isas Leibniz-Institut für Analytische Wissenschaften

BERGISCHE UNIVERSITÄT WUPPERTAL

Development and characterisation of quasi-simultaneous electrospray and plasma ionisation for the analysis of polar and less polar compounds in mass spectrometry

Dissertation

Zur Erlangung des akademischen Grades

Doktor der Naturwissenschaft (Dr. rer. nat.)

Vorgelegt von

Daniel Foest

Geboren in Dortmund

Bergische Universität Wuppertal

Physikalische und Theoretische Chemie

und

Institut für Analytische Wissenschaften – ISAS e.V.

Miniaturisierung

2023

Eingereicht als Dissertation in der Fakultät 4 – Physikalische und Theoretische Chemie der Bergischen Universität Wuppertal.

Mitglieder der Prüfungskommission:

1. PD Dr. Joachim Franzke
2. Prof. Dr. Thorsten Benter
3. Dr. Hendrik Kersten
4. Prof. Dr. Hans-Willi Kling
5. Prof. Dr. Peter Wiesen

The PhD thesis can be quoted as follows:

Insert Link

DOI:

Erklärung

„Ich versichere, die Arbeit selbstständig verfasst zu haben, nur die in der Dissertation angegebenen Hilfsmittel benutzt und alle wörtlich und inhaltlich übernommenen Stellen als solche gekennzeichnet zu haben, und dass die Dissertation in der gegenwärtigen oder einer anderen Fassung noch keiner anderen Fakultät, keiner Gesamthochschule und keiner anderen wissenschaftlichen Hochschule vorgelegen hat.“

Wuppertal, den 16.10.2023 Daniel Foest

Danksagung

Hiermit möchte ich allen Menschen danken, die mich unterstützt und es mir ermöglicht haben, diese Arbeit anzufertigen.

Ich danke Joachim Franzke für konstruktive Hilfestellungen und die wertschätzende sowie motivierende Arbeitsatmosphäre, die er durch seinen Führungsstil in der Arbeitsgruppe schafft. Dem gesamten Team Miniaturisierung möchte ich für die tolle Zusammenarbeit, die lösungsorientierten Diskussionen während der Kaffeepausen und schließlich für die lustigen Gespräche beim Mittagessen über neue Erkenntnisse aus dem Tierreich danken.

Abschließend bin ich meiner Familie für das liebevolle Umfeld, in dem ich lebe, sehr dankbar. Ich danke meinen Eltern für die Unterstützung und Zuversicht, die sie mir schenken. Ich möchte meiner Schwiegermutter Anne danken, die mir mit viel Mühe und Geduld bei der englischen Grammatik weitergeholfen hat. Ein besonderer Dank gilt meiner Frau und meinen Kindern. Vielen Dank, Lisa, für deine liebevolle Unterstützung, deine unendliche Geduld und unsere wertvollen Gespräche. Danke, Leonard, danke, Emilia, ihr beiden zeigt mir jeden Tag, was im Leben wirklich wichtig ist.

Abstract

The identification and determination of lipids as biomarkers is one of the most important tasks in the field of clinical and life science research. The challenge here is the enormous analyte diversity, which is given for example by the range of the molecular size and polarity present in complex sample matrices resulting from the high number of different biomolecules.

A very efficient and successful method for this task is the mass spectrometry. Depending on the ionisation source used, however, only molecules of a certain polarity range are accessible for mass spectrometers. Electrospray ionisation is able to ionise medium to polar and ionic compounds, whereas plasma-based techniques such as atmospheric pressure chemical ionisation are selective for medium to less polar compounds. As a result, simultaneous ionisation and detection of polar and less polar compounds from complex samples is not possible within a single measurement, making a time-consuming exchange of the ionisation source and subsequent recalibration of the mass spectrometer necessary.

To solve this problem, the present work deals with the combination of two ionisation techniques. The focus is on the development and characterisation of a combination consisting of the nano-electrospray ionisation and a modern plasma source, the flexible microtube plasma. A highly complex liver sample containing a large number of different polar and less polar biomolecules is selected as real life sample and reference for improvement and evaluation purposes. Investigations and improvements on this combination enables a selective activation of a dominanting ionisation technique solely by the plasma high voltage amplitude. A very fast alternating activation of a dominating ion source finally allows a quasi-simultaneous ionisation, leading to a simultaneous detection of polar and less polar compounds in ion trap mass spectrometers.

Contents

1 About this work

1.1 Motivation

The complexity of living organisms is very high and thousands of different biomolecules exist in every single cell of a human body. One of the largest groups among biomolecules are lipids. Categorised in different classes, they have multifarious functions in biochemical processes [1]. For this reason, lipids often are used in life sciences as biomarkers for a variety of diseases [2]. However, the identification and determination of biomarkers is challenging, due to the complexity of biological samples like blood, urine, saliva or tissue. Diverse separation and analysis techniques as well as sample preparation procedures are required to identify the entire spectrum of compounds or to determine a specific biomarker among thousands of molecules.

One of the most commonly used techniques in analytical chemistry is the mass spectrometry (MS) [3]. Since the past decade there is a growing trend to replace time-consuming separation and sample preparation treatments by the resolving power of modern mass spectrometers [4]. High-resolution mass spectrometric (HRMS) analysers as an Orbitrap™ are able to separate very similar compounds by the resolving power. An additional benefit of this

devices is the advantage of high mass accuracy. Resolving power and mass accuracy are closely linked and allow the determination of exact molecular masses with only minor deviations. Thus, a variety of different compounds can be accurately identified rapidly, making high-resolution mass spectrometry a powerful tool for the identification and determination of biomarkers in complex biological samples.

The first important step in mass spectrometric analysis is the ionisation of target analytes. Here, ionisation efficiency and selectivity are key parameters that indicate the application areas of a particular technique. For this reason, several ionisation sources are available for different analytical tasks.

The development of the electrospray ionisation (ESI) by Fenn et al. in 1984 represents a milestone in MS history and becomes the most common technique in mass spectrometric analysis [5–8]. The electrospray is able to ionise small and very large molecules up to several thousand mass units and is sensitive for medium to polar compounds [9,10]. In other words, the ionisation efficiency of the electrospray mechanism decreases with decreasing polarity of an analyte [4,11].

Another commonly used ionisation source is the atmospheric pressure chemical ionisation (APCI) [3]. Introduced by Horning et al. in 1975, the APCI is based on a plasma discharge that produces reactant ions which are able to ionise incoming neutral gas phase molecules [12]. As a consequence of the ionisation mechanism APCI and associated plasma based ionisation techniques are sensitive for medium and less polar compounds. This means that the ionisation efficiency of plasma-based techniques decreases with an increasing polarity of the analytes [11]. Due to the molecular preferences of ionisation techniques the determination of polar as well as non- and less polar analytes in a complex biological sample cannot be completed successfully in a single MS run. Performing two measurements with different ionisation sources is time-consuming and expensive. The technical switch of ion sources makes a readjustment and a recalibration of the MS setup necessary. Furthermore, acquired data of different ionisation sources are mostly difficult to compare.

In order to apply the full potential of high-resolution mass spectrometers within a single MS run, an ionisation source is required that is capable of ionising both polar and less polar compounds simultaneously. A possible solution could be the combination of two techniques.

The idea of a combined ionisation source is not new and a few publications are dealing with this topic. In 1998 Siegel et al. started to combine a conventional ESI source with an APCI. Antagonistic effects were recognised and mainly based on different temperature preferences of the ionisation sources [13]. The best conditions for ESI (depending on the specific source and solvents) are below 100 °C, higher temperatures lead to disrupting evaporation processes. In contrast to this, for the APCI mechanism a completely evaporated sample is necessary that requires high temperatures. Siegel et al. created a dual source, but the combined ESI-APCI operation showed only strongly reduced signal intensities. Altering between ESI and APCI prevents signal reduction, but multiple scan cycles are necessary for average spectra that is also time consuming due to the temperature gradient [13].

Further developments to combine electrospray and plasma ionisation techniques have been realised in several publications, but they lack in documentation, show recurrent weaknesses and comparisons to conventional sources are omitted. In these publications it is noticeable that signals acquired in APCI mode or in the combined mode (ESI+APCI) are an order of magnitude lower than those of the electrospray mode [14,15].

The antagonistic effects described above are still observed in combinations today and have an influence on the spectra. In the study "Hybrid Ionization Source Combining Nanoelectrospray and Dielectric Barrier Discharge Ionization for the Simultaneous Detection of Polar and Nonpolar Compounds in Single Cells", published in 2022, Liu et al. combine a nano-electrospray source with a dielectric barrier discharge ionisation (DBDI) to analyse single cells. In this excellent work the diagram of Figure 1 can be found that represents different ion chromatograms of polar and less polar compounds [16]. Here, the antagonistic effects of both electrospray- and plasma ionisation

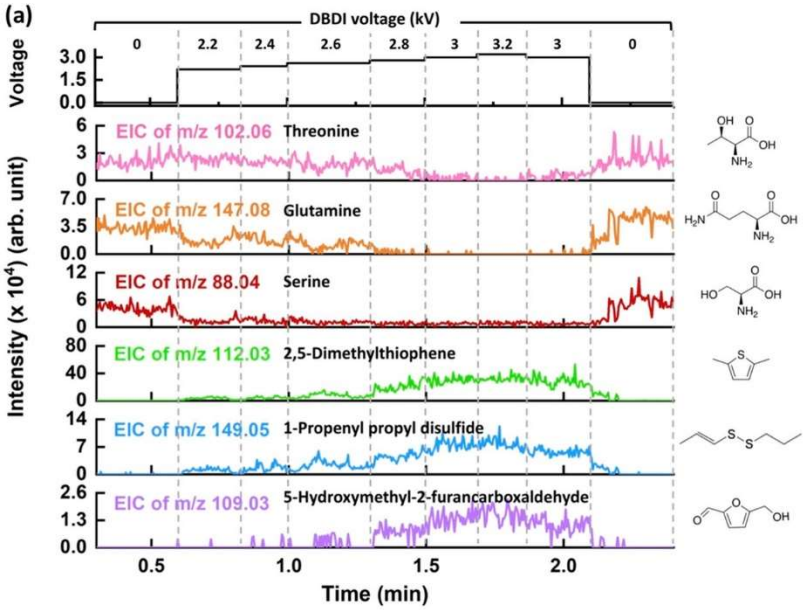

Figure 1: Part of a figure from the publication by Liu et al. shows that simultaneous ionisation of polar and less polar compounds is difficult to achieve. In areas of high polar analyte intensity the signals of less polar analytes are low and vice versa. This figure is reprinted with permission from Anal. Chem. 94, (2022), 2873–2881. Copyright 2022 American Chemical Society.

can be observed as well. With an increasing voltage of the dielectric barrier discharge ionisation (DBDI), the electrospray-generated signals of the polar amino acids decrease in intensity, while the plasma-ionised compounds increase. Either high electrospray signals of polar compounds or high DBDI generated signals of less polar compounds can be achieved, but a simultaneous ionisation is not truly given.

In order to understand these antagonistic effects and to solve this problem, a new type of discharge for plasma ionisation has been developed. Initialised by the work on novel miniaturised plasma techniques of J. Franzke et al. the Flexible Microtube Plasma (FμTP) was developed, characterised and introduced as ion source by S. Brandt in 2018. This type of plasma source shows an enhanced ionisation efficiency compared to conventional plasma sources and demonstrates its advantages and excellent appropriability in different analytical tasks [17–20]. In the dissertation by S. Brandt the FμTP was operated in combination with a nano-electrospray ionisation source for the first time, which represents the starting point for the present work [21].

1.2 Scope of this work

This work focuses on the development and characterisation of a dual ionisation source for the simultaneous mass spectrometric detection of polar and less polar compounds of complex biological samples. At the beginning of this work an overview of theoretical background knowledge of different sources, ionisation mechanisms as well as important analytical and statistical parameters is given.

The main work starts with a stepwise investigation and a detailed evaluation of the flexible microtube plasma as consecutive ionisation source for the less polar lipid cholesterol in electrospray mass spectrometry. For this comprehensive validation a challenging, complex real-life sample in form of a liver extract has been analysed in detail.

Furthermore, interesting observations and new findings are obtained by coupling the flexible microtube plasma with paper spray ionisation, which represents the second main part of the present work. The results, experiences and findings of this experiments lead to a confluence with the initial nESI-FμTP setup and to a further development that will be evaluated in the final main part of this work.

The combination and implementation of different insights lead to a technically and operationally revised version of the initially introduced combined nano-electrospray and flexible microtube plasma source. The resulting type of dual ionisation source allows a quasi-simultaneous ionisation of polar and less polar analytes within a single ion injection process of the mass spectrometric scan cycle of ion trap devices. Finally, the technique developed here is assessed and compared with conventional and commercially available ionisation techniques.

2 Fundamentals

2.1 Lipids

Lipids are essential biomolecules, forming one of the largest classes of natural compounds and fulfilling various vital functions in the body. They represent an important source of energy and also play a key role in the structure formation of cell membranes, signal transmission and the regulation of metabolic processes. The hydrophobic character makes them fat-soluble [1].

Lipid classification. There are different ways to classify lipid molecules. One possibility is the differentiation on the basis of their chemical structures. Here, lipids are basically divided into three classes which consist of various subgroups. These classes are fatty acid derivatives, isoprenoids and polyketides [1]. The polyketides are not described in detail here, as they are not of importance for this work. Fatty acid derivatives are subdivided and consist, among others, of neutral glycerolipids such as di- and triacylglycides (DG, TG) as well as of phospholipids such as phosphatidylcholines (PC) or phosphatidylethanolamines (PE). Within the class of isoprenoids, cholesterol is a relevant and well known representative. Cholesterol esters are directly related to cholesterol and fatty acids and can be counted to the fatty acid derivatives as well as to the isoprenoids due to their combined chemical structure [1].

Figure 2 exemplarly shows the chemical structures of relevant lipids for this work, including a phosphatidylcholine, a di- and triacylgylceride as well as cholesterol and a cholesteryl ester. This figure suggests a further classification that can be derived by comparing the chemical structures. The molecular polarity of the phosphatidylcholine is, due to the charged headgroup, increased compared to the other lipids of Figure 2. The classification by the molecular polarity of compounds is of central importance in mass spectrometric analysis, especially in the choice of a suitable ionisation technique.

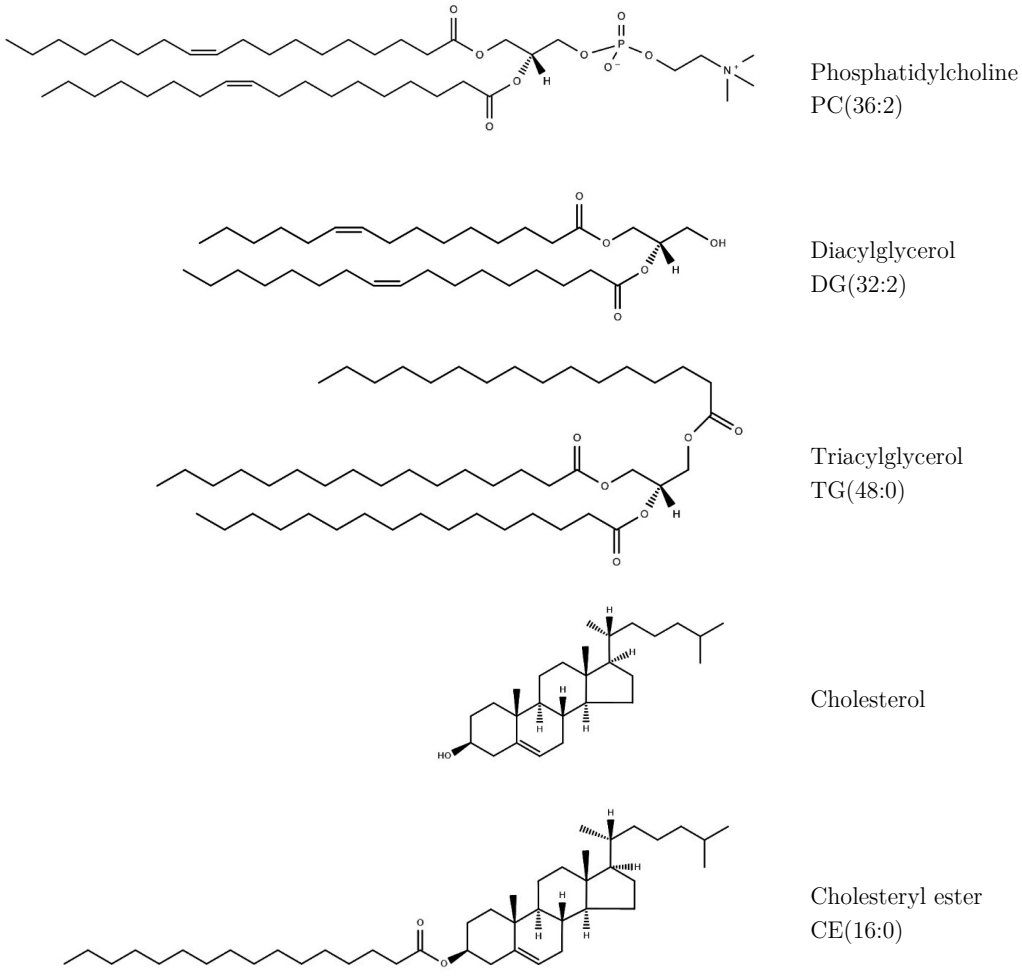

Figure 2: Exemplary compounds of the lipid classes that are relevant in this work. While phospholipids such as phosphatidylacetylcholines are considered as polar, triacylglycerides or cholesterol are considered as less polar lipids.

Molecular polarity. This fundamental property of a molecule is related to the dipole moment. An uneven distribution of electrons within a chemical bond caused by electronegativity differences creates a polarisation inside a molecule and leads to an electric dipole. The vector magnitude of two point charges ±q, which are separated by the distance d, can be calculated by the product of both and represents the dipole moment [22]:

Eq. 1

$$\vec{\mu} = q \cdot \vec{d}$$

In the case of several dipoles the total dipole moment of a molecule $\overrightarrow{\mu_M}$ results from the vector sum of all dipole moments [23]:

Eq. 2

$$\overrightarrow{\mu_M} = \sum_{i=1}^{n} \overrightarrow{\mu_i} = \sum_{i=1}^{n} q_i \cdot \overrightarrow{d_i}$$

Polar molecules have a permanent dipole. Due to the directional dependence, nearly symmetrical or completely symmetrical molecules have only a low to no dipole moment and are less or non-polar. The exact calculation of the dipole moment, especially for larger and more complicated molecules, can be very complex in practice. Therefore, quantum mechanical calculations by Hartree-Fock approximation or the density functional theory (DFT) are recommended for more accurate values [24]. In general, functional groups as well as the geometry or symmetry are decisive for the polarity of a molecule [22].

Lipids are basically hydrophobic, but can have non- or less polar as well as polar properties due to their diverse structures. Triglycerides, cholesteryl esters and cholesterol are less polar and are called neutral lipids in literature. In contrast, phospholipids such as phosphatidylchlolines or phosphatidylethanolamines are described as polar lipids [25].

Biomarker. All these biomolecules are linked via various biological processes, typically have several different functions in the human body and are therefore used for diagnosis, prognosis or risk assessment. Compounds used for this purpose are called biomarkers. For example, cholesterol serves

as a precursor of bioactive molecules such as vitamin D, bile acid, oestradiol and testosterone [26–28]. Furthermore, it regulates membrane fluidity and is involved in transmembrane signalling processes and plays a key role in the transport of hydrophobic molecules in hydrophilic media via lipoproteins [29,30]. Classified into different lipoproteins like low-density lipoproteins (LDL) and high-density lipoproteins (HDL), various diseases such as non-insulin-dependent diabetes mellitus, Smith-Lemli-Opitz syndrome, brain diseases, prostate cancer as well as cardiovascular diseases correlate with atypical cholesterol, LDL and HDL levels [31–36]. The determination of cholesterol in complex samples is not simple, for various reasons.

From the medical point of view different forms of cholesterol exist in the human metabolism. These forms are free cholesterol and cholesterol esters as shown in Figure 2. They are linked by the reverse cholesterol transport, in which excessive free cholesterol is absorbed and enzymatically esterified by HDL to transport it from the tissues to the liver [37]. Approximately 70 % of the cholesterol molecules in human plasma are found in the form of cholesterol esters [38]. Structurally, cholesterol esters differ strongly from the original, free cholesterol due to the additional long fatty acid chain, but extreme conditions in analysis processes such as high temperatures, electric fields or certain reaction conditions in the liquid phase can lead to the conversion of cholesterol esters to cholesterol creating interferences and incorrect values. For example, Lütjohann et al. found large deviations of the cholesterol concentrations in worldwide interlaboratory tests in 2019 [39].

Lipidomics. Mass spectrometry (MS) is an indispensable tool in lipid or biomarker analysis, which is demanding due to the high complexity of the samples. Especially the enormous quantity and diversity is a major challenge for analytics. Here, lipidomics represent a field of bioanalytics. With the development and commercialisation of high-resolution mass spectrometers a trend away from chromatographic separation methods towards high-resolution MS instruments could be observed in the field of lipidomics. Although these cannot replace chromatographic separation methods completely, many analyses can be performed more efficiently as selectivity

can be realised directly by the mass analyser rather than by a time-consuming pre-separation. However, this technique also has its challenges as there are a large number of lipids with very similar structures. For example, isomers or isobaric lipids can only be differentiated by using certain MS scanning techniques. Two isomeric lipids have a different chemical structure, but share the same mass and thus produce the same MS signals [3,4]. These isomeric lipids can be differentiated by MS^2 fragmentation experiments, which is also possible with less resolving mass spectrometers. Isobaric lipids on the other hand do not have the same molecular composition, but have very similar exact masses, often differing only by small decimal places [3,4]. The latter cannot be identified by less resolving mass spectrometers, thus high resolution MS instruments are necessary.

In addition, isotopic effects are present. Due to the naturally occurring isotope distribution of several elements isotope patterns can often be observed, especially in mass spectra of larger biomolecules. This becomes noticeable by additional signals. The probability that one or more carbon atoms represent a ^{13}C isotope increases with the number of carbon atoms in the molecule. Therefore, depending on the elemental composition of a molecule with the mass-to-charge ratio M, additional signals occur at m/z M+1, +2 and +3 (or more) for the carbon isotopy that has a ^{13}C abundance of 1.11 % [3,40]. The number and intensity of these signals depends on the abundance of carbon atoms in the molecule. As the number of carbon atoms in the molecule increases, the isotope signals become more intense compared to the stable isotope M and the number of signals increases [3]. Other elements with isotope distribution such as hydrogen, oxygen, nitrogen, phosphorus and sulfur can intensify this effect, but are less abundant.

In this work the lipid identification is realised using various techniques. High-resolution spectra with a high mass accuracy allow data matching with the database LIPID MAPS® and reduces the number of suitable lipids by the deviation to exact theoretical masses [41,42]. By this, a range of isobaric compounds can be almost excluded. The differentiation of isomers is realised by MS^2 experiments using collision induced dissociation (CID). By

fragmenting an isolated lipid, specific groups of the molecule can be removed and generate additional signals in the mass spectrum which can be identified [43]. These additional pieces of information can be interpreted and allow matching with lipid data bases like ALEX123 Lipid Calculator [44,45]. Finally, publications that deal with similar samples and analytical techniques are also of great relevance to confirm evaluated results.

As a result of the diverse chemical composition of lipids a large number of different analytical methods exists [1,46]. With the development of the electrospray, mass spectrometry has become one of the most important methods in the field of lipidomics [3,9,10,47,48]. This technique allows the ionisation of very large molecules and the direct transfer from the liquid to the gas phase without the need of high temperatures [3,10]. Coupled with improved instrumentation in mass spectrometry, this has led to a strong increase in research output in the field of lipidomics, especially in the last two decades [49,50].

2.2 Mass spectrometry

Mass spectrometry is an analytical technique with a large range of applications. Implemented in a variety of disciplines, tasks like quality controls, assessment of potential risks to health and environment, bioimaging and identification of diseases and disease mechanisms can be solved by MS analysis. In MS, different mass analyser technologies exist and this work focuses on ion trap devices.

As depicted in Figure 3, a mass spectrometer is composed of three major elements to determine the mass-to-charge (m/z) ratio of analytes. Usually molecules in the gas phase occur uncharged as neutral compounds. Hence,

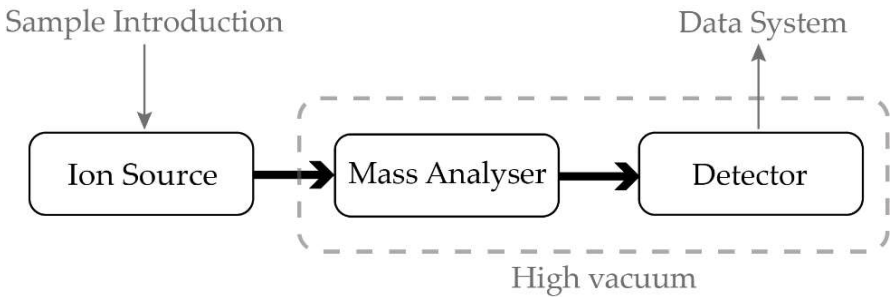

Figure 3: Schematic diagram of the major mass spectrometer elements.

ionisation is the first essential process to make neutrals accessible for electrical lenses, mass analysers and detectors.

Subsequent to the ionisation process, produced ions pass the MS inlet in a prevacuum and reach the mass analyser region inside the high vacuum. In ion trap mass analysers ions are accumulated and separated according to their mass-to-charge ratio. Ions ejected from the ion trap reach an electron multiplier which serves as a detector and generates electrically interpretable signals. In the following sections the relevant MS elements for this work are described in more detail.

2.2.1 Ion sources

For a mass spectrometer a liquid sample must be converted into a gaseous state and finally ionised. This is realised by the ionisation source which represents the interface between the sample and the mass spectrometer. Various ionisation techniques exist which are appropriate for different applications and classes of molecules.

Selectivity. The choice of a suitable ionisation technique depends on the physical state of the sample and the analytical aim. The latter is based on the already described molecular polarity of the target compound. Besides this,

another important property for the choice of a suitable technique is the molecular weight. Combining both leads to a very helpful visualisation as depicted in Figure 4. The diagram shows the selectivities of the individual ionisation techniques based on the accessibility for a specific molecular polarity and weight. Only ionisation sources that operate under atmospheric pressure, the so-called atmospheric pressure ionisation (API) sources, are listed here. [51].

The most common API sources are electrospray ionisation (ESI) and atmospheric pressure chemical ionisation (APCI). ESI is based on the electrospray mechanism, where the ionisation takes place directly in the liquid phase, making this approach sensitive for medium to high polar and ionic analytes. Hence, ionisation efficiency of ESI decreases with decreasing molecular polarity. Non- and less polar compounds are not accessible by ESI [3,51]. Appropriate for analytes of this polarity range is the atmospheric pressure chemical ionisation. The APCI is based on a plasma discharge which leads to gas phase reactions and finally to the ionisation mechanisms. Diverse

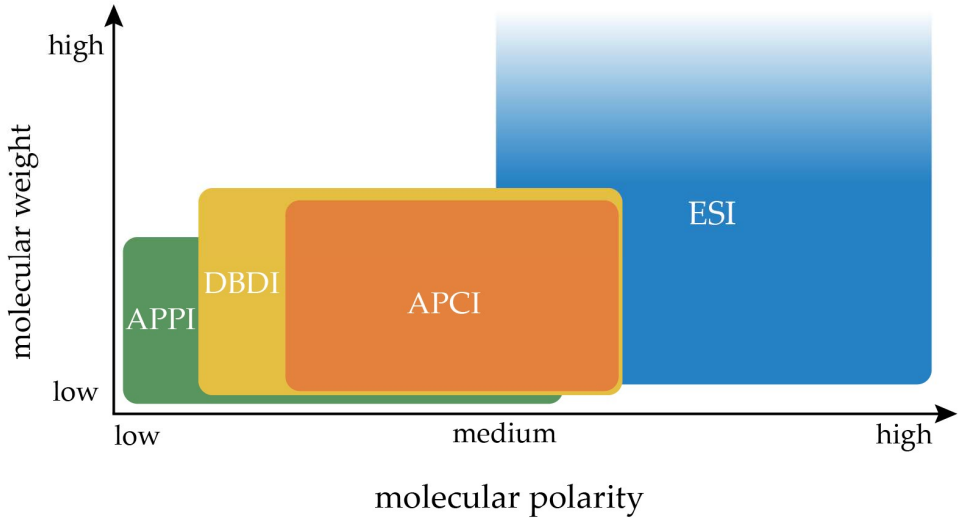

Figure 4: Molecular polarity range of common API sources. Classified by the molecular weight and the molecular polarity, the selectivity indicates the application range of an ion source. This diagram is illustrated according to the diagram of O.J. Schmitz and T. Benter, Advances in LC-MS Instrumentation, Journal of Chromatography Library, Vol. 72.

related developments like the direct analysis in real time (DART) [52], the low temperature plasma (LTP) [53] or the dielectric barrier discharge ionisation (DBDI) [54,55] represent modern types of APCI with enhanced ionisation efficiencies and polarity ranges [17,56,57]. Due to the ionisation mechanism of plasma-based techniques medium to low polar compounds are easily accessible. Another important approach that shares a similar polarity range of analytes is the atmospheric pressure photo ionisation (APPI). The process is based on photochemical reactions with dopants that lead to the formation of reactant ions and thus to the ionisation of target molecules [58,59]. In contrast to electrospay, both photoionisation and plasma-based techniques require the conversion of liquid samples into the gas phase prior to the ionisation process. The latter is usually achieved with vaporisers such as thermosprays.

Hard and soft ionisation. An important property of ionisation sources is the degree of hardness. A distinction is made between hard and soft ionisation. This property is directly linked to the conditions inside an ionisation source. Strong electric fields and high temperatures, for example, lead to unintended fragmentation processes before the molecules enter the mass analyser region [60]. For this reason, soft ionisation is usually desired in order to detect the entire molecule or to fragment the molecule in a controlled procedure, such as collision induced dissociation in the further course of the measurement. Therefore, ion sources that are able to remain molecules intact or show only low fragmentation products are categorized as soft techniques. Ion sources that show increased fragmentation patterns, such as electron impact ionisation, are considered as harder [60]. In principle, ESI and APCI are soft sources, although a gradation can already be made here. Due to the vaporiser temperature and the strong electric field in the direct vicinity of the corona needle, the APCI is slightly harder compared to the ESI. However, modern, alternative plasma based ionisation techniques as the dielectric barrier discharge ionisation (DBDI) can be softer than the classical APCI, due to differences in the ionisation mechanism. Yet, this fact has not yet been evaluated by data, but reflects the experience of handling these ion sources.

A mass spectrometer is able to analyse both positive and negative ions. However, it can be said that the positive ion mode is the standard and depending on the sample or target molecule, it may be necessary to work in the negative mode. This fact as well as the workload associated with evaluating the positive mode is the reason why this work deals theoretically as well as experimentally exclusively with the positive ion mode.

2.2.2 Electrospray ionisation

The development of electrospray as an ionisation source for mass spectrometry represents a milestone in MS history [5,9]. Two events are unique at this technique. Firstly, it allows the vaporisation and ionisation in one single process. Secondly, the electrospray is able to ionise extreme large (polar and ionic) biomolecules like polymers and proteins [10]. The latter is particularly the reason why this method has become established in the fields of lipidomics, metabolomics and proteomics. The electrospray mechanism is a multi-stage process in which ions of a liquid sample are transferred to the gas phase by nebulisation.

Principle. To generate an electrospray, a conductive liquid sample containing the target molecules passes a capillary where a high voltage amplitude is applied. The formation of charged droplets at the capillary tip finally leads to the ejection of gas phase ions. In electrospray ionisation different spray operation modes exist leading to aerosol production. The best characterised operation mode is the so-called cone-jet mode [61]. This entire electrospray mechanism and its multi-stage process is schematically visualised for the positive ion mode in Figure 5 [62].

A capillary with the conducting liquid sample inside is located several millimeters away from a counter-electrode which can also be represented by a mass spectrometer inlet. By applying a high direct current (DC) voltage

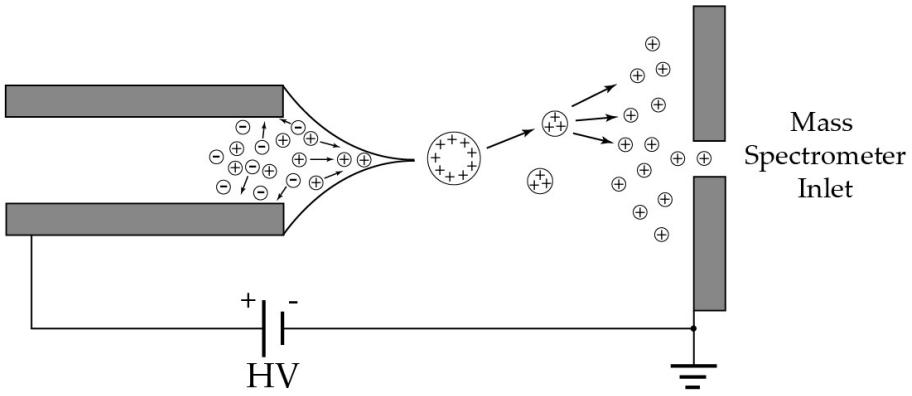

Figure 5: Schematic of the electrospray ionisation process. Charged droplets are generated at the Taylor cone and accelerate along the electrical field to the mass spectrometer inlet. This figure is a modified scheme according to P. Kebarle and M. Peschke. Modified reprint of Analytica Chimica Acta 406 (2000) 11–35 [62].

amplitude to the electrode of the electrospray, this system acts like an electrolytic cell. Ion movement along the electric field gradient is initiated and polarisation of the solvent molecules at the tip of the capillary leads to an accumulation of positively charged molecules. Negative ions move towards the anode and are removed by oxidation reactions [62]. The amount of positve ions at the meniscus increases until the coulomb repulsion forces of the ions exceed the surface tension. The solution surface expands in the shape of a cone towards the counter electrode (or mass spectrometer). This appearing cone is called Taylor cone in the literature [63,64]. The expansion of the meniscus is limited and when the applied voltage is sufficient, micro-droplets with an excess of charges are released from the Taylor cone towards the counter-electrode. Solvent evaporation reduces the size of the ejected droplets, whereas the amount of charges inside the droplet remains constant. Hence, the charge density at the surface increases with the shrinking process of the droplets. An effect similar to the formation of the Taylor cone described above now occurs at the droplet. The coulomb repulsion forces exceed the surface tension forces of the droplet and the droplet ejects a series of smaller droplets from a narrowed tail [3], which undergo the same procedure as shown in Figure 6. This process is called droplet jet fission and has been demonstrated via flash-shadowgraphs [65]. It continues until the micro droplets reach the

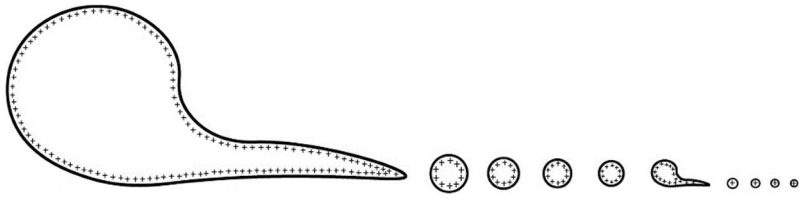

Figure 6: Schematic representation of the release of smaller droplets up to the size of charged nanodroplets. Similar to the Taylor cone the droplets form a shape distortion from which smaller droplets are ejected.

radii of a few nanometers [7]. Explanations of the electrospray process are based on investigations and models that underlie Gauss' law. This law states that electric charges on an insulated conductor generally move towards the outer surface. Accordingly, ions inside a microdroplet are localised at the droplet surface [7].

Ion release. The formation or release of gas phase ions has not been fully clarified and depend on the size of analytes. Three concepts exist to explain these processes [3,7]. The ion evaporation model (IEM) describes the formation of gas-phase ions for species of low molecular weight. By the high charge density of the droplet surface (Rayleigh-charged nanodroplets), an electric field is generated that is sufficiently large to eject solvated ions. This process has similarities to the droplet fission events that can be observed in larger droplets, as described above.

For the transfer of large, globular analytes such as folded proteins, a different model is required. The charge residue model (CRM) is used here for explanation. In the droplet a protein is surrounded by solvent molecules. It is folded in such a manner that non-polar parts are hidden inside and have no contact with the solvent. Solvent molecules evaporate from the Rayleigh-charged nanodroplets to dryness. During this evaporation process excess charges are ejected via the IEM of solvent molecules. The final solvent shell transfers the remaining charges to the large analyte. Due to the relevant lipid size of < 1000 mass units the CRM is of less importance for this work.

In certain solvent conditions proteins can be present unfolded. The CRM is no longer applicable here, as this disorder leads to non-polar parts also having contact with the solvent molecules. Here, the chain ejection model (CEM), which has similarities to the IEM, describes the process [7]. Due to the hydrophobic character the protein preferentially remains at the surface where it is released from the droplet by electrostatic repulsion. The charged protein enters the gas phase by stepwise ejection [7].

All three models are summarised graphically by Konermann et al. and reprinted in Figure 7. Both CRM and CEM describe the ejection process of large molecules such as proteins. Compared to these, lipids are rather small, which is the reason why the IEM model is of particular importance for this work. These processes are briefly summarised here, but can be found in more detail in the publication by Konermann et al. from 2012. It should be noted that not only ions but also neutral compounds with a certain minimum polarity can be ionised and sprayed by electrospray. In this case, very small ions such as H^+ or NH_4^+ associate with the neutral but polar analytes and ionise them [61]. This processes are called protonation and adduct formation. A protonated analyte molecule for example can be found at m/z $[M+H]^+$. Weak acids or bases are typically added to support this type of ionisation in

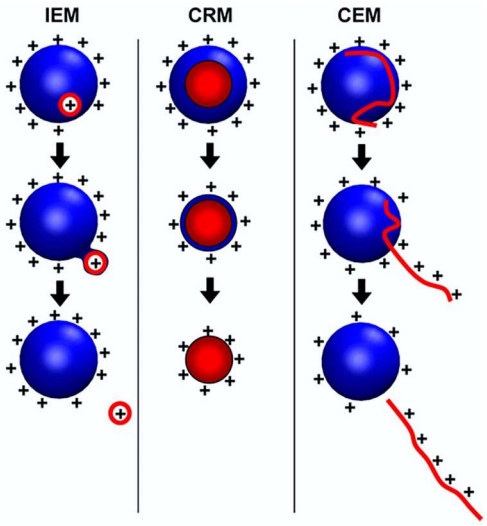

Figure 7: Graphical representation of the different ion release models such as the ion evaporation model (IEM), charge residue model (CRM) and chain ejection model (CEM). Reprinted with permission from Anal. Chem. 2013, 85, 1, 2–9. Copyright American Chemical Society 2013.

the liquid phase. This increases the conductivity of the sample and the probability of adduct formation, which leads to a higher ionsation degree. Typically, formic acid or ammonium actetate is used for this purpose [61].

If the molecular polarity of an analyte is below a certain level, it can no longer be ionised by the electrospray and consequently cannot be detected in the mass spectrometer. An analyte that is very close to this limit is cholesterol. This analyte can only be determined very poorly by ESI-MS. However, it is a fact that less polar compounds such as cholesterol or triacylglycols can also be found in complex samples and in the electrospray microdroplet cascade, as these can be measured using complex MS scan functions, even if only with very low signal intensities [66–68].

As described in the theories of ion release, charge carriers or ionised molecules prefer to stay on the droplet surface due to the repulsive forces. Surface active compounds such as polar lipids (PC, PE for example) are positioned in such a way that the non-polar side chains protrude out of the droplet [69]. As a result, molecules such as cholesterol and other low and non-polar molecules are preferentially located inside the droplet [70].

Nano-electrospray. A modern type of electrospray is the nano-electrospray. Compared to the conventional electrospray, capillaries with diameters in the lower µm range are used here. This leads to the ejection of smaller initial droplets as well as significantly reduced flow rates and sample consumption [3]. The nano-electrospray assembly used in this work is described in a following chapter 3.1.

2.2.3 Plasma based ionisation

Suitable for the ionisation of less polar compounds under atmospheric conditions is the APCI, which is besides the electrospray one of the most used API techniques in mass spectrometry. This technique, as well as its modern

variants (e.g. LTP, DBDI and FμTP), is based on a plasma which is a partially or fully ionised gas. The ionisation of a gas can be realised by adding energy, for example thermal energy, on a gaseous system. However, this requires extremely high temperatures of several thousand Kelvin. In practice, it is easier to create a plasma by applying electrical energy. To achieve this, an electrical discharge can be initiated by applying high voltage to electrodes that are separated from each other by a gas chamber. This capacitive coupling of a high voltage creates an electric field which initiates a series of excitation-, ionisation- and relaxation processes.

Plasma mechanisms. An atom or molecule A within an electric field can collide with an accelerated electron e^-. If the energy transfer of this collision is greater or equal to the ionisation energy of the particle, an electron is removed from the orbitals and the particle gets ionised (Equ. 3). This process is called electron impact ionisation [71]. If not enough energy is transferred, the particle A goes into an excited state A^* (Equ. 4). Particles that are already excited can also be ionised by a further collision (Equ. 5). The recombination of an electron e^- and an ion A^+ also leads to an excited state (Equ. 6). Excess energy of excited particles are emitted as photons, whereby the particle reaches the ground state (Equ. 7) [22].

Equ. 3 $$e^- + A \rightarrow A^+ + 2\,e^-$$

Equ. 4 $$e^- + A \rightarrow A^* + e^-$$

Equ. 5 $$e^- + A^* \rightarrow A^+ + 2\,e^-$$

Equ. 6 $$e^- + A^+ \rightarrow A^*$$

Equ. 7 $$A^+ \rightarrow A + hv$$

As mentioned above, strong ionisation conditions can lead to fragmentation processes. The resulting molecular fragments as shown in Equ. 8 - Equ. 10 can be neutral or ionised. The fragmentation within the ionisation region is usually not intended as described in the section about “Hard and soft ionisation”.

Equ. 8 $$e^- + AB \rightarrow A + B + e^-$$

Equ. 9 $$\rightarrow A^+ + B + e^-$$

Equ. 10 $$\rightarrow A + B^+ + e^-$$

In contrast, a controlled fragmentation of molecules by collision induced dissociation for example inside the MS device is a common technique for structure elucidation.

Excited states usually have a very short lifetime [22]. However, if the transition to the ground state is forbidden due to quantum mechanical selection rules, a much longer lifetime follows [72]. Particles in this state are called metastables A^M. These can only release their excess energy to reach the ground state by collisions with other particles [3]. The collision of a metastable particle and a collision partner B results in the formation of a high-energy intermediate stage AB^*. If the energy level of this transition state is higher than the ionisation energy of the collision partner B, the collision partner is ionised during the disintegration (Equ. 11). This ionisation process is called Penning ionisation [73].

Equ. 11 $$A^M + B \rightarrow AB^* \rightarrow A + B^+ + e^-$$

If analytes are introduced into the vicinity of the electrodes and thus into the electric field, they enter the plasma and can be ionised either by electron impact, Penning ionisation, proton transfer or adduct formation. In the case of the APCI source the sample is transferred via vaporiser into the gas phase of the ionisation chamber. A needle applied with high voltage produces a strong electric field at the tip, which leads to the ionisation mechanism of the equations Equ. 12 - Equ. 16 postulated by Horning et al. [74].

Equ. 12 $$N_2 + e^- \rightarrow N_2^+ + 2\,e^-$$

Equ. 13 $$N_2^+ + 2N_2 \rightarrow N_4^+ + N_2$$

Equ. 14 $$N_4^+ + H_2O \rightarrow H_2O^+ + 2N_2$$

Equ. 15 $$H_2O^+ + H_2O \rightarrow H_3O^+ + OH$$

Equ. 16 $$H_3O^+ + n\,H_2O \rightarrow H^+(H_2O)_{n+1}$$

Accelerated electrons cause electron impact ionisation of nitrogen molecules (Equ. 12) forming N_2^+ and subsequently N_4^+ ions (Equ. 13). An ionisation cascade (Equ. 14 - Equ. 16) finally leads to the formation of water cluster ions $H^+(H_2O)_n$ that are able to ionise incoming analytes.

The mechanism postulated by Horning et al. is generally accepted in the literature, but seems to be incorrect and/or incomplete. Current research results show that discharges in a pure nitrogen atmosphere are unable to ionise analytical molecules. Only by adding oxygen the process of analyte ionisation is able to operate [20,75]. A comprehensive study showed that in air, the radical cation O_2^+ is the dominant species [76]. Besides the direct formation of O_2^+ by the electric field, generated N_2^+ species react immediately with atmospheric O_2 and form O_2^+. It is assumed that the formation of the water cluster $H^+(H_2O)_n$ as described above (Equ. 16) is mainly formed by oxygen-water clusters [76]. Additionally, nitrogen oxides also contribute to the formation of these water clusters. A simplified overview of these reactions is given according to Allers et al. in Figure 8 [76]. However, the reaction of N_2^+ to $H^+(H_2O)_n$ clusters should be considered of minor importance and an additional reaction pathway from N_2^+ to O_2^+ should be mentoined.

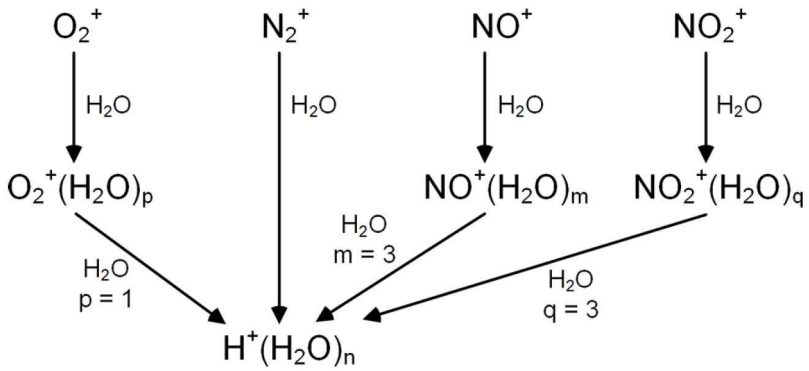

Figure 8: Overview of different APCI generated reactant ion species that lead to water cluster formation in air. Reprinted with permission from J. Am. Soc. Mass Spectrom., 31, 1291–1301. Copyright 2020 American Chemical Society.

The water cluster production is followed by a proton transfer that ionises the analyte molecule. In this process, the proton is transferred from the water cluster ion to the analyte M as shown in Equ. 17.

Equ. 17
$$H^+(H_2O)_n + M \rightarrow [M+H]^+ + n\,H_2O$$

Proton transfer reactions are possible if the proton affinity of the target molecule is greater than that of the water cluster ion. Furthermore, the proton affinity of water clusters depends on their size [76]. The reactions described above represent only a small, selected part of what occurs in reality. More information can be found in the excellent publication of Allers et al. [76].

The basic mechanism on generating reactant ions in modern plasma sources is the same as in APCI (described above). Major differences are in the geometric configuration and in some cases in the discharge gas and thus in the type of discharge. Compared to APCI, in which a metal needle surrounded by air is supplied with a direct current (DC), modern plasma sources usually consist of a glass capillary equipped with one or two electrodes. Helium passes through the glass capillary and a discharge is generated by applying alternating current (AC) to the electrodes.

The energy coupled into modern plasma-based ion sources is usually not sufficient to produce a significant amount of helium ions. Instead, the helium atoms are excited (He^*) and enter a metastable state (He^M) by emitting excess energy in the form of electromagnetic radiation as shown in the Jablonski diagram of Figure 9 [77]. Helium metastables collide with nitrogen molecules in the ground state $N_2(X^1\,\Sigma_g^+)$ and generate excited N_2^+ ions via Penning-ionisation. This assumption is based on the fact that the population of $N_2^+(B^2\,\Sigma_u^+)$ is comparable to that of the helium metastable state [77]. These excited $N_2^+(B^2\,\Sigma_u^+)$ ions also emit excess energy by electromagnetic radiation and enter the state $N_2^+(X^2\,\Sigma_g^+)$. As shown in the overview of the APCI mechanisms of Figure 8, these N_2^+ ions produce mainly O_2^+ ions, which in turn generate water clusters to ionise the analytes. How this process occurs at the end of the capillary is explained in more detail in the description of the flexible microtube plasma of chapter 2.2.4.

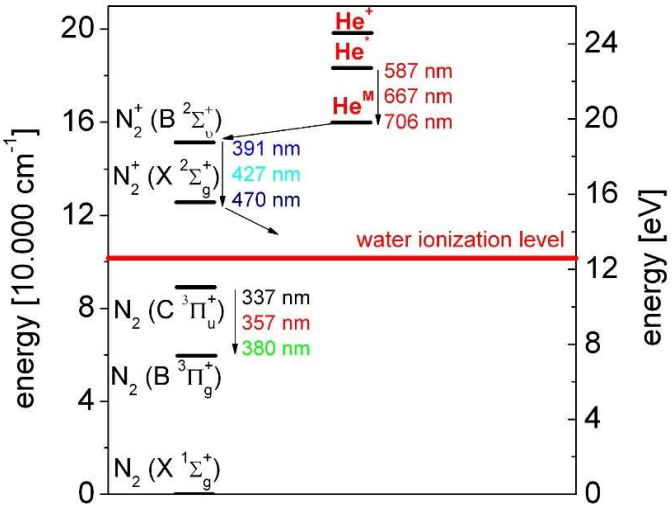

Figure 9: Jablonski diagram of different helium and nitrogen states. Reprinted with permission of Spectrochimica Acta Part B, 64, 1253–1258. Copyright 2009 Elsevier.

Both electrospray and plasma-based ion sources generate ions by electric fields. Disturbances of these electric fields can lead to obstructions in the ionisation process, which is the reason why interferences in a coupled system have to be avoided or at least minimised. The lower the voltages required to maintain the ionisation processes, the lower is the potential interference between two ion sources. Therefore, an important parameter to ignite a discharge is the breakdown voltage.

To describe the ignition process of low-pressure plasmas, the Townsend mechanism is applied from which Paschen's law (Equ. 18) can be derived. Simplified, Paschen's law gives the ignition voltage as a function of the product of the pressure p and the electrode distance d. Gamma corresponds to the 2nd Townsend coefficient, while A and B are gas-dependent parameters.

Equ. 18

$$U_Z = \frac{Bpd}{ln(Apd) - ln[ln(1+\gamma^{-1})]}$$

With identical electrode distances the ignition voltage of a low-pressure discharge is lower than that of a discharge at atmospheric pressure. Conversely, to ignite a plasma at atmospheric pressure the electrode distance

needs to be reduced. Hence, the miniaturisation of discharge geometries makes it possible to use plasmas at atmospheric pressure and moderate voltages.

Streamer mechanism. For the explanation of plasmas that operate under atmospheric pressure another mechanism plays an important role, the streamer mechanism. Under atmospheric conditions an electric field generated by an electrode is not able to produce ions over a longer distance, due to the high density of neutral particles at atmospheric pressure [78]. However, the ions generated by the electrode create an electric field by their own, which in turn accelerates electrons and thus ionises further neutral particles. Ions that have recently been generated recombine and become neutral particles. A new electric pulse is needed to repeat this process. This is the reason why AC voltage is used in this type of plasma. This process propagates through the capillary, as shown in the next section, so that the discharge moves along the capillary until it reaches the end.

2.2.4 The flexible microtube plasma

The plasma ion source used in this work is the flexible microtube plasma (FμTP) which is schematically illustrated in Figure 10. It consists of a fused silica capillary (Ø 360 µm; I.D. 250 µm) with an outer polyimide coating which, depending on the model, is typically removed at the end of the capillary (~ 10 mm). A tungsten wire (Ø 100 µm) that serves as the inner electrode, ends at a distance of 10 - 25 mm to the capillary end. Helium of purity 5.0 (purity 99.999 %) is used as plasma gas with a gas flow rate of 50 mL/min.

The AC plasma operating voltage is supplied by an in-house developed and manufactured square-wave generator. This AC generator delivers high voltage amplitudes up to 3.5 kV at a frequency of 20 kHz and a slope of 60 Vns^{-1}. The

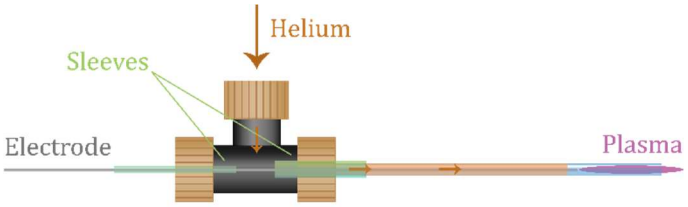

Figure 10: Schematic diagram of the flexible microtube plasma assemble. An IDEX high pressure PEEK micro tee introduces the electrode and the gas supply into the glass capillary.

generator also has a Bayonet Neill Concelman (BNC) input port to connect external frequency generators by transistor-transistor logic (TTL) signals. This enables the variation of the AC voltage frequency as well as the activation and deactivation of the HV generator. The latter is of particular importance in this work. The glass capillary is mounted in an IDEX PEEK tee-piece, which introduces the electrode and supplies the gas to the plasma capillary. In this configuration, the plasma ignites at ~1.2 kV, whereas typical values for ionisation of analytes are between 1.80 and 2.20 kV, which is about half of the voltages used in APCI. Several parameters of the FμTP can vary between experiments, which is why certain parameter descriptions are mentioned in the respective section. Further details about the flexible microtube plasma and its operational possibilities can be found in the Dissertation of Brandt et al. [79].

By applying a voltage, ions are formed at the electrode which generates further ions via the streamer mechanism and creates an excitation avalanche. This excitation avalanche moves towards the end of the capillary, whereby ions are deposited on the wall of the glass capillary and create a potential. At the end of the capillary there are probably two different effects that form oxygen-water cluster ions and water cluster ions leading finally to the ionisation of the analyte.

One of the effects is that N_2^+ ions generated inside the plasma reach the end of the capillary immediately and react with atmospheric oxygen to form O_2^+ ions as described before. However, the more important effect seems to be the potential that is created at the capillary wall. This potential is probably large enough to generate O_2^+ ions directly, which in turn causes also the

reactant ion cascade according to Figure 8 and Equ. 17. This mechanism is not yet fully understood and a subject of current research. In principle, the ionisation process is similar to that of an APCI, with the difference that this process is repeated frequently due to the chance of using AC voltage. The latter is probably the reason for the significantly higher ionisation efficiency of the DBDI or the FμTP compared to the conventional corona discharge.

2.2.5 Applied instruments and mass analysers

The major mass spectrometer used in this work is the commercially available LTQ Orbitrap XL from Thermo Scientific. This instrument has a linear trap quadrupole (LTQ) mass analyser as well as an Orbitrap mass analyser. In addition to this, in one experiment the successor model Orbitrap Velos Pro has been applied, which also consists of an LTQ and an Orbitrap.

Linear quadrupole ion trap. Due to the quadrupole construction the LTQ is a very fast mass analyser compared to other trap devices. It generates a high number of scans per time interval, but typically has a low resolution R of 3000 maximum [80]. Isobaric analytes are not resolvable and are represented as a single signal. The high velocity is ideal for coupling with chromatographic separation techniques to obtain many data points from the eluent signals. The principle of an electric quadrupole is based on an alternating field. Accelerated ions are introduced between two parallel rod electrodes to which alternating positive and negative electrical voltages are applied. A periodic alternating field is created that is able to separate ions by their mass to charge ratio (m/z). Ions of a certain m/z follow a stable path through the quadrupole, while other ions are deflected and do not reach the detector. By modulating the voltages, different m/z ranges can be selectively cycled [3]. In the case of the LTQ, the rod electrodes have a hyperbolic shape. Increased potentials at the front and back sections make it possible to retain the ions in the trap and eject them radially. The structure of such a linear

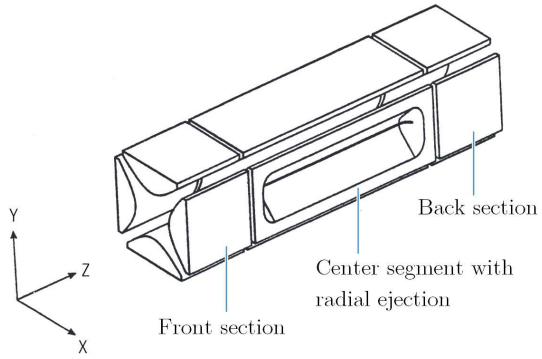

Figure 11: Scheme of the linear trap rod assemble of a Thermo Scientific LTQ orbitrap XL. Reprinted with the permission of Thermo Scientific, LTQ Series – Hardware Manual, 97055-97072 Revision D September, 2015.

quadrupole trap is shown schematically in Figure 11 [81]. This diagram is reprinted from hardware manual provided by Thermo Scientific (LTQ Series - Hardware Manual, 97055-97072 Revision D September, 2015) [81].

Orbitrap. In contrast to the LTQ, the Orbitrap mass analyser generates a significantly lower number of spectra per time interval. However, this mass analyser achieves a remarkable resolution of 7500 ≥ R ≤100 000 and a very high mass accuracy of < 3 ppm, classifying this instrument among high-resolution mass spectrometers (HR-MS). These devices are able to resolve even closely located signals such as isobaric molecules or isotopic patterns. The latter supports the investigation of complex samples and often makes chromatographic separations obsolete. Furthermore, due to the high mass accuracy, it is possible to obtain information on the structural composition of the molecules, which often makes comparisons of retention times with standards dispensable. In Orbitrap mass analysers, ions are also trapped in an electric field. This field is generated by a spindle-shaped central electrode and a barrel-shaped outer electrode. Stable ion trajectories result from the combination of rotation around the central electrode and axial oscillations whose frequencies depend on the m/z ratio [3]. The oscillating ion movements are acquired by image-current detection and subsequently converted into corresponding frequency and intensity signals by a Fourier transformation [3]. Figure 12 shows the construction of an Orbitrap mass analyser according to R. Zubarev and A. Makarov [82].

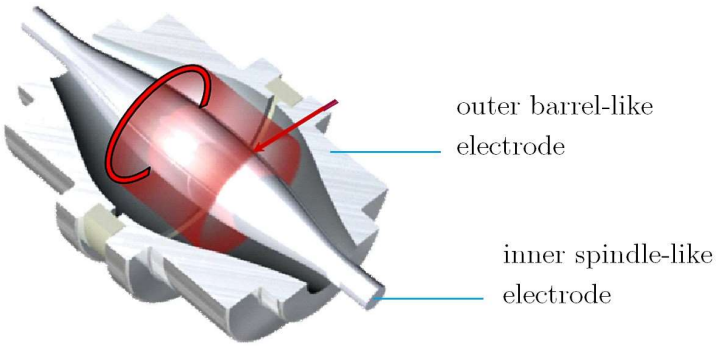

Figure 12: Scheme of the orbitrap mass analyser electrode assemble of the Thermo Scientific LTQ Orbitrap XL. Reprinted with the permission from Anal. Chem. 2013, 85, 11, 5288–5296. Copyright American Chemical Society 2013.

Both mass analysers are relevant for this work. The much faster LTQ part is used to generate data required for statistical purposes. The high resolution Orbitrap part is used to determine and identify analytes of the complex sample. The Orbitrap instrument has been mass calibrated to a deviation of < 3 ppm. The LTQ Orbitrap XL used here showed ghost peaks in the mass spectrum aquired with the high-resolution Orbitrap. The most conspicuous of these are at the m/z signals 552.293 and 657.473. Despite a resolution of R = 100 000, these show an unusually large width (m/z ±0.5) and are, according to the thermo technician, electronically induced. Data points of the ranges m/z 552.3±0.7 and 657.56±0.7 have been removed from the HR spectra presented in this work so that these artefacts do not complicate the interpretation of the spectra.

Scan cycles. According to Thermo Scientific, the procedure performed by a mass spectrometer during an analytical scan can be typically divided into five steps, as shown in Figure 13 [83]. An automatic gain control (AGC) based prescan determines the rate of incoming ions and sets the duration of ion injection. After ion accumulation in the trap, the first step in MS-MS experiments is the ion isolation. Only ions of the selected m/z remain in the trap so that it can subsequently be fragmented in the ion activation process. Finally, the resulting fragment ions are detected according to their m/z ratio, which represents the mass analysis [83]. In the case of the fullscan mode

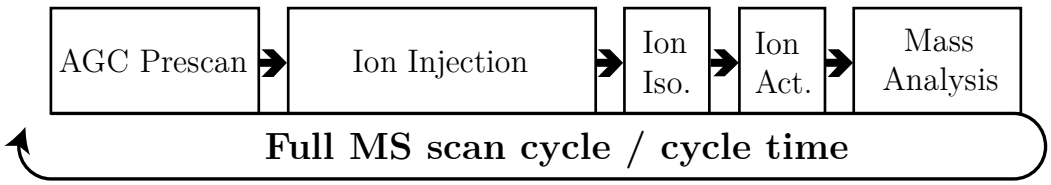

Figure 13: Scheme of the full MS scan procedure or scan cycle, which can be divided in five steps. Depending on the method of measurement, steps may be skipped or require different lengths of time.

isolation and activation are omitted. After accumulation of the ions in the trap they are detected sequential according to their m/z ratio. The time required for each step depends on various parameters. For example, in full scan mode isolation and activation are skipped, but due to the significantly increased mass range the duration of the mass analysis increases. Moreover, the AGC can be deactivated, which means that the prescan can be omitted. In this case, the time of the ion injection is specified by the user. This cycle is repeated throughout the entire measurement acquisition. In particular, the period of ion injection is of great importance for this work and will be discussed in more detail in a later chapter.

A mass spectrum shows the signal intensity as a function of the m/z ratio, whereby the relative abundance is usually used. However, in this work the relative abundance is only used when information is taken from only one mass spectrum. When comparing two or more mass spectra, the absolute intensity in arbitrary units (a.u.) or signal-to-noise ratios (SNR) are applied instead to ensure a direct comparison of the intensities.

2.3 Statistical methods

Various statistical approaches are used to interpret spectra and different analytical performance parameters. In this section, those that cannot be generally assumed will be explained.

Mass deviation. In the identification of lipids a comparison with databases is the first important step to exclude a large number of other lipids. Mass spectrometry is a realtive method of measurement and consequently has a certain inaccuracy. For this reason, database matching of lipids is based on the deviation of the measured mass ($m_{exp.}$) from the theoretical mass ($m_{theo.}$). The deviation δ in parts per million (ppm) can be calculated by the following Equ. 19 [3]:

Equ. 19
$$\delta\,[ppm] = \frac{m_{exp.} - m_{theo.}}{m_{theo.}} \cdot 10^6$$

For this purpose the monoisotopic mass is utilised. The monoisotopic mass is the mass of a molecule or ion which contained the most abundant naturally occurring stable isotopes of each atom [3].

Method of standard addition. Within the scope of this project, concentration series are analysed according to the method of standard addition. This method is a form of internal standard where known amounts of the analyte are added successively to the sample [84,85]. By adding the analyte the regression line is shifted along the axis on which the concentration is projected. The concentration of interest can be derived from the intersection of the regression line and the abscissa in the second quadrant (negative area) of the Cartesian coordinate system [84,85].

Linear dynamic range. Both linear dynamic range (LDR) and limit of detection (LOD) have been evaluated using this form of calibration. The linear dynamic range is the range in which the response of an instrument or method is proportional to the concentration of the analyte. It represents the span in which the accuracy and proportionality of the analysis is assured. Linearity is given when the slope of a linear regression in a double logarithmic diagram is calculated to one. The linear dynamic range can then be determined according to the International Union of Pure and Applied Chemistry (IUPAC) via the lower and upper limits that cross the confidence intervals [86]. Saturated signals of highly concentrated samples leave the regression and intersect the predicted confidence interval. At very low concentrations the signals leave the regression because the sensitivity of the method is insufficient, which

corresponds to the lower limit. The concentration at the lower limit is also called minimum detectability (MD). The LDR expresses intensity ratios on a logarithmic scale and can therefore be determined in the same way as decibel [dB] (or bel [B]) for sound volume levels by logarithmising the ratio of measured value and reference value [87]. In this case these values are given by the upper and the lower limit as depicted in Equ. 20 and result in the order of magnitude.

Equ. 20

$$\beta = 10\,log\left(\frac{upper\ Limit}{lower\ Limit}\right)[dB] \Rightarrow\ log\left(\frac{upper\ Limit}{lower\ Limit}\right)[B]$$

Limit of detection. Another important criterion of analytical methods is the limit of detection. The LOD corresponds to the lowest concentration of an analyte at which a signal can be distinguished from noise. A qualitative, but not a quantitative statement can be made about the analyte [3]. A large number of different methods for determining the detection limit exist [88]. In this work the method according to Hubaux and Vos has been applied [89]. Here the detection limit is determined using the confidence intervals, as shown in Figure 14. The intersection of the upper confidence interval y_c with the ordinate is projected onto the lower confidence interval which represents the limit of detection x_D on the abscissa. The variable confidence level represents the probability interval which is typically between 90 – 99 % and often defined as 95 % [90–92].

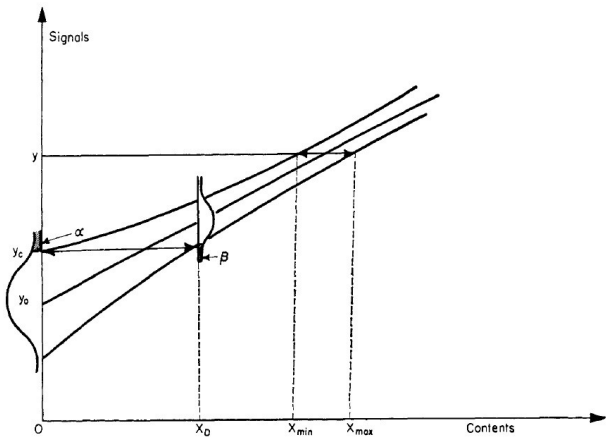

Figure 14: Scheme of the LOD determination via Hubaux and Vos. Reprinted with permission from Anal. Chem. 1970, 42, 8, 849–855. Copyright 1970 American Chemical Society.

2.4 Chemicals and sample preparation

For the experiments in this work a liver total lipid extract, produced by Avanti® Polar Lipids Inc. (181104C, Alabama, USA), has been used as a sample of a highly complex biological matrix. It is a chloroform extract of a bovine liver, which contains a high number of lipids with different molecular masses and polarities and is therefore excellently suitable as a real life sample. The following Table 1 summarises all lipid classes that are contained in the liver total lipid extract, according to the published analysis certificate of Avanti® Polar Lipids Inc. [93]. The stock solution has a concentration of 25 mg/mL in chloroform. In addition to the liver extract used for most of the analyses, a total heart extract (bovine) (Avanti Lipids, 171201C, Alabama, USA) with a stock concentration of 25 mg/mL in chlorofrom has been used.

The basic electrospray solution contains water/ethanol in a ratio of 1:1 (v/v). For conductivity and adduct formation ammonium acetate (purity $>$ 98 %, Merck, Darmstadt, Germany) in water (1 mol/L) has been added to this solution by one percent of the total volume. Ethanol in analytical grade (purity $>$ 99.5 %; Sigma-Aldrich, St. Louis, USA) has been used. The deionized water (conductivity 0.055 µS/cm) has been generated with a Millipore system. Other solvents that have been used in this work are methanol (purity $>$ 99.9 %; Sigma-Aldrich, St. Louis, USA) and acetonitrile (purity $>$ 99.9 %; Sigma-Aldrich, St. Louis, USA).

As described in the introduction, cholesteryl esters (CE) are able to produce the same product ion species as cholesterol. Here the cholesteryl ester CE(17:0) cholest-5-en-3ß-yl heptadecanoate (700186, Avanti Polar Lipids Inc., Alabama, USA) with a concentration of 1 mg/mL in chloroform serves as a representative of CE to determine the influence of cholesteryl esters to the cholestadiene signal.

Two ketones have been used as potential biomarker candidates for studies with paper spray ionisation, including 3-octanone (purity > 98 %; Alfa Aesar Massachusetts, USA) and 2-nonanone (purity > 99 %; Sigma-Aldrich, St. Louis, USA).

Specific dilution steps, final concentrations and further parameters will be described in the respective sections. Chemicals and solvents that have been used in this work necessitate protective equipment in compliance with material safety data sheets as well as trained personnel.

Table 1: Composition of the total liver lipid extract of a bovine according to Avanti lipids [29].

Component	Fraction (wt/wt) [%]
Phosphatidylcholine	42
Phosphatidylethanolamine	22
Phosphatidylinositol	8
LysoPhosphatidylinositol	1
Cholesterol	7
Neutral Lipids / Other	20

3 The nESI-FμTP

This chapter focuses on the first combination of a nano electrospray and the flexible microtube plasma. At the beginning, the experimental realisation of this approach will be described. After the investigation of essential parameters, possible interferences as well as the performance are evaluation on the basis of important analytical properties. The results obtained here are discussed, assessed and compared with current literature values in the corresponding sections. Finally, the performance and characteristics of the combined nESI-FμTP technique are summarised for further developments. Parts of this chapter are published in the publication "Flexible Microtube Plasma for the Consecutive-Ionization of Cholesterol in Nano-Electrospray Mass Spectrometry" [98].

3.1 Coupling the nESI with the FμTP

In this study, the nano electrospray serves as first stage ionisation source for polar compounds of a complex sample as well as nebulizer for the second

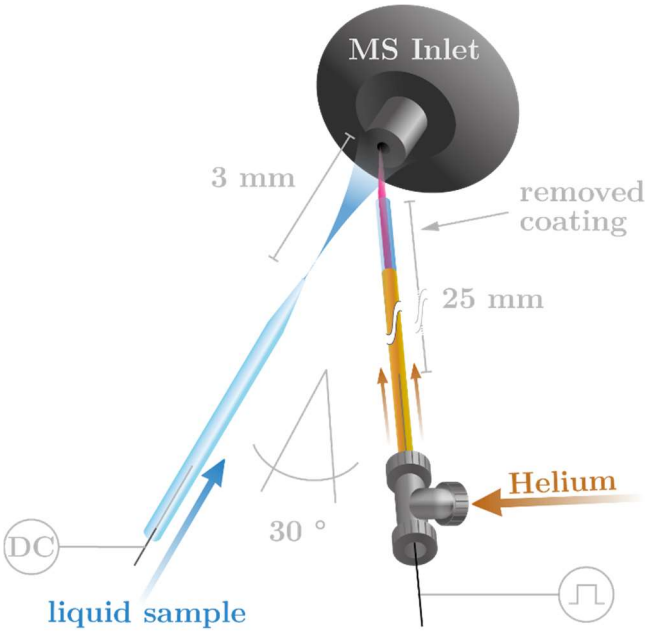

Figure 15: Schematic diagram of the nESI-FµTP setup in front of the mass spectrometer inlet (top) with the nESI emitter on the left and the FµTP on the right. The plasma is positioned into the electrospray particle trajectory. This diagram is based on the publication according to Anal. Chem. 2023, 95, 22, 8423–8432. Copyright 2023 American Chemical Society.

stage, the plasma ionisation. In the following, the first stage is named nESI-mode and the second stage is named nESI-FµTP-mode.

Figure 15 shows a schematic diagram of the combined setup with the relevant geometrical parameter. The nano-electrospray (left) is mounted axially to the MS inlet (top) in a distance of 3 mm. Classical nESI sources typically are mounted in a distance of 1 - 2 mm to the front of the MS. However, in order to generate some space for the additional FµTP, the nESI is moved slightly backwards in this setup. The FµTP is arranged at an angle of 30° to the nESI emitter. The FµTP capillary ends in the ionization area in front of the mass spectrometer with a distance of 1 mm to the inlet. A fused silica capillary with an inner diameter of 50 µm and an outer diameter of 360 µm is sharpened to a tip and was applied as the nESI emitter. The sharpening of the capillary is realized with the help of a rotating sandpaper surface. However, commercially available emitters can also be used, which provide smaller internal tip diameters and a more stable electrospray at lower sample flow rates. The advantage of the in-house made emitters is their robustness. While commercial emitters are quickly blocked due to their inner tip diameter (typically 8 µm - 10 µm), the homemade emitters used here are applicable for several months.

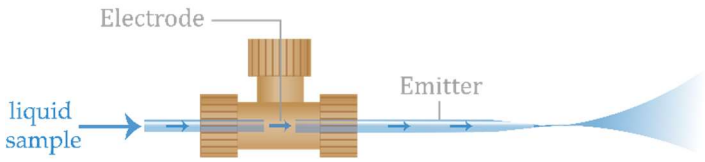

Figure 16: Schematic diagram of the nano electrospray assemble. A Supelco PEEK micro Tee connects the sample introduction capillary, the electrode contact via platinum electrode and the emitter tip.

In this setup, the sample flow rate passing through the nESI emitter is typically set to 0.7 - 1.0 µL/min. The electrospray voltage is supplied by the MS instrument and the high voltage amplitude typically is set to 2.6 kV, but depends on the nESI position, the FµTP position and the applied plasma voltage amplitude. The nESI emitter is mounted in a polyether ether ketone (PEEK) micro T-Piece (PEEK micro Tee, Supelco) as depicted in Figure 16. This connects the liquid sample introduction capillary with the nESI emitter tip and ensures the electrical contact between the sample and the platinum electrode. Fitting sleeves maintain a successful sealing. The sample is supplied via direct infusion using a syringe and the MS integrated syringe pump.

As introduced in chapter 2.2.4, the FµTP is composed of a fused silica capillary with an outer diameter of 360 µm and an inner diameter of 250 µm. The polyimide coating is removed on a distance of 8 mm to the capillary's orifice. The tungsten wire that serves as internal electrode and ends 25 mm away from the end of the capillary. With a volumetric flow rate of 50 mL/min, the plasma operating gas is helium 5.0 (purity 99.999 %). Information on the high-voltage supply can be found in chapter 2.2.4 "The flexible microtube plasma".

Both, nESI emitter and flexible microtube plasma, are embedded in a PEEK micro interface, which has been manufactured by micromachining in the in-house workshop. Figure 17a shows this interface in front of the MS inlet. The nESI passes through the centered and the FµTP through the right channel. Covering these channels with a glass plate (fixed by magnets) both ion sources keep their position and relative height to each other. The entire

structure is mounted on a translation stage with an in-house 3D printed holder. The holder also allows the implementation of a microscope camera, which is used for adjustment purposes as well as for the observation of micro processes. Figure 17b shows the view on the ionisation region taken from the microscope camera.

It should be noted that a large number of preliminary measurements have been carried out with the nESI-FμTP setup. The best signals of this approach were obtained when the nano electrospray and the flexible microtube plasma were arranged axially, with a slight offset of about 1 mm in the direction of the nESI. This offset can also be seen in Figure 17b. Furthermore, this fact will be discussed in one of the following chapters.

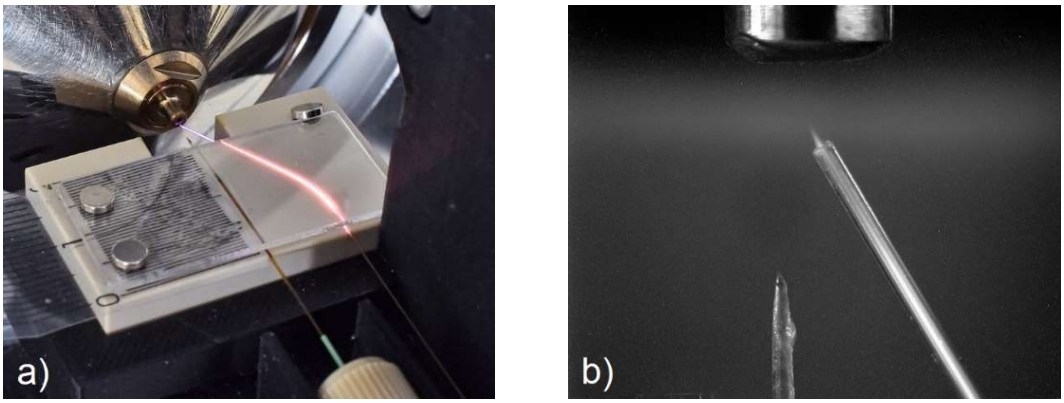

Figure 17: The left photo shows the arrangement of nESI to FμTP and the micro interface in front of the mass spectrometer. Photo b on the right shows the nESI-FμTP in the direct vicinity of the inlet capillary. The photo on the left is reprinted with permission from Anal. Chem. 2023, 95, 22, 8423–8432. Copyright 2023 American Chemical Society.

3.2 Application to liver extract

The nESI-FμTP approach allows two operational modes. In the first mode, the FμTP is deactivated and solely the nESI generates a typical electrospray

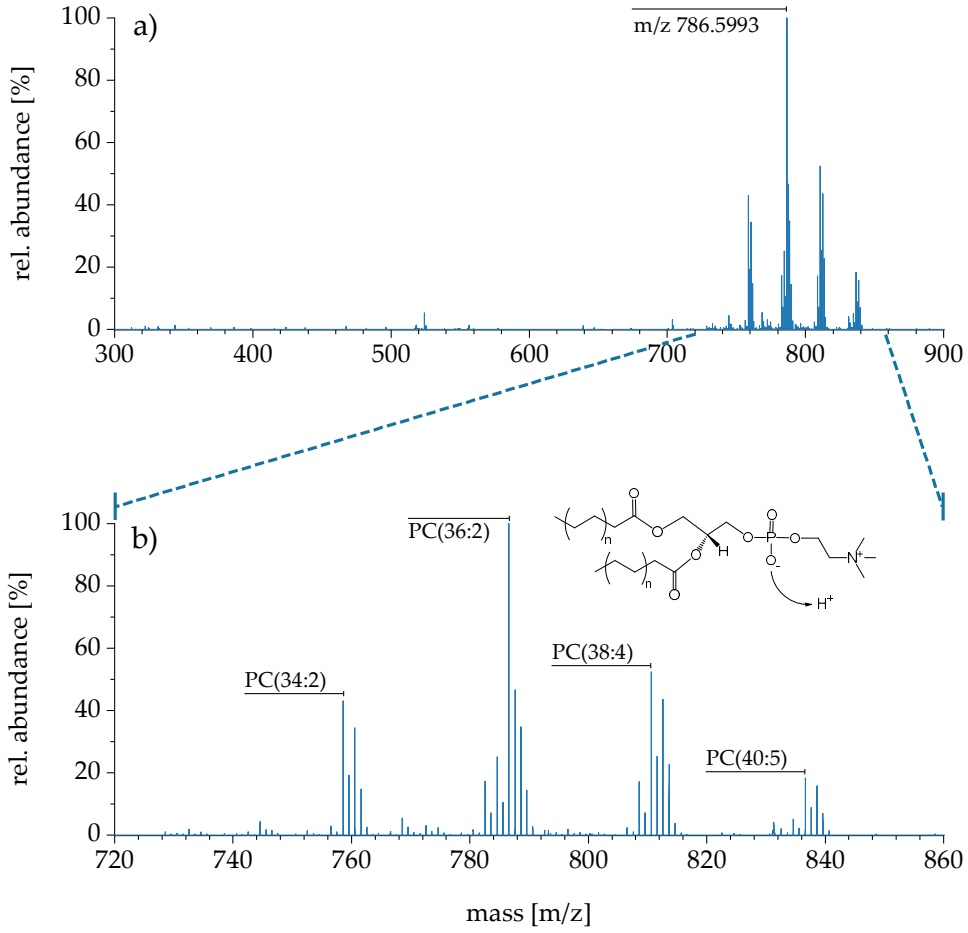

Figure 18: Mass spectrum of the liver total lipid extract, recorded with the LTQ-Orbitrap XL in FT mode (R=100 000). A high number of polar lipids can be observed, especially in the m/z range of 720 – 860.

mass spectrum of polar compounds. Figure 18 a shows the spectrum of the liver total lipid extract measured in the nESI-mode. A high number of different polar lipid species can be detected in the m/z range of 720 – 860. These signals correspond to diverse phosphatidylcholines (PC) and phosphatidylethanol-amines (PE) as published in the analysis certificate of Avanti® Lipids, which is depicted and described in the previous chapter 2.4. The spectrum shown in Figure 18a inlcudes an averaging of 20 scans with a microscan number of one. The voltage supply and the volume flow rate of the nESI source have been set to 2.1 kV and 1 µL/min.

Compared to the total spectrum in Figure 18a, spectrum b shows a detailed view of the m/z range between 720 – 860. The most abundant signal is represented by m/z 786.5993, which corresponds to the PC(36:2). The latter, together with the three other most abundant signals, are identified and assigned in Figure 18b. Based on the particularly good signal-to-noise ratio of the lipid PC(36:2) at m/z 786.5993, this signal is frequently used in ongoing interpretations and represents the electrospray ionisation mechanism. The identification of the observed lipid species in Figure 18 is based on a combination of different publications, data base matching using LIPID MAPS® and ALEX[123] lipid calculator as well as MS^2 fragmentation experiments as described previously in chapter 2.1 [94–96].

Figure 19 exemplarily shows the identification of the most abundant lipid species by MS^2 fragmentation. This spectrum is generated with the LTQ mass analyser by isolating the signal at m/z 786.6 with an isolating width of m/z 2. Using the collision induced dissociation (CID), a normalised collision energy of 10 a.u. has been applied to fragment the PC(36:2). The fragment pattern in Figure 19 shows clearly the loss of a trimethylamine and the loss of a PC headgroup. In addition to this, the loss of the two fatty acids FA(18:0) and FA(18:2) shows that this signal belongs mainly to the PC(18:0/18:2). Besides

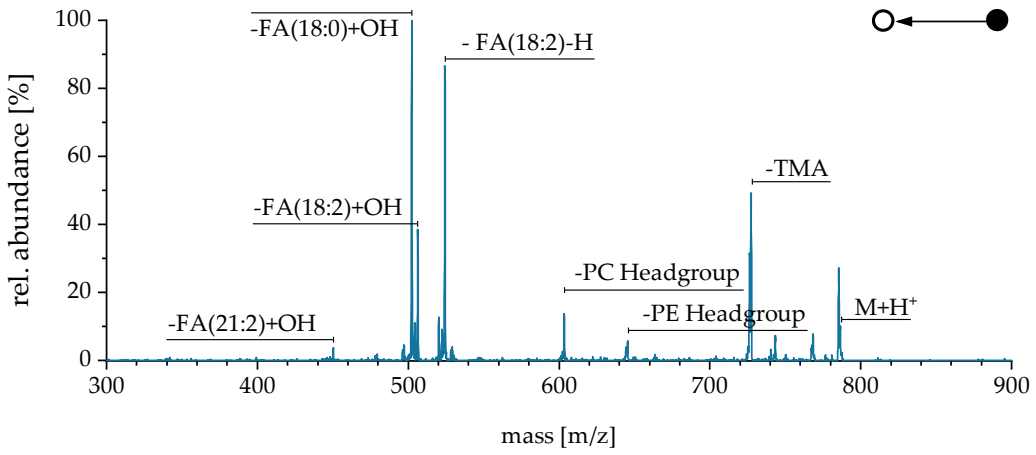

Figure 19: MS^2 fragmentation of the polar lipid signal at m/z 786.6. The fragmentation pattern shows clearly that this signal comprises mainly the PC(36:2), but includes a smaller amount of PE(39:2).

this, the loss of a PE headgroup can be observed, too. This indicates the existence of a PE(39:2), which has the same mass as the PC(36:2). A weak signal also shows the loss of a FA(21:2) and suggests the presence of a PE(21:2/18:0).

On the basis of the signal ratios, the PE(39:2) exist in a significantly smaller amount compared to the PC(36:2). This hypothesis is supported by the analysis certificate according to Avanti Lipids as shown in Table 1 of the chapter 2.4. The liver sample comprises 42 % of PC and 22 % of PE species.

A collection of the most abundant m/z signals, which are found in the nESI-MS analysis of the liver extract in Figure 18b, is depicted in the following Table 2. The latter summarises the relative abundances, the measured and theoretical masses, the mass deviations, the ion types and corresponding lipid species. If the signal comprises two or more lipids, the more abundant lipid is entered to Table 2. MS^2 fragmentation spectra, which lead to the identification of the lipids listed in Table 2, are added to Figures A1 - A6 of the appendix.

Activating the plasma of the nESI-FμTP setup (nESI-FμTP-mode) leads to a significantly changed mass spectrum. Now, the plasma ionisation process dominates as shown in the following Figure 20. The polar lipid pattern

Table 2: Major lipid signals of the liver extract detected by nESI-MS. The relative abundance reflects the signal intensities. The Δmass shows the deviation of the measured m/z to the theoretical mass in ppm. Finally, the columns lipid species and ion type summarises the identified lipids.

m/z	Rel. abundance [%]	Theo. mass [g/mol]	Δmass [ppm]	Lipid species	Ion type
758.5682	42.58	758.5694	-1.58	PC(34:2)	$[M+H]^+$
760.5836	34.49	760.5851	-1.97	PC(34:1)	$[M+H]^+$
786.5993	100.00	786.6007	-1.78	PC(36:2)	$[M+H]^+$
788.6145	34.59	788.6164	-2.41	PC(36:1)	$[M+H]^+$
810.5992	52.76	810.6007	-1.85	PC(38:4)	$[M+H]^+$
812.6146	43.46	812.6164	-2.22	PC(38:3)	$[M+H]^+$
836.6147	19.35	836.6164	-2.03	PC(40:5)	$[M+H]^+$

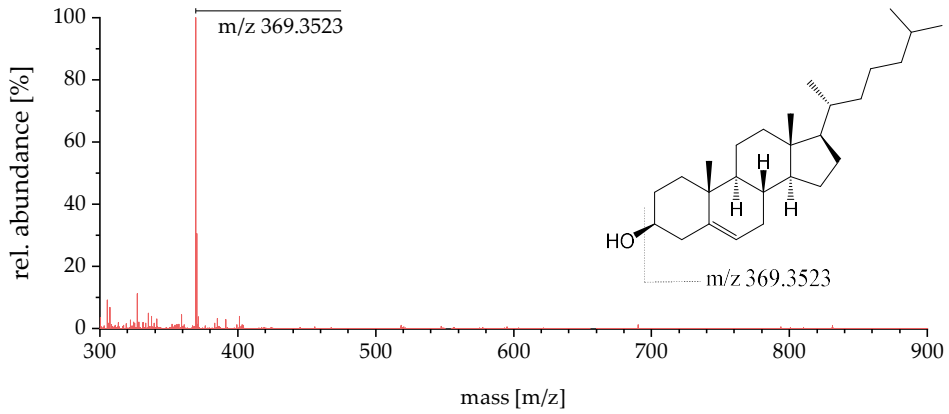

Figure 20: Mass spectrum of the liver extract, analysed with the nESI-FµTP-mode. Due to the dominating plasma ionisation process, the mass spectrum changes completely in contrast to the nESI-mode. Now the most abundant signal is the cholestadiene ion at m/z 369.3523, which represents a product ion of cholesterol. This spectrum shows an average of 20 scans.

disappears and the most intense signal can be observed at m/z 369.3523. This signal corresponds to a protonated cholestadiene, which is a product ion of cholesterol [67,97]. By protonation and subsequent dehydration of cholesterol, a protonated cholestadiene ion $[M+H-H_2O]^+$ is formed and detectable at a theoretical mass of 369.3516 [42,68]. The mass deviation of the experimentally detected mass with m/z 369.3523 to the theoretical mass can be calculated to 1.9 ppm. In this measurement, the voltage of the nESI source was set to 2.5 kV, whereas the voltage of the FµTP was set to 2.0 kV.

Compared to a classical nESI, the nESI emitter of the nESI-FµTP setup is slightly moved backwards as described in chapter 3.1. For this reason, a comparison with a conventional nESI-source as reference seems meaningful. Therefore, a measurement with a classical nESI in optimised position is the next step to compare the results measured with the nESI with those of the nESI-FµTP.

Figure 21 shows the liver extract analysed in three different ways. The spectrum in Figure 21a represents the nESI reference in green. In spectrum b the nESI-FµTP approach is depicted with deactivated plasma (blue; nESI-mode) and with activated plasma (red, nESI-FµTP-mode) in a comparative

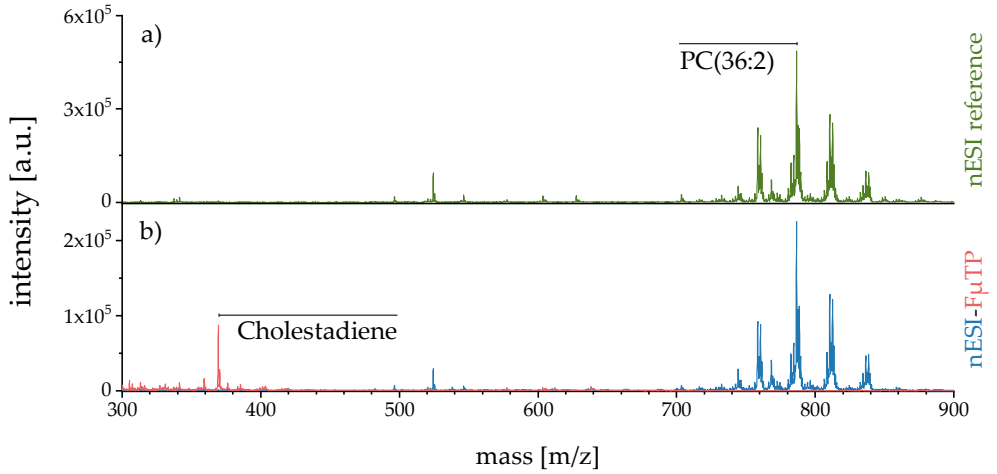

Figure 21: Comparison of a classical nESI source (nESI reference, top spectrum) to the nESI of the nESI-FμTP approach (spectrum below). In spectrum b, the nESI-FμTP spectra with deactivated plasma is shown in blue and with activated plasma in red. The lipid pattern intensity of the nESI reference is approximately twice as the nESI-FμTP. The cholestadiene signal reaches a relative abundance of 39% of the PC(36:2) in the nESI-mode. This diagram is based on the publication according to Anal. Chem. 2023, 95, 22, 8423–8432. Copyright 2023 American Chemical Society.

view. These spectra are acquired with the LTQ mass analyser and represent an average of 100 spectra.

The lipid pattern intensity of the nESI reference (green) is approximately twice as the nESI FμTP (blue). This phenomenon is based primarily on the increased nESI-to-MS distance of the nESI-FμTP mentioned above. Activating the plasma (nESI-FμTP-mode) leads to a strongly increased cholestadiene signal which reaches a relative abundance of 39 % of the PC(36:2) signal. For a representative comparison, the signal-to-noise ratios (SNR) of the cholestadiene and PC(36:2) signals are calculated for each ionisation process of Figure 21. The SNR is given as the quotient of the absolute signal intensity and the background noise. Latter is determined by the median (0.5 quantile) of the related mass spectrum.

As observed previously, the SNR of the PC(36:2) signal decreases by 54 % (factor ~2) from 843.7 to 382.3 by using the nESI source of the nESI-FμTP instead of the nESI reference. In contrast, the cholestadiene SNR increases from 1.3 in the nESI-mode to 386.3 by activating the plasma (nESI-FμTP-

mode). Therefore an increase factor of 304 can be achieved. Relative to the nESI reference (SNR = 6.7), the cholestadiene signal of the nESI-FμTP-mode shows an increase factor of 57. If the plasma is activated in the nESI-FμTP, the SNR of polar lipids decreases strongly to zero. The reason for this behavior remains unclear. Conceivable are neutralisation processes of the already produced ions or deviations in the ion trajectory, caused by the additional electrical field of the plasma source. The following Table 3 summarises the determined absolute intensities, the medians and calculated signal-to-noise ratios for a direct comparison.

Table 3: Comparison of the PC(36:2) and cholestadiene signals, generated by the nESI reference and the nESI-FμTP with inactive and active plasma. The absolute intensities and the medians have been used to calculate the signal-to-noise ratios.

Signal	Abs. intensity [a.u.]	±Error [a.u.]	Median [a.u.]	SNR
nESI ref. – PC(36:2)	$4.8 \cdot 10^5$	$4 \cdot 10^4$	573	843.7
nESI ref. – cholestadiene	$3.9 \cdot 10^3$	$3 \cdot 10^3$	573	6.7
nESI-FμTP deactivated – PC(36:2)	$2.3 \cdot 10^5$	$3 \cdot 10^4$	599	382.3
nESI-FμTP deactivated cholestadiene	757	$1 \cdot 10^3$	599	1.3
nESI-FμTP activated – PC(36:2)	18	92	233	0.1
nESI-FμTP activated – cholestadiene	$9.0 \cdot 10^4$	$2 \cdot 10^4$	233	386.3

3.3 Signal quality and stability

The plasma of the nESI-FμTP approach is electrically switchable and activating the plasma leads to significant change in the mass spectrum. This raises the question of repeatability of the plasma ionisation process. How large are appearing deviations in the intensity with repeated activation of the plasma? To evaluate the relative error of repeatability E_{Rep}, a temporal acquisition of five switching processes is performed. Therefore, the plasma was switched on and off ten times. Each ionisation process remained for ~ 25 s. For the E_{Rep}, the deviation of the switching processes in relation to the average

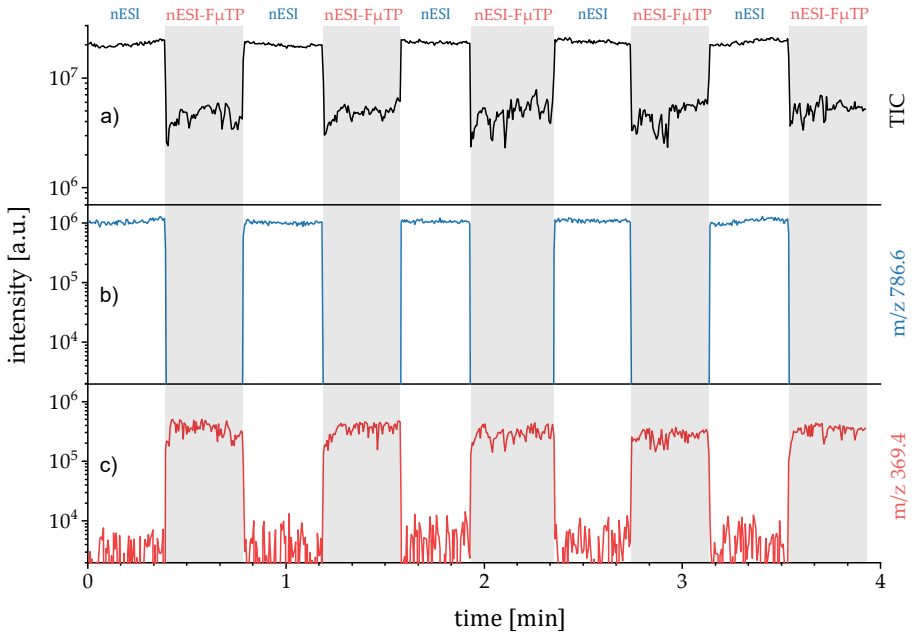

Figure 22: Temporal acquisition of the total ion current (TIC) and the extracted ion currents at m/z 369.4 and m/z 786.6. Ten activation and deactivation processes (each process 5 times) are performed to evaluate the error of repeatability and the relative standard deviation of the switching processes. This diagram is based on the publication according to Anal. Chem. 2023, 95, 22, 8423–8432. Copyright 2023 American Chemical Society.

of all five switching processes is calculated by using 50 scans of each step. The scans comprise a micro scan number of three. The ion currents with a mass tolerance of 200 mmu are extracted from the data acquired in full scan mode with a range of m/z 300 - 900. In Figure 22a the ion chromatogram shows the total ion current (TIC), coloured black. Ion chromatogram b and c shows the extracted ion current (EIC) of the signal m/z 786.6 (PC36:2) in blue and the signal m/z 369.4 (cholestadiene) in red. The areas marked in grey represent the nESI-FμTP source with activated plasma (nESI-FμTP-mode), whereas the unmarked areas represent the nESI-mode of the nESI-FμTP (plasma inactive). A logarithmically-scaled ordinate highlights the differences in the signal intensities of the modes. In addition to Figure 22, Table 4 summarises the results of the E_{Rep} calculation. Similar to Figure 22, results generated with activated plasma (nESI-FμTP-mode) are labeled in grey here.

The E_{Rep} values of the TIC (3.6 % in nESI-mode and 4.6 % in nESI-FμTP-mode) are very close to each other. In contrast to the EICs, the TIC comprises the full spectrum in the range of m/z 300 - 900, including the background noise, which leads to very stable and repeatable TICs. The EIC of m/z 786.6 shows in the nESI-mode a comparable value (3.4 %). This is based on the fact that this signal is the most abundant signal and constitutes a major part of the ion amount in the nESI process. With activated plasma, the m/z 786.6 signal decreases towards the background noise. On the basis of the low intensity and SNR of this signal in the nESI-FμTP-mode the relative deviation rises, which has a large influence on the E_{Rep} value. The latter is also applied for the m/z 369.4 signal in the nESI-mode.

Compared to the very low E_{Rep} of the m/z 786.6 in the nESI-mode (3.4 %), the cholestadiene E_{Rep} in the nESI-FμTP-mode of 13.3 % is four times larger. Disturbances of the resulting electrical field could be the reason for this phenomenon. Every ionisation technique has specific sources of error. Adding a second ionisation source (including its own specific error) leads to a combination of both error sources, making an E_{Rep} value of 13.3% probable.

Another important aspect, which can be observed in Figure 22, is the larger signal fluctuation (within a switching process) of the cholestadiene signal (nESI-FμTP-mode; red) compared to the PC(36:2) signal in nESI-mode (blue). The temporal signal fluctuation can also be described as signal quality and can be expressed by the relative standard deviation (RSD). The RSD

Table 4: Summarised results of the E_{Rep} determination. The error of repeatability is calculated by the average of the signal and the corresponding ±Error, which is given as relative standard deviation.

Operation-mode	Ion current type	Average [a.u.]	±Error [a.u.]	E_{Rep} [%]
nESI-mode	TIC	$2.1 \cdot 10^7$	$7.5 \cdot 10^5$	3.6
nESI-FμTP-mode	TIC	$4.9 \cdot 10^6$	$2.3 \cdot 10^5$	4.6
nESI-mode	EIC (m/z 786.6)	$1.0 \cdot 10^6$	$3.5 \cdot 10^4$	3.4
nESI-FμTP-mode	EIC (m/z 786.6)	85	17	19.7
nESI-mode	EIC (m/z 369.4)	$3.7 \cdot 10^3$	778	21.1
nESI-FμTP-mode	EIC (m/z 369.4)	$3.4 \cdot 10^5$	$4.4 \cdot 10^4$	13.3

determines the deviation of the data points from the average within a measurement. To calculate the RSD of each ionisation process, the same data as in the E_{Rep} calculation have been used. For a RSD comparison with a conventional nESI source, a further measurement with the nESI reference setup has been performed and interpreted. Here, 50 scans with a micro scan number of three were acquired. The ion chromatogram of the nESI reference (EIC of the PC(36:2) signal) is not included here, but can be found in the Figure A7 of the appendix.

Table 5 summarises the resulting RSD values. As previously stated, the rows marked in grey highlight the nESI-FµTP-mode (activated plasma). The unmarked rows, on the other hand, show the nESI-mode (deactivated plasma). Related to the PC(36:2) signal, the nESI-mode of the nESI-FµTP approach shows a marginally better RSD value of 6.0 %, compared to that of the nESI reference 6.4 %. On the basis of the very low abundance of the PC(36:2) signal in the nESI-FµTP-mode, the relative error increases strongly and the RSD rises up to 221 %. Similar results are obtained with the cholestadiene signal in the nESI-mode and the nESI-reference. The very low abundance of the cholestadiene signal in the nESI-reference and nESI-mode of the nESI-FµTP leads to high RSD values of 60.2 % and 82.9 %, which is not acceptable for analytical measurements. Only with activated plasma the nESI-FµTP approach reaches a relative error of 19.2 %. On the one hand a RSD of 19.2 % is significantly higher than typical nESI RSDs. On the other

Table 5: Determined RSD values of the nESI reference and the nESI-FµTP with activated and deactivated plasma for the EIC of the PC(36:2) at m/z 786.6 and cholestadiene at m/z 369.4.

Operation-mode	Extracted ion current (EIC)	Average [a.u.]	±Error [a.u.]	RSD [%]
nESI-reference	m/z 786.6	$2.1 \cdot 10^6$	$1.3 \cdot 10^5$	6.4
nESI-mode	m/z 786.6	$1.0 \cdot 10^6$	$6.3 \cdot 10^4$	6.0
nESI-FµTP-mode	m/z 786.6	85	190	221.1
nESI-reference	m/z 369.4	$1.4 \cdot 10^4$	$8.7 \cdot 10^3$	60.2
nESI-mode	m/z 369.4	$3.7 \cdot 10^3$	$3.1 \cdot 10^3$	82.9
nESI-FµTP-mode	m/z 369.4	$3.3 \cdot 10^5$	$6.3 \cdot 10^4$	19.2

hand, activating the plasma improves the cholestadiene signal quality of a typical nESI source 3 – 4 times.

The parameter RSD or signal quality only describes temporary signal fluctuations. Another source of error can be a signal variation over a long period of time. To evaluate possible long-term signal drifting, a long-term measurement of the nESI-FμTP was performed and interpreted by extracting the ion current of cholestadiene at m/z 369.4 over a duration of 30 min. The long-term measurement was acquired with the LTQ mass analyser. The ion source parameters are the same as described in the previous experiments. To reduce the data size of the acquisition here, a micro scan number of 10 has been selected.

The long-term observation of the extracted cholestadiene ion current is depicted below. The ion chromatogram in Figure 23a shows the conventional line plot of the extracted ion current (m/z 369.4) as a function of time. The calculated average is added to the line plot. A slightly different representation of the same data is given in the scatter plot of chromatogram b. Omitting the

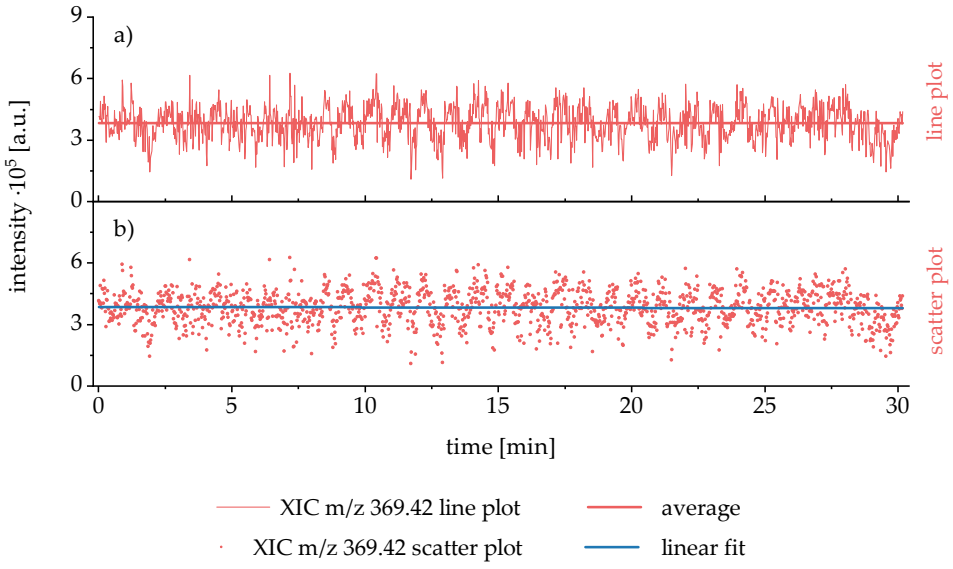

Figure 23: Long-term measurement of the nESI-FμTP generated cholestadiene signal. The top chromatogram shows the acquired data in a typical line plot. In contrast to this, chromatogram b depicts the same data set in a scatter plot, which facilitates a better visualisation and interpretation of a large amount of independent variables.

connection line reduces the graphical representation creating a focus on the individual data points. The result is a cloud of points without a supposed progression, which enhances the visualisation and facilitates the interpretation of a large amount of independent variables. Instead of an average as added in chromatogram a, a linear regression is inserted to chromatogram b. To exclude a signal drift, the data of a long-term measurement should ideally show a slope of zero. Furthermore, the average over all values should be equal to the intersection of the linear regression with the ordinate. Both are given in the case of the nESI-FµTP approach.

The experimentally determined average of $3.83 \cdot 10^5$, shown in the ion chromatogram b of Figure 23, is very close to the interception of the regression line in chromatrogram b with $3.86 \cdot 10^5$. The slope of the linear regression is calculated to - 239.2 min^{-1}, which corresponds to a signal drift of 0.061 %/min and is therefore negligibly small.

A residue analysis gives information about the distribution of acquired variables. In the case of a linear regression, a Gaussian distribution should be achieved. Therefore, a residual analysis has been carried out and clearly indicates the normal distribution of the measured values as shown in Figure

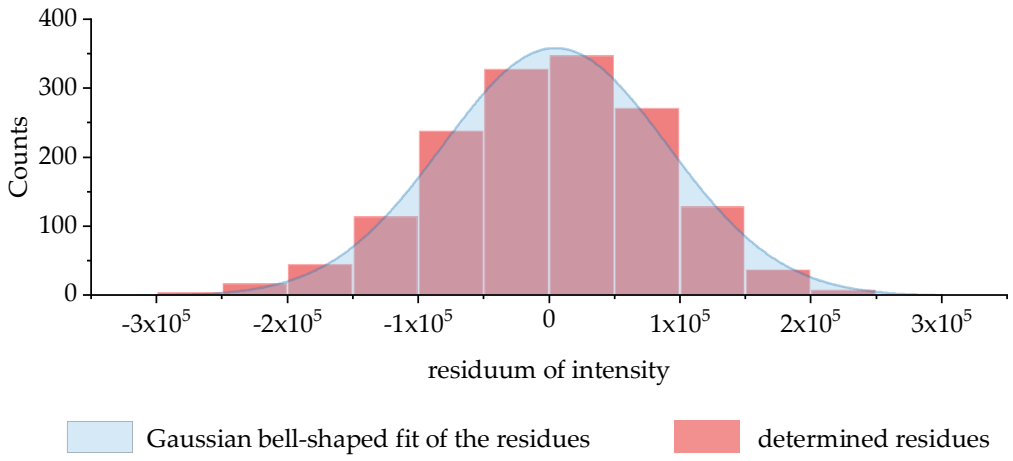

Figure 24: Residual analysis of the measured values, generated by the long-term observation (red). The overlaid Gaussian fit (blue) shows clearly normal distributed values of the long-term measurement. This diagram is based on the publication according to Anal. Chem. 2023, 95, 22, 8423–8432. Copyright 2023 American Chemical Society.

24. Here, a Gaussian distribution can be observed in compliance to the calculated residues. The area beneath the Gaussian fit is filled to highlight the bell-shaped normal distribution. Overall, it can be stated that the results obtained here indicate a stable ionisation process of the nESI-FμTP setup without any evidence of a significant signal drift during a period of 30 min.

3.4 Cholesteryl ester interferences

Free cholesterol (FC) and cholesteryl esters (CE) are directly related and participate at the cholesterol reverse transport as described in chapter 2.1. Due to the rough conditions inside a mass spectrometer, CE undergoes fragmentation processes inside the mass spectrometer device according to Figure 25. This insource fragmentation can be forced or attenuated by changing the MS parameter. A low MS capillary temperature (or MS inlet temp.) as well as a low tube lens and capillary voltages are able to reduce the insource fragmentation of cholesteryl esters. In this case, the signal ratio between the intact molecule ion und the fragment ion shifts to the first one. A small, device specific amount of the CE fragment ion remains, but the signal can be minimised to very low intensities.

The major problem of CE fragmentation is the resulting product ion. As shown in Figure 25, both cholesteryl ester fragmentation and cholesterol share the resulting product ion. Consequently, the presence of cholesteryl esters can interfere with the determination of free cholesterol. Compared to “soft” electrospray ionisation sources, plasma based ionisation techniques are classified as “less soft” (s. chapter 2.2.1.). Therefore, the possibility exist that

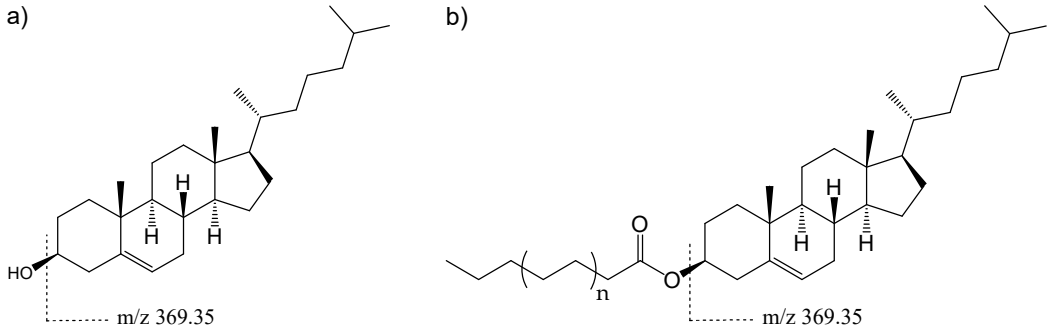

Figure 25: Ionisation processes of cholesterol and cholesterol esters. The dehydration process of cholesterol shown on the left leads to a product ion with an exact mass of 369.35. The same species is formed by the cholesteryl ester fragmentation on the right. This process could lead to signal interferences of the determination of free cholesterol.

plasma-based techniques, such as a FµTP, may increase the fragmentation rate of CE and generate interferences to the free cholesterol signal.

To identify potential cholesteryl ester interferences, a cholesteryl ester standard has been analysed with the nESI-FµTP-MS. The CE(17:0) (cholest-5-en-3-yl heptadecanoate, Avanti® Polar Lipids) is purchased with a concentration of 1 mg/mL. The stock solution has been 100-fold diluted with ethanol. Here, 10 µL of the CE(17:0) stock solution have been mixed with 980 µL ethanol. Finally, 10 µL of an ammonium acetate solution (1 mol/L) has been added to the solution. This results in a CE concentration of 0.01 mg/mL. The sample has been analysed with the nESI-FµTP in the nESI-mode (inactive plasma) and the nESI-FµTP-mode (active plasma).

The acquisition of the spectra are performed with the LTQ mass analyser. To attenuate the insource fragmentation of CE(17:0), several MS parameter are decreased. In this measurement, the value of the capillary temperature is reduced to 200 °C. The tube lens voltage has been set to 60 V and the capillary voltage to 10 V. Each spectrum represents an average of 200 spectra acquired in full scan mode with a m/z range of 300 - 800.

Figure 26 illustrates the relevant sections of the recorded spectra with a tolerance of eight mass units, the detected m/z values and molecular structures. On the right, the intact CE(17:0) can be observed as an

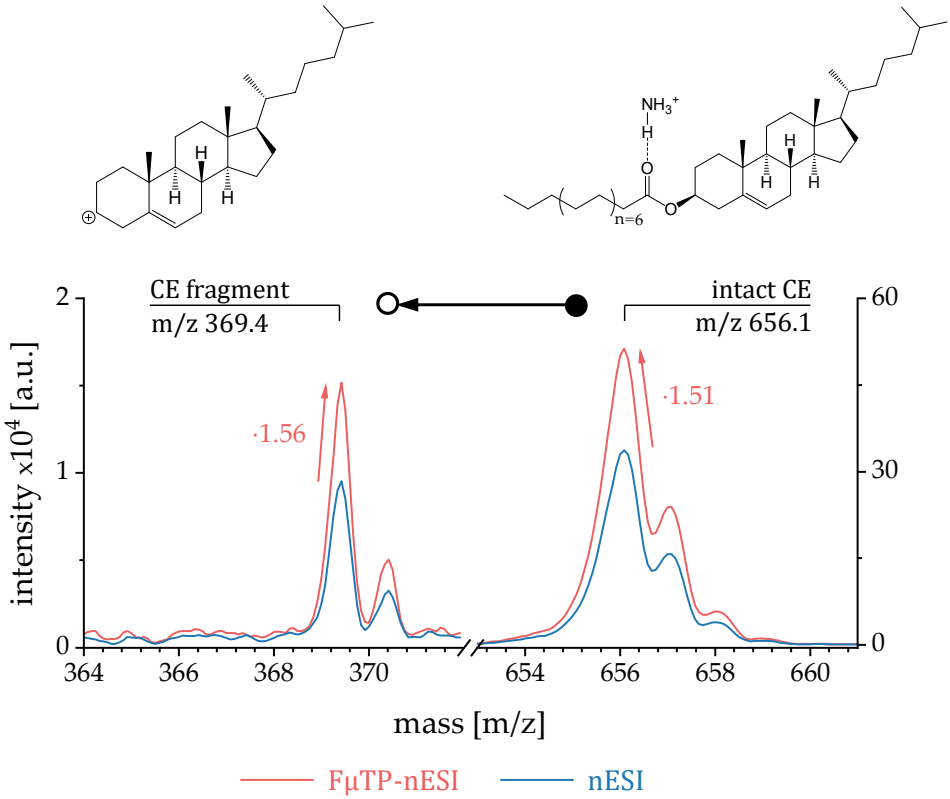

Figure 26: Measurement of the cholesteryl ester fragmentation (CE(17:0)), generated in nESI-mode (blue) and in nESI-FµTP-mode (red) to evaluate potential interferences to the signal of free cholesterol. The intact CE ion with ammonium adduct (right) fragments to the cholestadiene ion on the left. Both ionisation modes show similar fragmentation ratios. This diagram is based on the publication according to Anal. Chem. 2023, 95, 22, 8423–8432. Copyright 2023 American Chemical Society.

ammonium adduct $[M+NH_4]^+$ at m/z of 656.1. The fragmentation process leads to the cholestadiene ion at m/z 369.4 on the left. In order to evaluate the additional amount of cholestadiene ions generated by the plasma, the fragmentation process has first been determined using only the nESI-mode (blue line). The ratio of the intact ion to the fragment ion serves as reference (base value) for the subsequent measurement. Finally, the same measurement has been carried out in the nESI-FµTP-mode (activated plasma; red line) to calculate the additional cholestadiene amount generated by the plasma.

In contrast to the liver sample, in which the polar lipids disappear when the plasma is activated, the intact CE remains here. In addition, both the

intact molecule ion and the fragment ion increase in intensity. This could lead to the hypothesis that the disappearance of lipids in the nESI-FµTP analysis (related to the liver sample) might be caused by matrix effects. Inside the ionisation area in front of the MS inlet, ions are in competition. Ions produced by the plasma might be advantaged due to the smaller distance and a stronger electric field. It should be emphasised that this is only an assumption and has not yet been proven by any measurements.

Both signals, the intact CE ion and the fragment ion, are amplified by activating the plasma. The absolute intensity of the intact CE(17:0) increases by the factor of 1.51, while that of the fragment ion increases by the factor of 1.56. Comparing the signal-to-noise ratios of the detected ions in both modes (active and inactive plasma) shows that the background noise also increases with activated plasma. The SNR increase factors of 1.15 for the intact ion and 1.19 for the fragment ion show that the signal amplification is less pronounced than the signal intensities would suggest. The relative increase of the signal intensities are 15.4 % for the intact CE ion and 18.8 % for the fragment ion. Therefore, an increase is given, but is smaller than expected at the beginning. The reason for this general signal amplification lies probably in the slightly shifted geometry of the nESI emitter. The nESI-FµTP geometry is optimised for the nESI-FµTP application with activated plasma. Therefore, compared to a classical nESI emitter tip, the emitter of the nESI-FµTP is slightly shifted to the left (and backwards) as described in chapter 3.1. Activating the plasma leads to a change of the Taylor cone orientation at the emitter tip towards the plasma, what could be responsible for the increased signal intensity. This change in orientation of the Taylor cone can be observed with the help of the microscope camera. Figure 27 illustrates captured photographs of the microscope camera mounted above the nESI-FµTP setup. The photo in Figure 27a with inactive plasma shows a straight orientation of the Taylor cone at the emitter tip. In contrast to this, by activating the plasma, the Taylor cone sprays to the right in the direction of the FµTP.

The relative signal increase of the intact CE ion of 15.4 % and that of the fragment ion of 18.8 % shows that the fragment ion only rises slightly by

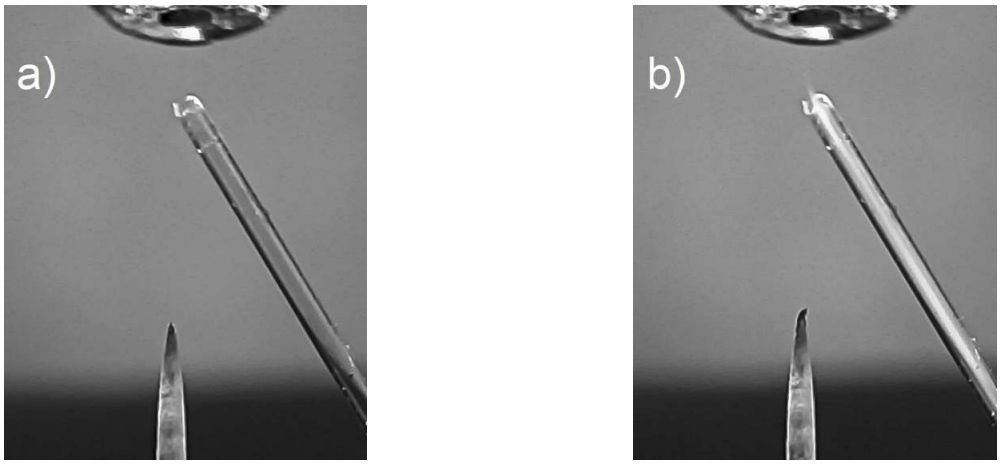

Figure 27: Photographic images of the nESI-FμTP assembly, taken with a microscope camera. In the left photo the plasma is inactive, the orientation of the electrospray is straight foreward. In photo b on the right, the plasma is active and the Taylor cone of the electrospray changes the orientation towards the FμTP.

3.4 % (factor 1.034). To better assess this value, the effect of the tube lens to the fragmentation process has also been measured. For this purpose, a tube lens voltage variation has been performed by using only the nESI-mode (plasma inactive). The resulting spectra of the fragment ion are depicted in an overlaid spectra of Figure 28. The following values are calculated by using an average of 50 scans, with a micro scan number of one and a mass tolerance of 200 mmu. In this measurement, an initial tube lens voltage of 40 V (corresponds to soft MS conditions) has been selected and successively elevated to 220 V, which corresponds to hard MS conditions.

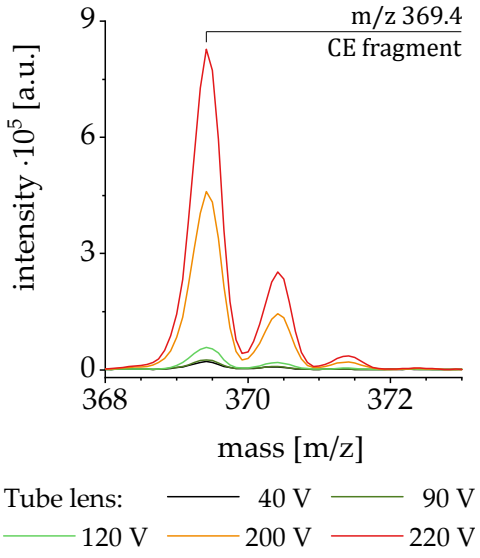

Figure 28: Signals of the CE fragment ion at m/z 369.4, generated in nESI-mode to evaluate the effect of the tube lens voltage to the CE fragmentation process.

The step from 40 V (black) to 90 V (dark green) results in an

increase factor of 1.18, which exceeds the nESI-FµTP approach with a signal increase of 1.034 easily. The increase to 120 V (green) results in a factor of 2.7 and ends with a 58-fold signal amplification at 220 V. This clearly highlights the very strong effect of the tube lens voltage to the fragmentation process of the CE(17:0) and also shows the very small effect of the plasma on the fragmentation process. It should be noted that already produced interferences of cholesteryl esters during electrospray- or in-source fragmentation processes are not removable, but this measurement shows that the additional fragmentation, which is generated by the activated FµTP of < 4 %, can be considered as negligibly small, compared to insource parameters like the tube lens voltage. Based on the knowledge gained here, it can be stated that the major part of the m/z 369.4 signal is generated almost exclusively by the presence of free cholesterol (regarding on the liver sample). For this reason, the cholestadiene signal will also be titled as cholesterol signal in the further development of this work. Parts of the data determined here can also be found in the corresponding publication “The Flexible Microtube Plasma for the Consecutive-Ionisation of Cholesterol in nano-Electrospray Mass Spectrometry” [98].

3.5 Influence of voltage and temperature

The voltage of an nESI is an important operating parameter and has a direct influence on the resulting electric field generated at the end of the emitter tip. If the applied voltage is too low, no Taylor cone will be formed, which does not lead to an ion production. If the applied voltage is too high, the nESI process becomes unstable and the nESI does not operate efficiently. The FµTP behaves in a similar way. A certain voltage is required to ignite

the plasma. However, overvoltage can lead to a reduced ionisation efficiency. Furthermore, electric breakdowns to the inlet are possible in the latter, which could destroy important electrical components of the MS device.

Electric fields are dependent on many factors like distances and voltage amplitudes. Combining two ion sources leads to mutual influences of their electric fields. Therefore, the distance of an ion source to the MS inlet, the distance between both ion sources and as well as the voltages are essential parameters. Matching the two ion sources to each other is therefore of great importance for a successful operation.

In this section, the operating voltage of the plasma will be optimised for a successful cooperation of the FμTP with the nESI. For this purpose, other parameters are kept constant. The geometry of the nESI-FμTP approach and the composition of the sample also remain constant. The plasma serves as a consecutive ion source, therefore the voltage of the nESI is predefined at 2.6 kV. The data are acquired in full scan mode and interpreted with the extracted ion currents (EIC ±200 mmu mass tolerance). Each data point represents a spectrum averaged over 20 scans, recorded with a micro scan number of one. The results are illustrated in Figure 29, which presents the determined SNR values as a function of the applied voltage. The SNR data generated by the EIC of the polar lipid PC(36:2) are coloured blue and stands for the nESI process. The SNR of the less polar cholesterol are coloured red and stands for the consecutive plasma ionisation process. The data points are connected by a modified Bezier curve, which does not represent a fit of the data, but rather highlights the progression of the signals. Below the diagram of Figure 29 six photos captured at different plasma voltages show the growth process of the plasma inside the fused silica capillary.

It can be observed that plasma voltages below 1.8 kV have no effect on the lipid signals generated by the nESI or the cholesterol signal. Here, the deviation of the data points remain within the error range. The plasma does not reach the anterior part of the capillary, which can be seen in photo a. At a voltage of 1.8 kV, the plasma reaches the front region of the capillary, which is depicted in photo b. Here, the electrospray signal drops slightly. At 1.85

kV the plasma reaches the end of the capillary (photo c) and further increase of the voltage up to 1.9 kV (photo d) leads to a strong reduction of the nESI signal. Here, the cholesterol signal appears weak. A further increase of the plasma voltage leads to a strong amplification of the cholesterol signal. It reaches a maximum at 2.0 kV, where the plasma already extends far out of the capillary and moves towards the MS inlet (photo e). In contrast to the raised cholesterol signal, the nESI signal goes close to zero. Further increase

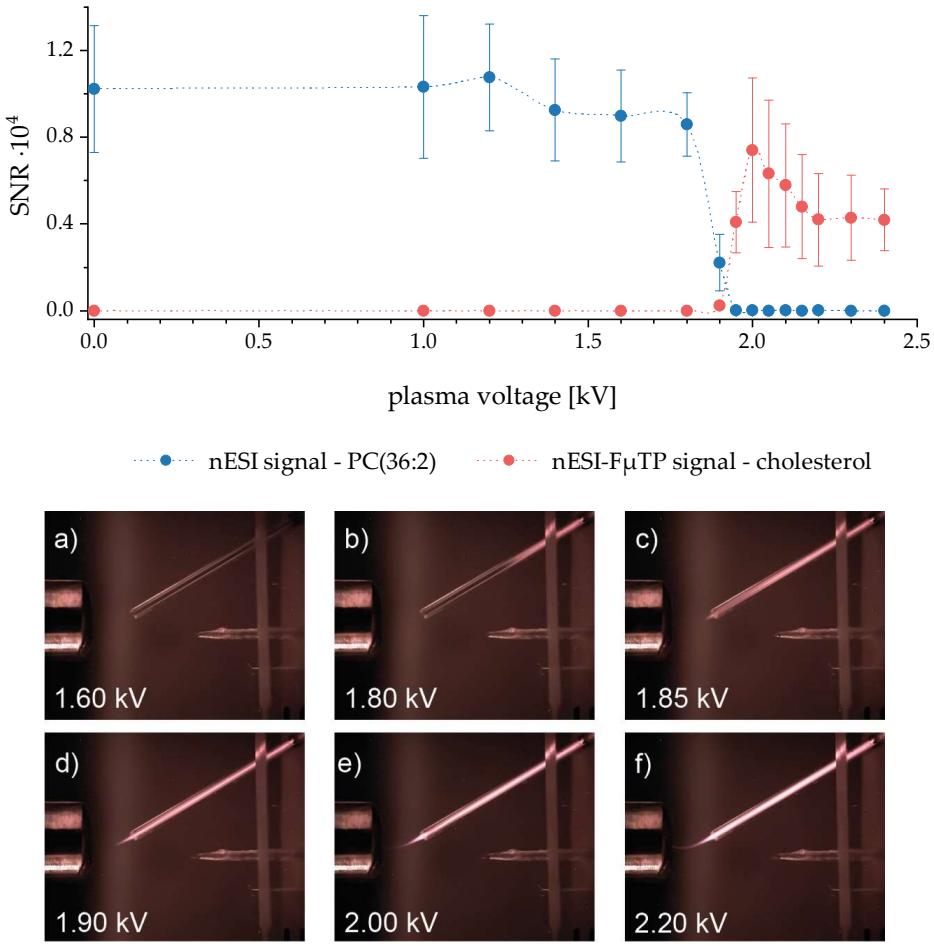

Figure 29: The top diagram shows the SNR of PC(36:2) and cholesterol as a function of the plasma voltage amplitude. With an increasing voltage amplitude the intensity of the nESI process decreases, whereas the cholesterol SNR rises. A maximum cholesterol SNR can be observed at 2.0 kV. The Photos a - f visualise the plasma growth process and correspond to different plasma states of the diagram above. Photos a – f are reprinted with permission from Anal. Chem. 2023, 95, 22, 8423–8432. Copyright 2023 American Chemical Society.

of the voltage amplitude leads to a reduction of the cholesterol SNR. From a voltage of 2.2 kV and higher, the plasma is very long and touches the MS inlet surface (photo f). From here, the SNR of cholesterol no longer changes and remains constant.

Primarily, this measurement shows that there exists an optimal plasma voltage for a defined arrangement of both ion sources at which the cholesterol signal can be maximised. Secondly, it can be shown that the optimal plasma voltage in this case is at 2.0 kV. For this reason, a voltage between 2.0 and 2.1 kV is usually selected in the following experiments.

As mentioned previously, the MS inlet temperature plays an important role and has a large influence on MS analysis. The same applies to the nESI-FµTP approach for cholesterol determination here. Typical MS inlet temperatures ranging from 200 to 300 °C. Therefore, in order to evaluate a suitable temperature for cholesterol determination, a study has been performed in which all nESI-FµTP parameters have been kept constant, but the MS inlet capillary temperature has been varied between 160 °C and 400 °C. The same parameters were used as in the previous experiment. The voltage amplitudes of the nESI and the FµTP have been set to 2.6 kV and 2.0 kV. Data were acquired in full scan mode. The results has been calculated from spectra (generated by the LTQ analyser) with an average of 200 scans.

At the beginning of this investigation, an observation was made, which will be interpreted prior to the interpretation of the temperature variation. At very high temperatures, further signals have been observed in addition to the cholesterol signal. Figure 30 shows two mass spectra acquired at different MS inlet temperatures. The first spectrum is recorded at 240 °C and shows the cholesterol signal at m/z 369.4 with an excellent intensity. Signals beyond m/z 450 cannot be detected. By increasing the temperature above typical inlet capillary temperatures different, previously unobserved signals appear. At 340 °C, a series of additional peaks can be found, which is shown in spectrum b of Figure 30. These are located in the mass range m/z 500 - 700 and m/z 820 - 900.

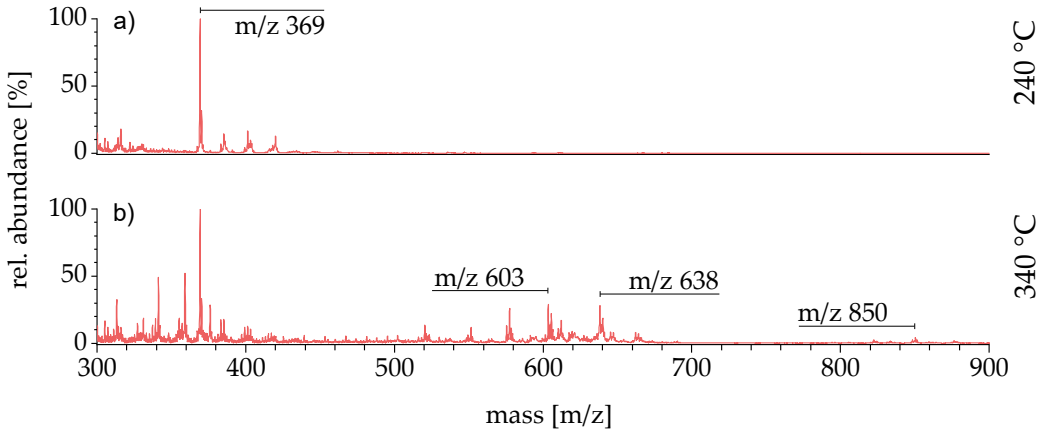

Figure 30: Two spectra of the liver sample acquired at different MS inlet capillary temperatures. The top spectrum was recorded at 240 °C and shows an excellent cholesterol signal. By increasing the inlet capillary temperature to 340 °C, the spectrum below can be observed. The cholesterol signal at m/z 369.4 decreases, but a range of additional signals appear. This shows the importance and influence of the MS inlet temperature on the acquired spectra.

On the one hand, these could be signals of further non- or less polar lipids, which are ionised exclusively by the plasma. On the other hand, they could be caused by fragmentation processes. The identification of these additionally detected signals is not part of this experiment and will not be explained in detail here, but shows the importance and influence of temperature on acquired spectra. The identification of these signals will be covered by one of the following chapters. As these signals appear with an increase in temperature, three selected signals are included in the interpretation of this experiment. These selected signals represent the most abundant signals of each signal pattern and are located at m/z 603.5, m/z 638.3 and m/z 850.5.

The aim of this experiment was to verify the optimal temperature for the analysis of free cholesterol. For this purpose, the SNR of cholesterol was determined as a function of the MS inlet temperature. In addition to cholesterol, the SNR of the three selected signals that only occur at higher temperatures were also determined. The diagram in Figure 31a shows the influence of the inlet temperature on the SNR. At lower temperatures ($<$ 200°C) no cholesterol can be detected. Beyond an inlet temperature of 220 °C, a cholesterol signal is detectable, but it contains a large relative error of 65

%. The highest SNR is achieved at a temperature of 240 °C. However, the relative error here is also large at 66 %. Further increase of the temperature to 280 °C leads to a slight reduction of the intensities, but also reduces the relative error by 13 % to 53 %. The signal here is significantly more stable compared to the signal at 240 °C. At temperatures of 300 °C and more, the cholesterol signal decreases and disappears in the background noise. The signals at m/z 603.5, m/z 638.3, and m/z 850.5 become visible only at a temperature of 320 °C and more. It should be noted that the SNR of cholesterol ($\cdot 10^4$) is significantly larger than the SNR of the other signals ($\cdot 10^2$). While the signal at m/z 638.3 reaches its optimum at 340 °C, the m/z 850.5 reaches its maximum at 380 °C. The signal at m/z 603.5 does not reach an optimum below 400 °C. Accordingly, it is not possible to detect both cholesterol and the other non polar lipids simultaneously with the nESI-FμTP approach. The differences in optimal inlet temperatures and signal intensities

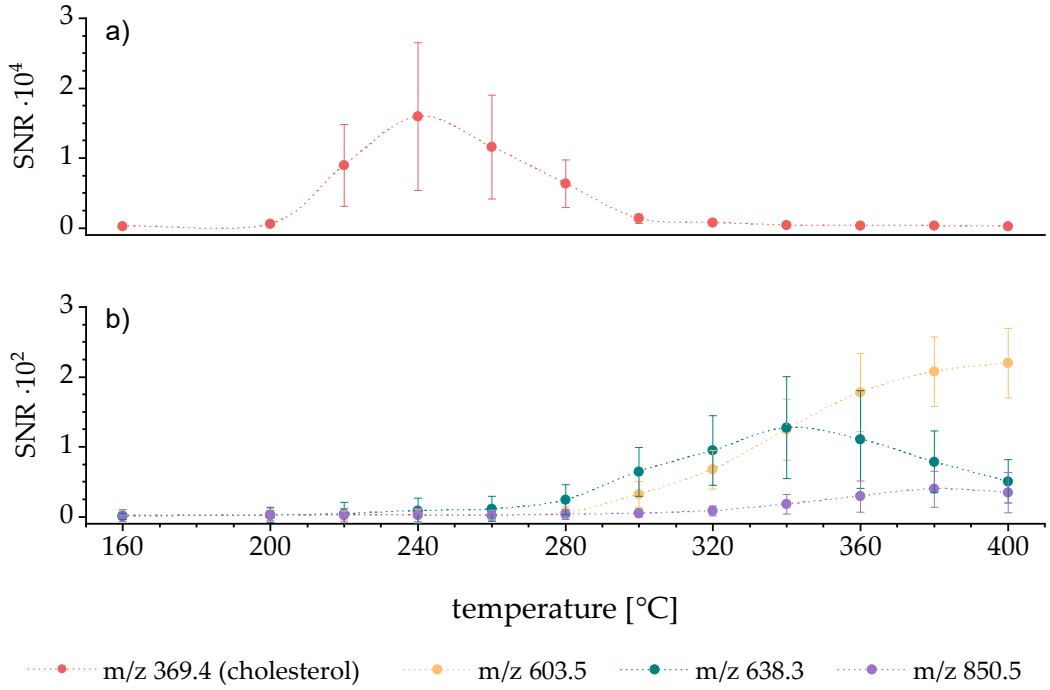

Figure 31: SNR of different signals as a function of the MS inlet capillary temperature generated with nESI-FμTP approach. The diagram on top shows the progression of the cholesterol signal with an increasing temperature. The diagram below shows the three most abundant additional lipids observed at very high temperatures. It should be noted that the SNR of cholesterol at ·10⁴ is significantly larger than that of the other signals at ·10².

are too large to cover all signals in one measurement. In order to measure the entire spectrum of non polar lipids, at least two measurements at different temperatures are necessary. This is an extremely strong disadvantage of the nESI-FμTP source and makes it only useful for one of these two applications. In the publication "Flexible Microtube Plasma as Consecutive Ionisation Source for Cholesterol in nano-Electrospray Mass Spectrometry", published prior to this work, the determination of the optimum temperature was carried out solely by the signal intensities. This showed that the optimal temperature for cholesterol analysis is 280 °C. In the progress of this work, the same data have been revised and the SNR has been used for evaluation. These calculations clearly show that the temperature at 240 °C produces the highest SNR, but also has a percentage error of 66.4 %. In comparison, the SNR of cholesterol at 280 °C has a 13 % lower error.

Consequently, this should not result in a significant difference for the following measurements, since both the determination of the linear dynamic range and the determination of the accuracy strongly depend on the errors of the measured values. Therefore, the following measurements were not acquired at 240 °C MS inlet temperature as would be expected, but at 280 °C.

3.6 Linear dynamic range

A performance indicator of analytical techniques is the linear dynamic range (LDR). As described in chapter 2.3 "Statistical methods", the LDR is the range of concentrations where the signals are directly proportional to the concentration of the analyte in the sample. To determine the LDR, a calibration series has been measured according to the method of standard addition. The latter represents a variant of the internal standard and is suitable for the analysis of complex samples, where matrix effects can occur. In comparison to the internal standard, where a similar substance is added,

in the method of the standard addition the same substance is added to the samples of a calibration series. To determine the LDR, the calibration series should cover a large concentration range, otherwise the limits may not be covered. Therefore, preliminary experiments were necessary to evaluate the potential concentration range. In order to determine the final LDR, a calibration series was generated in which the liver extract had to be diluted by a factor of 1:1000 (v/v). In this calibration series the added cholesterol amounts ranged from 2.19 mg/L to 217.51 mg/L. Exact dilution steps, added cholesterol amounts and resulting concentrations of the first calibration series can be found in Table 6.

In contrast to the previous measurements for optimisation, where different parameters of the setup were changed, here instead of the SNR for evaluation, the signal intensity was used. A mass tolerance of 200 mmu was applied for the EICs. The LTQ analyser operated in full scan mode with a m/z range of 365 - 375 and the micro scan number of one. Each data point consisted of 250 scans and the error bars representing the standard deviation of the average cholesterol intensity. As described in the previous experiments, the voltage amplitudes of the nESI and the FμTP were set to 2.6 kV and 2.0 kV.

Table 6: Composition of calibration series I. Exact dilution steps, solvent quantities and added amounts of cholesterol are summarised in this table. Each sample contains 1 μL of the liver extract stock solution to yield a dilution of 1:1000 (v/v).

Sample No.	Ethanol [μL]	Stock solution (Cholesterol) [μL]	Electrospray solution [μL]	Added cholesterol [mg/L]
1	197	2	800	2.19
2*	195	4	800	4.37
3*	189	10	800	10.93
4*	179	20	800	21.86
5*	149	50	800	54.65
6*	49	150	800	163.95
7	0	199	800	217.51

* Samples used to calculate the regression.

Furthermore, the MS inlet capillary temperature was at 280 °C and the tube lens voltage was set to 65 V.

To determine the LDR the measured intensities (with errors) are plotted in a diagram with double logarithmic scale. As described in chapter 2.3, the slope b of a linear fit represents the exponent of an exponential fit in normal scale and stands for the linearity of the present data. For high linearity, an exponent or slope b of one should be achieved. The more this value deviates from one, the greater the deviation of the linearity.

Figure 32 shows the acquired data of the calibration series as well as the calculated regression line (red) with the 95 % confidence interval hyperbolas in double logarithmic scale. Here, five of the seven measured concentrations could be used to determine the regression. The lowest and highest concentrations show a strong negative effect on the linearity, are therefore not part of the regression and are used to determine the lower and upper limit of the nESI-FμTP approach. A dotted line (modified Bezier curve) to highlight the progress connects the acquired data.

The coefficient of determination R^2 with 0.9945 indicates a high correlation between the acquired data in the range of 4.37 – 163.95 mg/L and the linear regression. The calculated slope of 0.9901 ± 0.0367 is very close to the expected value of one. Hence, the nESI-FμTP shows a very good linearity in this range. The intersection of the connecting line and the 95 % confidence intervals mark the upper and lower limits. The lower limit can be determined to 3.71 mg/L. The lower limit, together with the upper limit of 189.37 mg/L, shows according to Equ. 20 a resulting linear dynamic range of 17.1 dB. This corresponds to an LDR of 1.7 orders of magnitude. These results are also accessible in the corresponding publication [98].

The lower limit of 3.71 mg/L is also known as minimum detectability (MD) and represents a type of limit of detection (LOD) [99]. The latter is also a widely used performance indicator and enables the comparability of different methods. However, due to the fact that the method is based on standard addition, the amount of cholesterol already contained in the sample must be

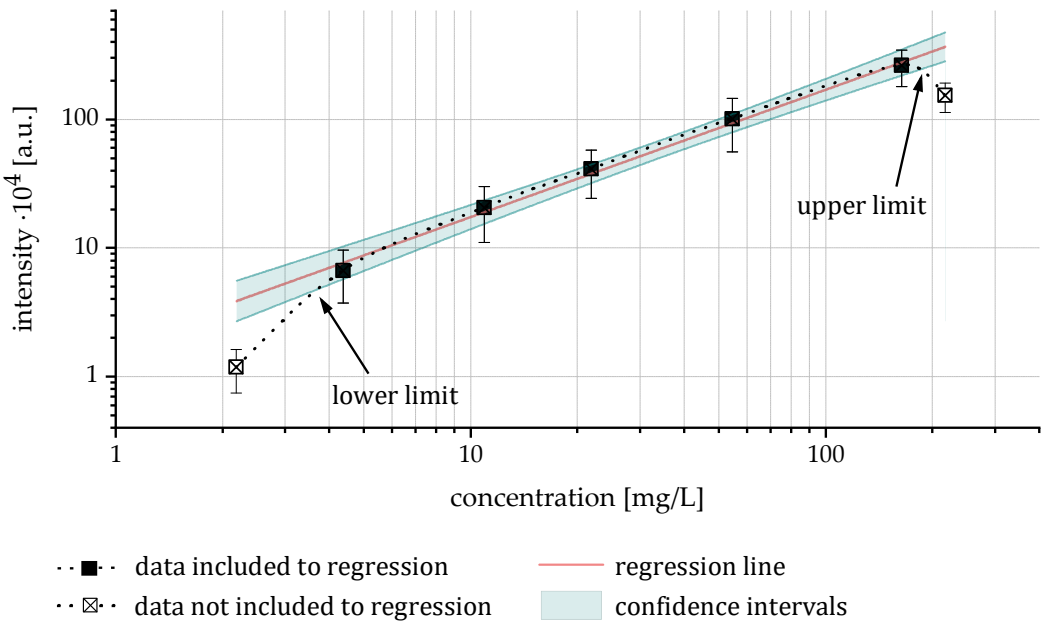

Figure 32: Determination of the linear dynamic range by linear regression of the acquired data in double logarithmic scale. The regression has a slope of 0.9901 ± 0.0367 and shows a good linearity. The interception of the dotted connection line with the 95 % confidence interval hyperbolas represents the lower and the upper limit. With these limits the LDR has been calculated to 1.7 orders of magnitude. This diagram is reprinted with permission from Anal. Chem. 2023, 95, 22, 8423–8432. Copyright 2023 American Chemical Society.

added to the determined value of 3.71 mg/L to obtain the minimum detectability. According to Avanti® (s. Table 1, page 35), the 25 mg/mL liver extract contains 7 % cholesterol, which results in a concentration of 1.75 mg/L (in this 1:1000 (v/v) dilution) [93]. A more precise specification with an error is not given by the analysis certificate of Avanti®. The lower limit obtained from Figure 32, together with the concentration already present in the sample, gives a minimum detectability of 5.46 mg/L.

The highest concentration (217.51 mg/L) of the calibration series one (Figure 32) shows an unexpected underperforming intensity. The signal drops too strong for an intensity saturation or an overloaded ion trap. During the measurement of sample No. 7, periodically repeating droplet accumulation and ejection has been observed. This also reflects the cholesterol signal, which

is shown in Figure 33. The extracted ion current of free cholesterol at m/z 369.4 shows a rapid periodic increase in intensity which can be detected at frequencies of 0.33 – 0.5 Hz.

It is not known on which of these the effect of droplet accumulation is based. In fact, over-concentration of analyte or matrix seems to destabilise the nESI-FuTP process, which is the reason for the underperformance of sample No. 7. Comparing the LDR of 1.7 orders of magnitude determined here with those of other methods, the linear range nESI-FμTP is somewhat lower, but absolutely sufficient and acceptable for routine measurements. Table 7 shows some common literature values. Compared to an LC approach with a UV detector (0.5 orders of magnitude), the nESI-FμTP presented here has a three times larger linear range (even without chromatographic separation) [100]. The measurement by GC-MS is a common method to determine the total cholesterol (FC + CE) and is currently used as laboratory routine measurements [46]. With 2.2 orders of magnitude this exceeds the range of nESI-FμTP slightly, but requires time consuming derivatisation steps and is not selective for free cholesterol. It should be noted that both of these analytical methods are based on chromatographic separation techniques. In

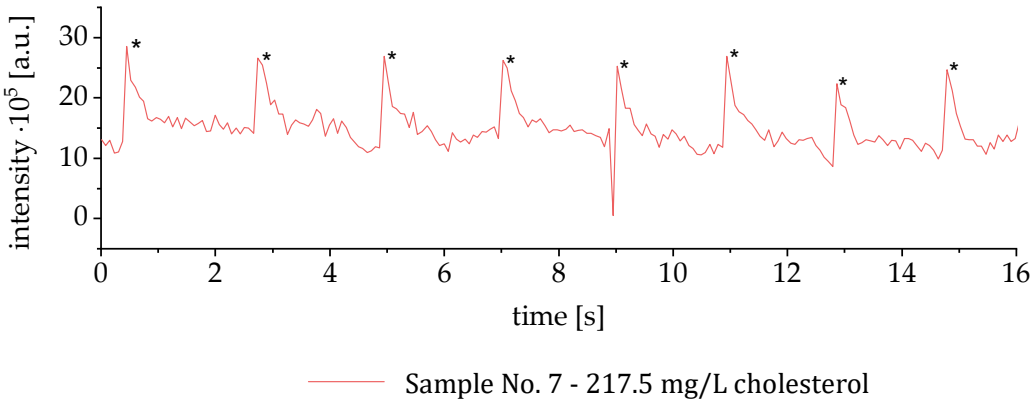

Figure 33: The extracted ion current at m/z 369.4 of the highest concentration of the calibration series I shows clearly a pulsating ion ejection, which is generated by droplet accumulation at the nESI emitter tip. This is the reason for the underperforming of sample No. 7 with 217.51 mg/L. This diagram is based on the publication according to Anal. Chem. 2023, 95, 22, 8423–8432. Copyright 2023 American Chemical Society.

Table 7: Linear dynamic ranges of different methods for the determination of free cholesterol. The linear ranges are given in orders of magnitude.

Instrumen-tation	Methode	Medium / Matrix	Lin. range	Reference
RP-LC	UV Detection	Serum	0.5	[46,100]
GC-MS	Derivatisation	Serum	2.2	[102]
HR-ESI-MS	FTMS (scan mode)	Plasma	≤ 2	[67]
HR-ESI-MS	MSX (scan mode)*	Plasma	≤ 3	[67]
HR-ESI-MS	PRM (scan mode)*	Plasma	≤ 3	[67]
nESI-FμTP-MS	Modified Ion Source	Liver	1.7	[98]

* An Orbitrap Fusion Tribrid MS device was used in this study

comparison to the nESI-FμTP, which applies direct infusion, in separation techniques an enrichment takes place on the chromatographic column, whereby the analyte elutes with increased concentration for a short time.

Although ionisation by ESI is not efficient, modern Tribrid MS devices show a large linear range regarding to free cholesterol. The advantage of such devices is the fusion of a quadrupole, an ion trap and an Orbitrap mass analyser in a single device. As already described in chapter 2.2.5, due to their physical construction, different MS devices have specific fields of application. Quadrupole MS unfold their performance in quantification. Incoming ions enter the detector without any accumulation processes. Due to their linear construction, they achieve extremely high scan velocities and have a very large ion transmission to the detector. As a result, they are linear over a wide range and achieve low detection limits compared to ion traps, but are lacking in resolving power. In contrast, ion trap instruments such as the Orbitrap are characterised by an extremely high mass accuracy and resolving power. However, due to the ion accumulation in the trap the loss of ions during the mass analysing process is larger.

The Orbitrap Fusion Tribrid combines these mass analyser classes and has a large linear range despite its high resolving power. MS devices like this, together with complex scanning techniques such as MSX and PRM, are able

to achieve a linear range of around 3 orders of magnitude in spite of the poor ionisation efficiency of the electrospray (regarding cholesterol). However, Orbitrap Fusion - Tribrid devices are extremely cost-intensive and generate these results by enhancing the signal-to-noise ratio, but not by improving the ionisation efficiency. The analysis with a modern Orbitrap without complex scan methods (ESI-FTMS) is able to generate a linear range of ≤ 2 orders of magnitude, which is comparable to the approach presented here.

The nESI-FμTP developed here improves the ionisation efficiency of the nESI source. This technique does not change the scanning process of the MS instrument and does not require any additional sample preparation or derivatisation steps. On the contrary, complex scan modes such as MSX or PRM and chromatographic separation techniques can be applied additionally, which should lead to further improvement. It can be used with less expensive, older or modern MS devices and is therefore much more flexible than other methods.

3.7 Accuracy and limit of detection

For the determination of accuracy, the concentration of free cholesterol in the liver extract is determined by the nESI-FμTP approach and afterwards compared with the literature value given by Avanti. The value of accuracy can also be referred to as recovery rate. For the determination of the FC concentration by the method of standard addition, a calibration series in the range of the true concentration value is required. Hence, a second calibration series has been prepared and measured by using the nESI-FμTP. To avoid measuring in the range of the lower limit, dilutions of 1:200 have been prepared and spiked with different cholesterol amounts as described

previously. Exact dilution steps and added amounts of the calibration series II can be found in the following Table 8. Each data point represents an average of 100 scans measured in LTQ full scan mode (m/z 365 – 375) with a micro scan number of three. For this measurement, the same MS settings and the same interpretation parameters as in the previous experiment have been selected (inlet temp. 280 °C, tube lens 65 V, 200 mmu mass tolerance).

By using the method of standard addition, the unknown concentration is given by the interception of the extrapolated regression line (fitted for the positive concentrations in first quadrant (QI)) and the abscissa in the negative, second quadrant (QII). As already described in the previous section, the cholesterol concentration in the liver extract according to Avanti® is 7 % (wt/wt). At a dilution of 1:200 (v/v), this results in a target concentration of 8.75 mg/L.

To yield a high coefficient of determination (R^2) and therefore the highest method accuracy, only four of the five generated samples have been taken into account of the regression. The samples used for the regression are marked with an asterisk in Table 8. Sample No. 2 shows abnormal high signal intensities. Including sample no. 2 in the linear regression demonstrates that this value lies outside the 95 % confidence intervals and thereby reduces the coefficient of determination to $R^2 = 0.9295$. Repeated abnormally high values

Table 8: Composition of calibration series II. Exact dilution steps, solvent quantity and added amounts of cholesterol are summarised in this table. Each sample contains 5 μL of the liver extract stock solution to yield a dilution of 1:200 (v/v).

Sample No.	Ethanol [μL]	Stock solution (cholesterol) [μL]	Electrospray solution [μL]	Added cholesterol [mg/L]
1*	195	0	800	0.00
2	193	2	800	2.19
3*	189	6	800	6.56
4*	185	10	800	10.93
5*	155	40	800	43.72

* Samples used to calculate the regression.

of this sample indicate a systematic error in sample preparation. Therefore, sample No. 2 (2.19 mg/L) can be considered as an outlier and is not included in the following regression calculations. A faulty pipetting process could be a possible reason for this deviation.

Figure 34 shows the intensity of the recorded data as a function of concentration in a linear plot. Furthermore, the linear regression and the

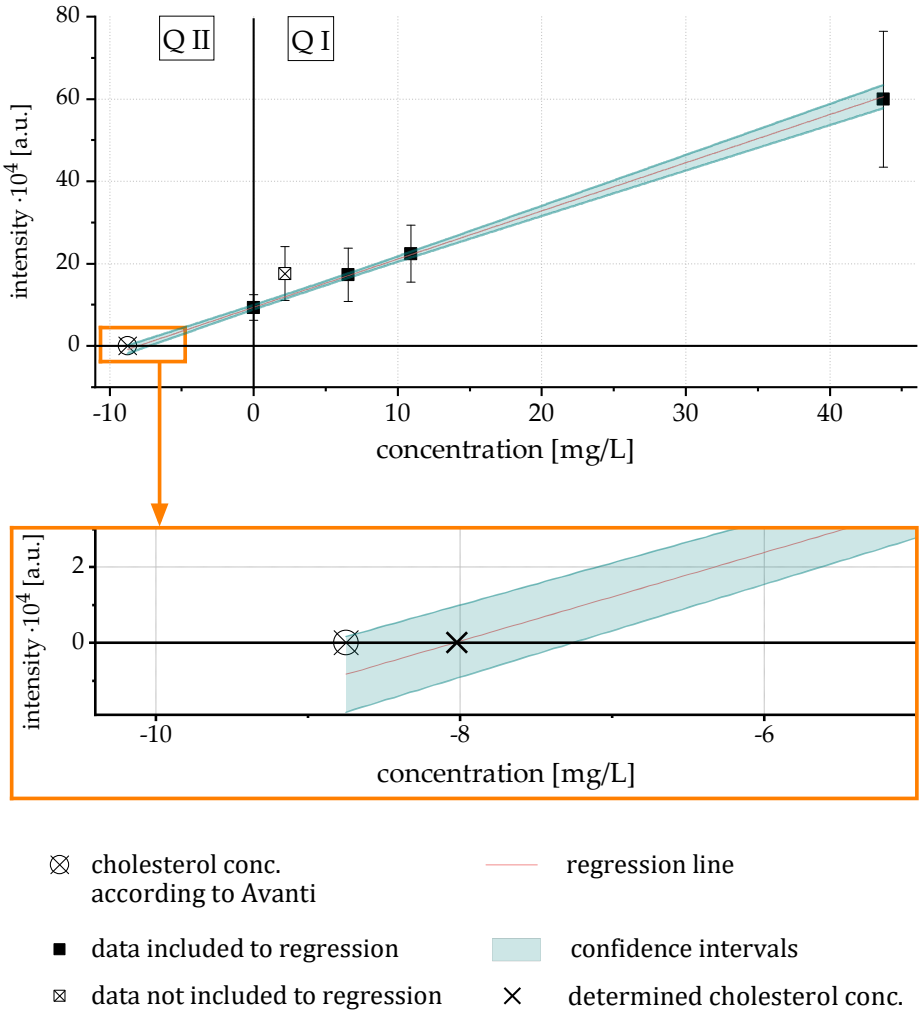

Figure 34: Determination of accuracy (recovery rate) via calibration series II. In the method of standard addition, the unknown concentration can be taken from the intersection of the regression line with the abscissa in the second quadrant. The calibration in total is shown at the top. The region of the unknown concentration is shown enlarged below. This diagram is based on the publication according to Anal. Chem. 2023, 95, 22, 8423–8432. Copyright 2023 American Chemical Society.

corresponding 95 % confidence intervals are added to this figure. As described above, sample No. 2 is not part of the linear regression and is marked as a crossed square in Figure 34. The coefficient of determination of the regression can be determined to $R^2 = 0.9994$ and indicates a high correlation. For a better overview the important region of the abscissa in QII that indicates the target concentration has been optically enlarged.

The experimentally determined concentration has been calculated to 8.04 ± 0.19 mg/L and is marked by a bold cross in Figure 34. Comparing the experimental value with the literature value according to Avanti® Lipids (8.75 mg/L; marked as a crossed circle), a deviation of -8.1 % could be achieved, which results in a relative recovery rate of 91.9 % ± 2.4 %. The value, according to the literature is within the calculated confidence interval hyperbolas. As noted before, an error of this value is not available by the distributor's literature. Deviations of current cholesterol quantification techniques range from 10 % (110 % accuracy), over 7.2 % (92.8 % accuracy) to 0.5 % (99.5 % or 100.5 % accuracy) [101–103]. For this reason, the value determined here can certainly be regarded as valid and acceptable for analytical methods.

With the concentration series of free cholesterol measured here, the limit of detection (LOD) can be evaluated by the method according to Hubaux and Vos. For this purpose, the determined concentration of 8.04 mg/L has been mathematically added to the cholesterol concentration of each sample of the second calibration series. The resulting calibration and corresponding regression is depicted in Figure 35. The intersection of the upper confidence interval and the ordinate can be used to determine the intensity at which the lower confidence interval reaches the detection limit on the abscissa. This process is shown in Figure 35 with a dotted arrow on the right. The result is a detection limit of 1.56 mg/L, which differs slightly from the minimum detectability of 5.46 mg/L as calculated in chapter 3.6 "Linear Dynamic Range". The reasons for this deviation are on the one hand the different concentration ranges of the applied calibration series and on the other hand the different mathematical approaches of the determination. The calibration

for the determination of the LDR covers a wide range and becomes less precise at the limits. The second calibration is more accurate in the lower range due to the fact that the generated samples are closer to the true cholesterol concentration. Even though there is a discrepancy between the two values, they are in a similar concentration range.

Due to the complexity, there is not a large number of publications dealing with the determination of free cholesterol in complex matrices. The majority of publications only focuses on the total cholesterol concentration (FC + CE). Table 9 summarises different methods that have been used for the quantification of free cholesterol in difficult matrices. The "direct analysis in real time" (DART) works with a plasma source for the ionisation of cholesterol. Here, the sample is desorbed from a paper and ionised with the plasma. A detection limit of 21.5 mg/L could be achieved [104]. Another possibility to quantify cholesterol is the use of an atmospheric pressure chemical ionisation as ionisation source for mass spectrometry. In combination with liquid chromatography, an LOD of 0.1 mg/L can be achieved [105]. However, this method is time-consuming due to the LC separation.

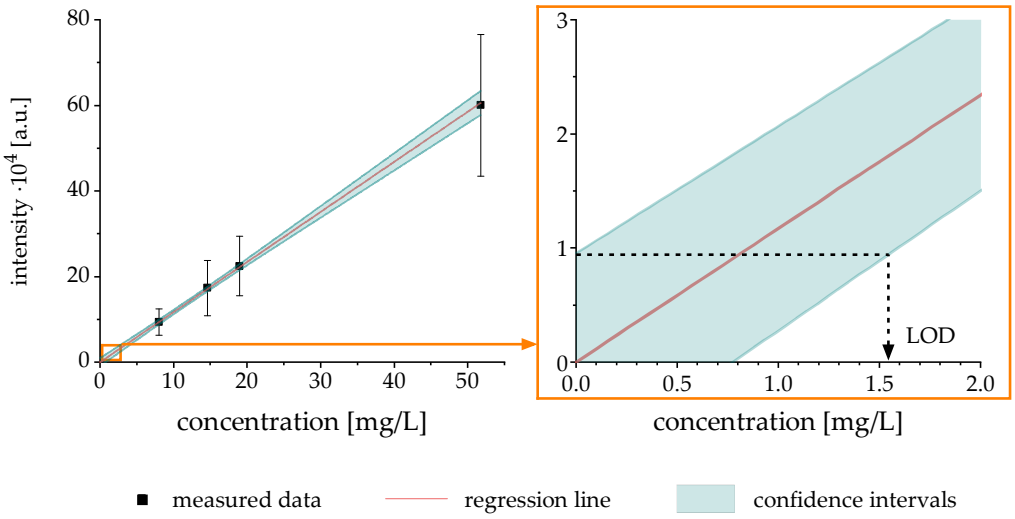

Figure 35: Evaluation of the limit of detection (LOD) with the calibration series II and corrected cholesterol concentrations. Using the method according to Hubaux and Vos, a detection limit of 1.56 mg/L can be determined. A deviation to the minimum detectability of 5.46 mg/L can be observed and based on various concentration ranges of the calibration series and different mathematically approaches.

In 2006 Liebisch et al. published a derivatisation method using acetyl chloride. However, converting free cholesterol to the cholesteryl ester CE(2:0) exacerbates cholesteryl ester interferences and necessitates either LC separation or complex scan modes [106]. The major disadvantage of this method is the very time-consuming derivatisation steps which take at least 60 minutes. In principle, derivatisation is frequently an excellent technique, but requires additional effort due to elaborate sample preparation. The scan functions used by Gallego et al. (MSX, PRM), already presented in the section "linear dynamic range", show excellent detection limits which is comparable to the LC-APCI-MS approach, but as already described previously, these Tribrid MS devices are very cost-intensive.

Compared to the methods presented, the nESI-FuTP ion source developed in this work can be combined with either complex scan functions, modern tribrid mass spectrometers or liquid chromatohraphy, which leads to the expectation that the detection limit of 1.6 mg/L can be significantly lowered and the LDR presumably increases by using modern MS techniques like these.

Table 9: Comparison of cholesterol detection limits generated by different methods.

Instrumentation	Method	Medium / Matrix	Limit of detection [mg/L]	Reference
DART-MS	Paper loaded	Serum	21.5	[103]
LC-APCI-MS/MS	LC separation	Serum	0.1	[104]
ESI-MS/MS	Derivatisation	Plasma	0.2	[106]
ESI-MS (Fusion-Tribrid)	MSX, PRM	Plasma	~ 0.1	[67]
nESI-FμTP-MS	Dual ion source	Liver	1.6	[98]

3.8 Summary and conclusion of the nESI-FμTP

The combination of the nano electrospray and the flexible microtube plasma is the starting point for the development of a hybrid ionisation source in mass spectrometry. This chapter describes the experimental setup and investigations and performance evaluations of this approach.

The nESI-FμTP approach allows two operational modes. In the first mode (nESI-mode), the FμTP is deactivated and the nESI generates a typical electrospray spectrum of polar compounds. Analysing a liver total lipid extract in the nESI-mode leads to a high number of polar lipid species which are detectable in the m/z range of 720 – 860. A collection of the most abundant Lipids in the nESI-mode has been identified and correspond to diverse phosphatidylcholines (PC) and phosphatidylethanolamines (PE). The most abundant lipid signal can be detected at m/z 786.5993, which corresponds to the PC(36:2). By activating the plasma, the second mode (nESI-FμTP-mode) dominates and leads to a significantly changed mass spectrum. Here, the polar lipids disappear and the most intense signal can be observed at m/z 369.3523. This signal corresponds to a protonated cholestadiene which is formed by protonation and subsequently dehydration of cholesterol $[M+H-H_2O]^+$.

Due to the modified construction of the nESI-FμTP relative to a conventional nESI, a reference measurement with a typical nESI in optimised position is performed and for the PC(36:2) shows a reduction by approximately 2 (relative to the nESI reference). In contrast to that, plasma activation leads to a signal increase of cholesterol by a factor of 57.

The repeatability of the switching processes between the nESI- and nESI-FμTP-mode is evaluated by a temporal acquisition of ten switching processes. The resulting relative error of repeatability (E_{Rep}) for the cholestadiene signal

in the nESI-FμTP-mode with 13.3 % shows a four times higher value than the PC(36:2) signal with 3.4 %. Here, a larger temporal signal fluctuation of the cholestadiene signal (in nESI-FμTP-mode) compared to the PC(36:2) signal in nESI-mode also can be observed. This signal fluctuation is evaluated by the relative standard deviation (RSD) and can also be described as signal quality. In relation to the cholestadiene signal, both the nESI-mode and the nESI reference show very poor signal qualities (large RSD values of 60 % and 83 %). Using the nESI-FμTP approach, the RSD could be reduced to 19.2 %, which corresponds to a 3 - 4 fold improvement in signal quality. Furthermore, a long-term measurement over 30 min indicates a stable signal with an insignificant drifting of 0.061 %/min. The residue analysis of the data acquired over this duration showed a typical Gaussian distribution of the measured values.

The presence of cholesteryl esters (CE) can interfere with the determination of free cholesterol (CF). This is due to the same product ions at m/z 369.35 which are formed during the ionisation processes. To identify potential cholesteryl ester interferences, the cholesteryl ester CE(17:0) has been analysed with the nESI-FμTP-MS. Comparing the signal-to-noise ratios of the detected ions in both modes (active and inactive plasma) shows that with activated plasma the fragment ion only rises by slightly 3.4 % (factor 1.034). In contrast to this, a very large influence on the fragmentation has the MS integradet tube lens. Increasing the tube lens voltage leads to additional fragmentation factors between 1.18 - 58, which shows that the increase factor of the nESI-FTP with ~1.03 is very small. Therefore, the signal at m/z 369.4 produced by an active plasma is almost exclusively generated from free cholesterol.

The ionisation and analysis of compounds like cholesterol by the nESI-FμTP is strongly affected by the plasma voltage amplitude and the MS inlet temperature. To investigate the analysis, both parameters are varied over a defined range. The best signal-to-noise ratio (SNR) is achieved at plasma voltages of 2.0 - 2.1 kV while keeping the nESI voltage constant at 2.6 kV. Varying the MS inlet temperature showed that the temperature has a

significant impact to the number of detected species. At high temperatures above 320 °C, additional signals can be observed. These signals should be further non- or less polar lipids that are present in the sample, but undetectable so far. Besides the cholesterol signal, three additional signals (m/z 603.5, m/z 638.3, and m/z 850.5) have been selected to study the behavior under variation of inlet temperature. A good SNR of cholesterol has been observed between 240 - 280 °C. The signals at m/z 603.5, m/z 638.3, and m/z 850.5 are only visible at temperatures of 320 °C and higher, which leads to a problem. The optimal inlet temperatures of cholesterol and the other lipid signals are largely separated, which makes a simultaneous detection almost unfeasable. This represents a significant disadvantage of the current nESI-FμTP source, making it only useful for analytes accesible in a specific temperature range. In addition, the ion source is not device-independent and depends on the capillary temperature of the MS.

In order to determine the linear range of the nESI-FμTP approach, a calibration series according to the method of standard addition has been produced and investigated over a large range of concentration. With the limits of 3.71 mg/L and 189.37 mg/L, the linear dynamic range can be determined to 1.7 orders of magnitude. Here, high cholesterol concentrations have shown droplet accumulation at the emitter tip, resulting in a decreased intensity and consequently in a reduced LDR. Better results can be expected if the nESI-FμTP is combined with a modern trap device or a triple quadrupole device.

For the evaluation of the accuracy of this technique, the recovery rate has been evaluated with a second calibration series. According to the literature or certificate the cholesterol concentration has to be 8.75 mg/L. By utilising the method of standard addition, a concentration of 8.04 ± 0.19 mg/ml was determined. This leads to a deviation of -8.1 % and corresponds to a relative recovery rate of 91.9 ± 2.4 %. Relative recovery rates obtained from the literature vary between 10 % - 0.5 % deviation, which makes 8.1 % to an acceptable value. Finally, the limit of detection according to Hubaux and Voss is determined with calibration series II. Here, a detection limit of 1.56 mg/L has been achieved.

Even if the plasma dominates during activation and a hybrid ionisation is not possible, the nESI-FμTP approach shows great potential for the analysis and quantification of cholesterol. The cholesterol ion yield can be multiplied many times without the need of derivatisation- or chromatographic separation techniques. Although the nESI-FμTP approach performs somewhat lower than the other current research approaches mentioned above, the enhancement of the nESI-FμTP begins here. For example, a combination of the nESI-FμTP and a modern MS trap instrument with complex scan functions (MSX, PRM) would lead to significantly better results which probably exceed the performance of other techniques as both the ion yield in the ion source and the signal-to-noise ratio in the MS system would be improved. With the nESI-FμTP approach a successful cholesterol analysis by ESI-MS is not longer dependent on expensive, state-of-the-art equipment.

The mechanisms of the nESI-FμTP ionisation processes remains unclear to a certain extent. It can be assumed that the evaporation processes or the release of the different non-polar lipids from the μ-droplets do probably not proceed completely or are too slow. By increasing the MS inlet temperature, the release of other less polar lipids to the gas phase can be supported. This fact clearly shows that temperature plays a key role for the ionisation processes applied here.

The development and investigation of the nESI-FμTP approach is the first step towards a development of a hybrid ionisation source. However, the aim has not been reached yet. For this reason, the nESI-FμTP setup has to be enhanced by several elements to enable the simultaneous detection of different lipid classes inside complex biological samples.

4 The PSI-FμTP

Within the scope of the work on coupling an electrospray ionisation and the flexible microtube plasma, another project has been evolved. The motivation for this project was the versatile applicability and low cost of paper spray ionisation and whether this can also be combined with flexible microtube plasma. This resulted in unexpected insights that were of relevance for paper spray analysis as well as helpful for the further development on the previously presented nESI-FμTP approach. In this chapter, important experimental parameters are followed by the results and their interpretation with a subsequent summary and conclusion. Some of the illustrations and diagrams are taken in modified form from the corresponding publication [107].

4.1 Coupling the PSI with the FμTP

In this experiments the classical nano electrospray in front of the mass spectrometer inlet is replaced by an in-house made paper spray ionisation (PSI). Paper spray ionisation is an electrospray variant in which the sample

is applied to a paper substrate and sprayed along the edge of the paper. The PSI comprises of an isosceles triangle-shaped paper, cut from Whatman chromatography paper (Grade 1; CAT No. 3001-861), measuring 16 mm in length, 10 mm in width and an angle of 35° at the tip. The paper triangle is held by a copper clamp that is linked directly to the power supply of the MS device. The high voltage amplitude is generated by the mass spectrometer's integrated high voltage generator. A typical amplitude value for the experiment performed here is at 3.0 kV, but will be described in the respective section. To ensure easy adjustability, the copper clamp is mounted on a precise 3D translation stage. The schematic diagram in Figure 36a illustrates the main area in front of the mass spectrometer inlet, where the PSI is positioned axially with a distance of 2 mm to the MS inlet.

For the first measurements, the paper spray has been used exclusively, but the flexible microtube plasma has been added later in this project. The combination of both is shown in Figure 36b. The paper spray has not changed in dimension or position from the first measurements. In order to keep the influence of the plasma on the paper spray as low as possible, the plasma has been moved away from the paper spray source so that the angle between the PSI axis and the plasma capillary is now 75°. Apart from its position the FμTP has changed only slightly. The fused silica capillary, the electrode wire and the power supply have been retained. However, the electrode wire ends

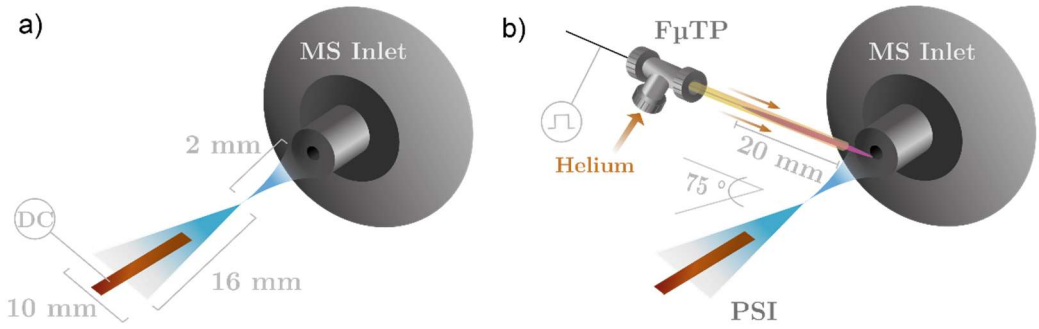

Figure 36: Schematic representations of the applied ionisation sources and their essential geometric parameters. The paper spray ionisation in front of the MS inlet is shown on the left and the combination of the paper spray ionisation with the flexible microtube plasma is given on the right. This graphic is partially reprinted with the permission from Anal Chim Acta. 2022, Vol 1201; 339619. Copyright 2022 Elsevier.

in a distance of 20 mm to the capillary orifice. In experiments where the plasma is added and activated, the plasma voltage amplitude is typically set to 2.2 kV and therefore somewhat higher than in the nESI-FµTP measurements. Furthermore, the distance between FµTP and MS inlet has been reduced to 0.5 mm. Figure 37 shows a macro photograph of the ionisation region in front of the mass spectrometer. Due to the increased plasma voltage amplitude, the jet of the plasma is significantly longer than in the nESI-FµTP measurements and extends to the MS inlet capillary as shown in Figure 37.

A sample volume of 2 - 5 µL is applied to the centre of the paper triangle. After this, the paper remains in the fume cupboard until it is completely dry. In this project, the same liver sample as introduced in the previous chapter has been used here as well as a heart extract. More information on the heart extract can be found in chapter 2.4. Furthermore, several different compounds are applied here. One of these compounds is the alkaloid reserpine. The latter is a drug for the treatment of hypertension that is rarely used today, but represents an excellent model compound for electrospray ionisation mass spectrometry [108,109]. Further compounds are two potential oral cancer biomarker candidates which have been added to the heart extract later on. These are 2-nonanone and 3-octanone as introduced in chapter 2.4.

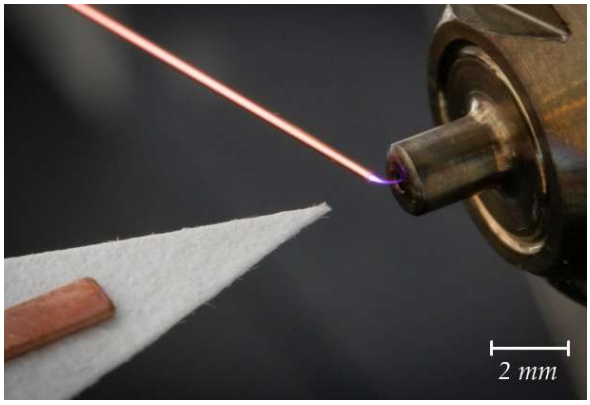

Figure 37: Macro photograph of the ionisation region with the paper spray ionisation and the flexible microtube plasma in front of the MS inlet. This photo is reprinted with the permission from Anal Chim Acta. 2022, Vol 1201; 339619. Copyright 2022 Elsevier [108].

After drying the sample treated paper, the paper triangle is placed in the copper clamp in front of the MS inlet. 35 µL of the spray solvent and the electric voltage amplitude is applied to generate the paper spray ionisation. The basic spray solvent has already been introduced in the previous parts and is described in detail in chapter 2.4. In addition, other spray solvents

containing methanol, ethanol, acetonitrile and water (with ammonium acetate) have been prepared and used in some experiments.

Because of its complex composition, the liver sample is applied as an indicator for different ionisation mechanisms. Here the detection of polar lipids indicates the electrospray mechanism, while signals of neutral lipids (less polar compounds) indicate the plasma-based ionisation process.

4.2 From paper spray to corona discharge

The spray duration of a paper spray depends on various factors. The main factors are the applied solvent, the amount of solvent, the type of paper and the ambient temperature. The latter, however, varies only slightly due to temperature-controlled laboratories. The type of solvent has the greatest influence. While solvents such as acetonitril (ACN) or methanol (MeOH) are highly volatile and only generate a short spray duration of around 1 min, ethanol or water generate a significantly longer spray duration of up to several minutes.

To present different spray durations, Figure 38 shows a reserpine sample analysed with different solvents and a solvent mixture. The reserpine sample used here is a 100 µM solution which corresponds to a concentration of 0.061 mg/mL. Similar to the basic spray solution, in this measurement each solvent also contains one percent of the total volume of a 1 mol/L ammonium acetate solution. 2 µL of the reserpine solution have been positioned on the paper which was fixed in the copper clamp after the drying process. 35 µL of solvent has been added before the high voltage of the power supply has been activated.

In the case of acetonitril (ACN) and methanol (MeOH), the spraying process observed by the $[M+H]^+$ of reserpine at m/z 609.27 is completed after a 1.3 min and 1.4 min respectively, whereas ethanol (EtOH) sprays somewhat longer (3.1 min). The longest spraying time is achieved with a mixture of EtOH and H_2O (ratio 1:1; basic electrospray solution). Here a spray duration of 6.5 min can be achieved, but requires a long initiation or stabilisation phase.

During the first measurements of the liver sample an unusually long spray duration has been recognised. The liver sample has been applied and measured as described above. 5 µL of the Avanti liver extract resulting in an absolute mass of 125 µg on the paper substrate. Analysing the liver sample by paper spray ionisation mass spectrometry, a spectrum as shown in Figure 39 is obtained. Due to the electrospray mechanism this paper spray spectrum shows the same signals as already observed with the electrospray technique of the previous chapter. The intensity ratios of the signals also show strong similarities. The PC(36:2) signal is the most abundant peak at m/z 786.9.

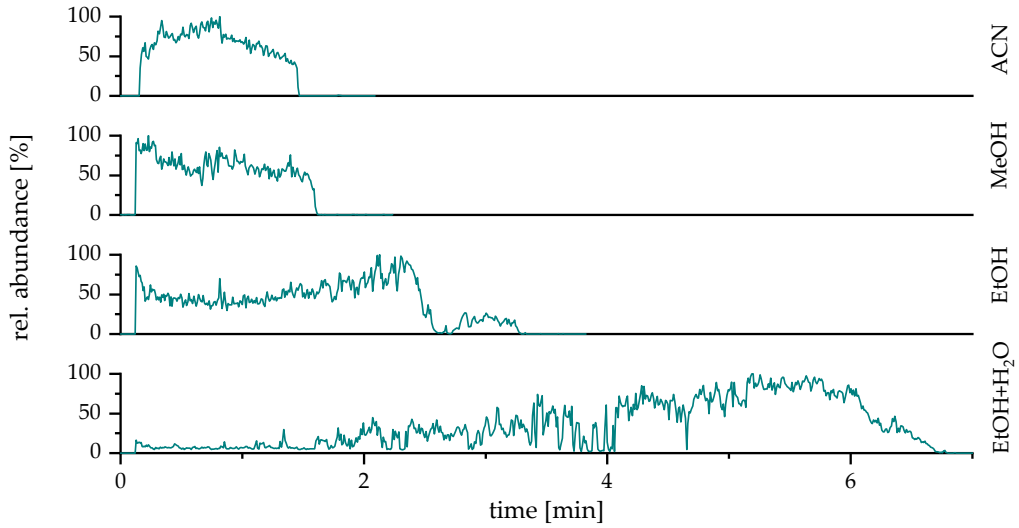

Figure 38: Spray durations of different spray solvents in paper spray ionisation acquired by the reserpine signal at m/z 609.27. The spray duration depends primarily on the solvent type. ACN and MeOH show a short spray duration, EtOH a somewhat longer one. The mixture of EtOH and H_2O (ratio 1:1) sprays for the longest time. Here a spray duration of maximum 6.5 min can be observed. A voltage amplitude of 2.5 kV has been applied to the paper. Due to the high resolution of the orbitrap analyser, the mass tolerance for the extracted ion currents has been set to 10 mmu.

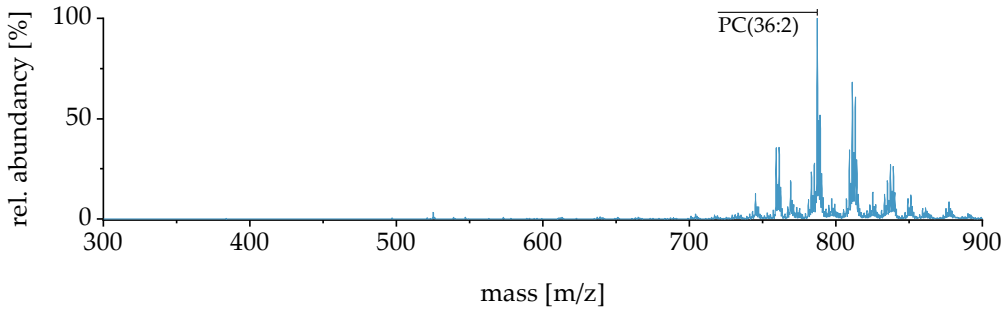

Figure 39: Mass spectrum of the total lipid liver extract generated by paper spray ionisation mass spectrometry. The lower resolution LTQ part of the MS has been used. The detected signals are identical to those of the nESI measurements of the previous chapter.

Investigating the spray duration of the liver sample, an additional process has been observed. To illustrate this additional process, Figure 40a and b shows the ion chromatograms of the polar lipid PC(36:2) at m/z 786.9 and of the less polar cholesterol at m/z 369.5.

This paper spray measurement can be divided into different phases, which are separated by grey lines and numbered periods in Figure 40. At point (1) the DC high voltage of 3.1 kV has been applied. The first ions already reach the MS directly. Larger analytes as lipids move through the paper slower, due to the paper chromatographic effect. Hence, the signal of the PC(36:2) increases in a stabilisation phase of period (2). This is followed by period (3) with a stable spray resulting in a stable signal of the PC(36:2) over a duration of 6.5 minutes. At minute 8.5 (beginning of period (4)) an unexpected signal increase can be observed in the ion chromatogram.

The reason behind the increase in signal from period (3) to (4) could be attributed to the drying process of the paper. As the spray solvent evaporates it leads to a higher concentration of charge carriers on the paper, resulting in a slightly increased conductivity. This creates a stronger electric field at the paper tip and thereby increasing the intensities of the lipid signals. However, this effect of concentration is marginally present in phase (3) due to the solvent-saturated paper. During period (4), where most of the solvent is

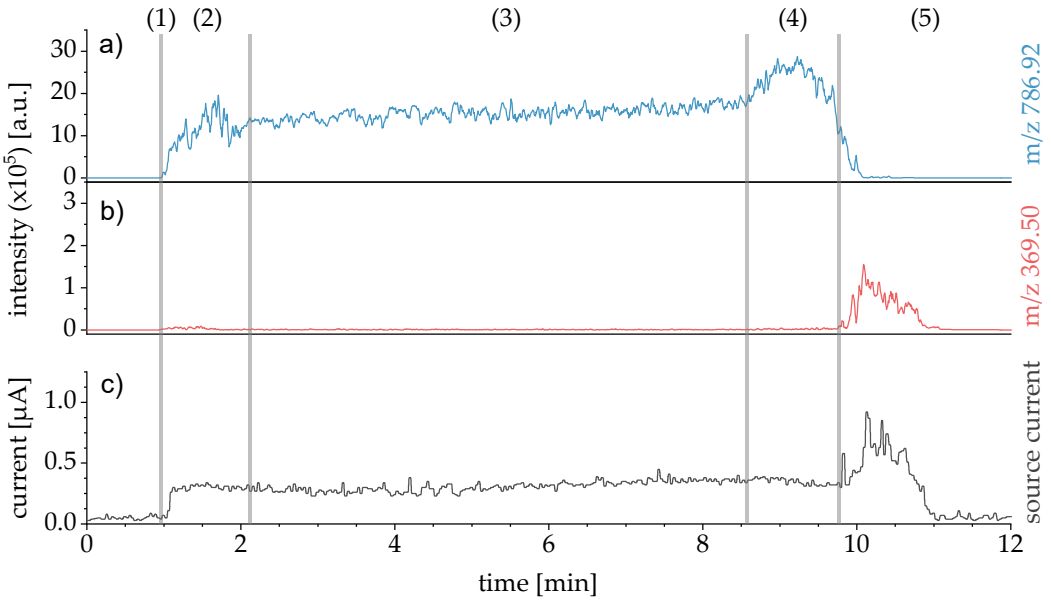

Figure 40: Measurement of the liver sample analysed with paper spray ionisation mass spectrometry. Chromatograms a and b show the extracted ion currents of the polar PC(36:2) and the less polar cholesterol as a function of time. The process of paper spray ionisation can be separated into different periods. After the voltage is applied (1), a stabilisation phase follows (2). A stable paper spray can be observed in (3). In period (4) the intensity of the PC(36:2) increases briefly before it stops spraying. This is followed by a corona discharge which allows the ionisation of cholesterol. The change from electrospray to a corona discharge can also be detected by acquiring the electric current of the MS power supply as shown in c. The measured source current remains constant until it transits to a corona discharge. Here the current increases rapidly. The LTQ analyser has been used with a mass tolerance of 200 mmu. The ion signals have been acquired at an inlet capillary temperature of 260 °C, a capillary voltage of 50 V and a tube lens voltage of 112 V. According to Anal Chim Acta. 2022, Vol 1201; 339619. Copyright 2022 Elsevier [108].

evaporated or already sprayed, the concentration effect is enhanced, resulting in a significant increase in signal intensity. Since cholesterol is not accessible via electrospray ionisation, no signal can be detected in Figure 40b during period (1) to (4). However, after the paper spray process the signal intensity of the less polar cholesterol at m/z 369.5 increases in a subsequent phase (5). This indicates a change from the electrospray ionisation process to a corona discharge.

The measured electric current depends on the type of discharge and can be used as an additional indicator for occuring mechanisms. However, the

software Xcalibur available from Thermo Scientific does not offer the opportunity to extract the electric source current. Therefore, a python file reader program code according to F. Allain is developed to extract the source current from MS RAW data files and create a text-based ASCII file [110]. The latter can be interpreted by using data analysis software as OriginLab.

In Figure 40c the extracted source current is shown as a function of time, which rises insignificantly from 0.30 µA to 0.38 µA between phases (3) and (4) despite the increase in intensity. After that the source current increases in the period of phase (5) by a factor of 2.5, reaching 0.92 µA and seems to exceed the source current of a paper spray ionisation. Of course, the absolute current value of a discharge depends on many factors and can be poorly compared with other assembles or discharge techniques, but a strong relative increase of the current within a measurement as in period (5) clearly indicate a switch of the operating discharge process.

The explanation for the increase in current when changing from electrospray to plasma ionisation is based on the current-voltage characteristics of electric discharges. Basically, the electrospray represents a type of electric discharge as well. However, it delivers significantly lower current values at the same voltage amplitudes compared to a plasma discharge. This effect is probably a consequence of the different ionisation mechanisms in electrospray- and corona discharges. While electrospray initially forms droplets which release ions into the gas phase by coulomb fission, a plasma ionises the ambient atmosphere directly. Consequently, more charge carriers are moved within a certain period of time (s. chapter 2.2) during the corona discharge than in the case of an electrospray. Both, the appearing cholestadiene ion signal and the increased source current, indicates the existence of a corona discharge as a temporal consecutive-ionisation process subsequent to the electrospray ionisation.

It should be noted that the maximum cholesterol signal intensity in Figure 40b is more than an order of magnitude smaller than that of the PC(36:2) in Figure 40a. Based on the highest signal intensities (with a PC(36:2) intensity of $28.8 \cdot 10^5$ and a cholestadiene ion intensity of $1.5 \cdot 10^5$), the cholesterol signal

only reaches a relative abundancy of around 5 % of the PC(36:2) signal. This is despite the fact that the cholesterol fraction of 7 % in the liver sample is very high [93]. In comparison, when using nESI-FμTP the cholestadiene ion can reache a relative abundancy of 39 %. Therefore, higher cholestadiene signals should be expected, which leads to the assumption that the appearing corona discharge is not particularly efficient. Furthermore, the corona discharge only exists for a short duration of about one minute. After this corona discharge in period (5) the ionisation process interrupts completely. Not only the ion currents of m/z 786.9 and m/z 369.5 disappear, also the total ion current (TIC) stops.

The generation of the corona discharge can therefore be described as follows. If enough spray solvent is present to maintain an electrospray, droplet ejection takes place. If there is not enough spray solvent, the spraying process ends, but due to the ions generated in the liquid by the electrospray, a conductivity to the tip of the paper still exists. As long as this condition persists, a corona discharge occurs at the tip of the paper. If there is no longer enough solvent to ensure the generation of ions and the conductivity, the corona discharge also disappears.

The working group around R. G. Cooks already showed an occuring corona discharge under specific conditions during paper spray ionisation in 2011. According to Li et al., this so-called paper spray chemical ionisation (PSCI) only occurs if non-polar solvents such as n-hexane or dichloromethane are utilised [111]. Due to the high vapour pressure of these solvents, here a continuous supply of solvent is necessary. Furthermore, a very high voltage amplitude of 6 - 7 kV (DC) is required. In 2017, Kim et al. used this method to analyse oil-contaminated sediment and showed a successful ionisation of low polar compounds such as 4,6-dimethyldibenzothiophenes and anthracenes [112,113].

In contrast to these publications, in this work the effect of paper spray chemical ionisation has been observed with a standard polar electrospray solution consisting of water and ethanol (with ammonium acetate). To investigate the phenomenon of a subsequent corona discharge and whether

this occurs primarily in complex samples with polar solvents, another sample has been prepared. Instead of the highly concentrated liver extract (25 µg/µL), a standard that contains 0.031 µg/µL reserpine and 0.547 µg/µL cholesterol. Therefore the analyte concentration has been significantly lower compared to the liver sample. The distinctly higher cholesterol concentration relative to the resperin has been chosen because of the lower ionisation efficiency of the molecule. Here 4 µL of the samples have been spotted, resulting in absolute masses of 0.12 µg reserpine and 2.2 µg cholesterol on the paper. After drying, the paper spray ionisation processes generated by different spray solvents (MeOH, EtOH, ACN and the basic electrospray solution) have been examined for the occurence of a corona discharge. Similar to the previous experiment, this has been evaluated on the basis of the extracted ion current of cholesterol and the temporal characteristic of the source current.

The acquired ion chromatograms of reserpine (m/z 609.27) and cholesterol (m/z 369.35) are shown at the top of each measurement presented in Figure 41a - d. Below these there are the extracted source currents which have been read out by applying the programmed python code as already described. Looking at the measurements of ethanol (a) and the basic electrospray solution (ethanol+water; in b), no cholesterol can be measured during the acquisition process. This is probably the major reason why no corona discharge subsequent to the paper spray ionisation has been detected in preliminary experiments. In contrast, the source current shows a clear indication of an occurring corona discharge. With the disappearance of the reserpine signal the source current increases up to 4 µA, indicating a change in the dominant ionisation mechanism. In the previous measurement (analysis of the liver extract by PSI) the current has only increased up to 0.92 µA. The reason for the strong increase up to 4 µA in this experiment is unclear, but in this measurement here a different MS device (Thermo Velos Pro) has been used, which could explain the difference. Exclusively when using methanol, an increase in the cholesterol signal as well as in the source current can be observed, whereby the cholesterol signal is clearly shorter than the duration

of the corona discharge indicated by the soure current. This means that cholesterol is not permanently available and is being consumed. The reason for this is unclear up to this point and will be examined in more detail in the following experiment. Acetonitrile, on the other hand, is the only solvent that does not produce a corona discharge and thus no cholesterol signal. The reason for this is unknown, nevertheless compared to the other ones acetonitrile is an aprotic solvent.

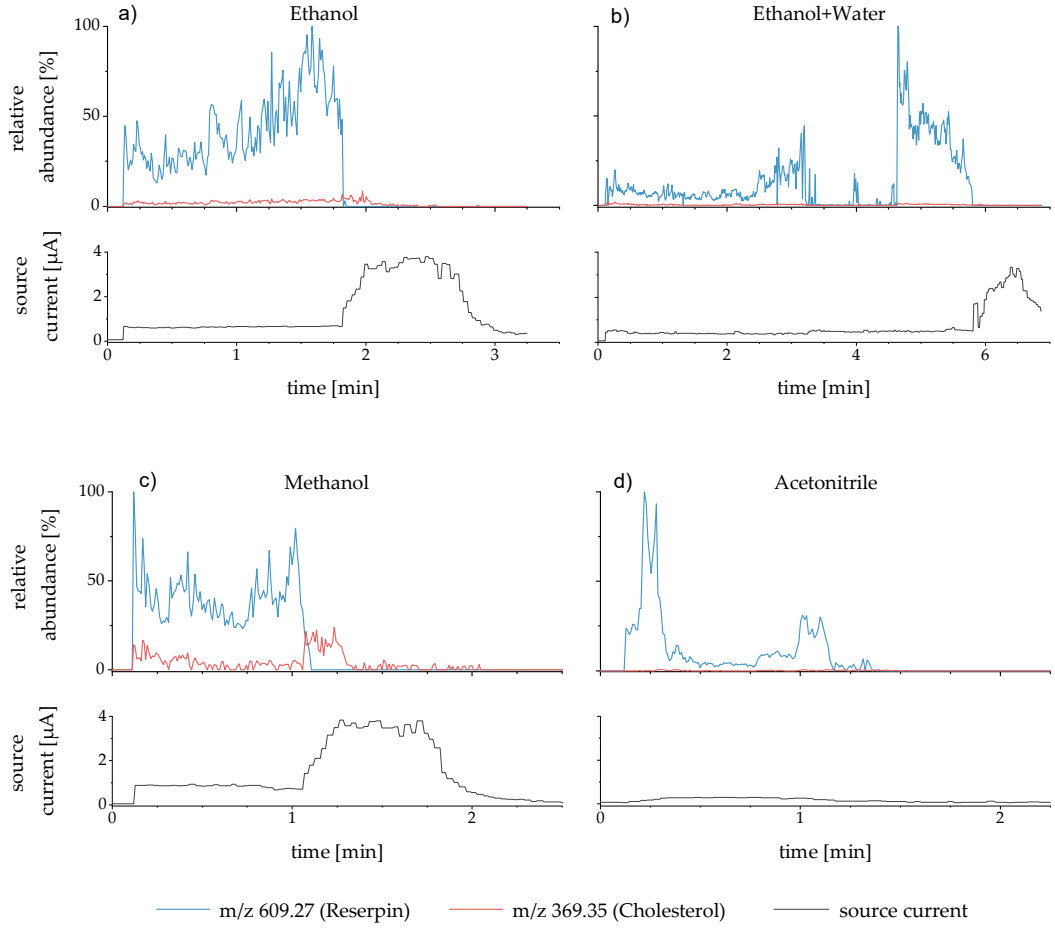

Figure 41: Paper spray ionisation of a reserpine and cholesterol consisting standard. Different solvents have been applied to generate the paper spray in order to observe the formation of a corona discharge subsequent to the electrospray ionisation. Within a measurement, the ion currents are shown at the top and the source current at the bottom. Especially on the basis of the source current the appearance of a corona discharge can be detected for MeOH, EtOH and EtOH+H_2O. No corona discharge is observed by using ACN. A voltage amplitude of 2.5 kV has been applied in this measurement to generate the ionisation process.

This shows that a corona discharge also appears using polar solvents with non-complex samples such as standards and is thus independent of the sample itself and rather dependent on the solvent (see acetonitrile). Literature on corona discharges during paper spray ionisation with polar solvents is rare and difficult to find. Two other publications describe this phenomenon [114,115]. Here, however, the occurrence of a corona discharge is regarded as an artefact to be avoided and is attempted to be suppressed by variation of the spray solvent [115]. Consequently, further research is needed to describe this phenomenon in detail, but this is beyond the scope of this thesis.

In fact, a corona discharge as a subsequent discharge to the paper spray process is an interesting approach, but not sufficiently efficient for the analysis of less polar compounds such as cholesterol. For this reason, in the following experiment the paper spray is combined with a flexible microtube plasma as introduced at the beginning of this chapter in order to increase the ionisation yield of the cholesterol.

4.3 Ionisation modes

Similar to the nESI-FµTP approach, the combination of the PSI and the FµTP enables three different operating modes. The first mode represents the paper spray ionisation (PSI mode) that is generated by a voltage amplitude of 3.1 kV. The second mode combines the activated PSI and FµTP (PSI-FµTP-mode). In the third mode, only the plasma source with a voltage amplitude of 2.2 kV is activated (FµTP-mode). These different modes are illustrated in Figure 42a and b. Here the extracted ion current of the polar PC(36:2) signal is shown in chromatogram a and the extracted ion current of the cholesterol signal is shown in chromatogram b. In this experiment the LTQ analyser of an LTQ Orbitrap XL has been used and the ion currents have been evaluated with a mass tolerance of 200 mmu.

The chromatograms in Figure 42 are separated in 9 periods. Each period corresponds to one of the three ionisation modes as mentioned before. After wetting the sample treated paper triangle with 35 µl of the basic spray solvent in period (1) only the FµTP is activated, in order to identify cholesterol which perhaps entered the gas phase by solvent evaporation. This process is performed in the time span between minute 0 an 1 of Figure 42a and b. Neither a PC(36:2) signal nor a cholesterol signal can be detected.

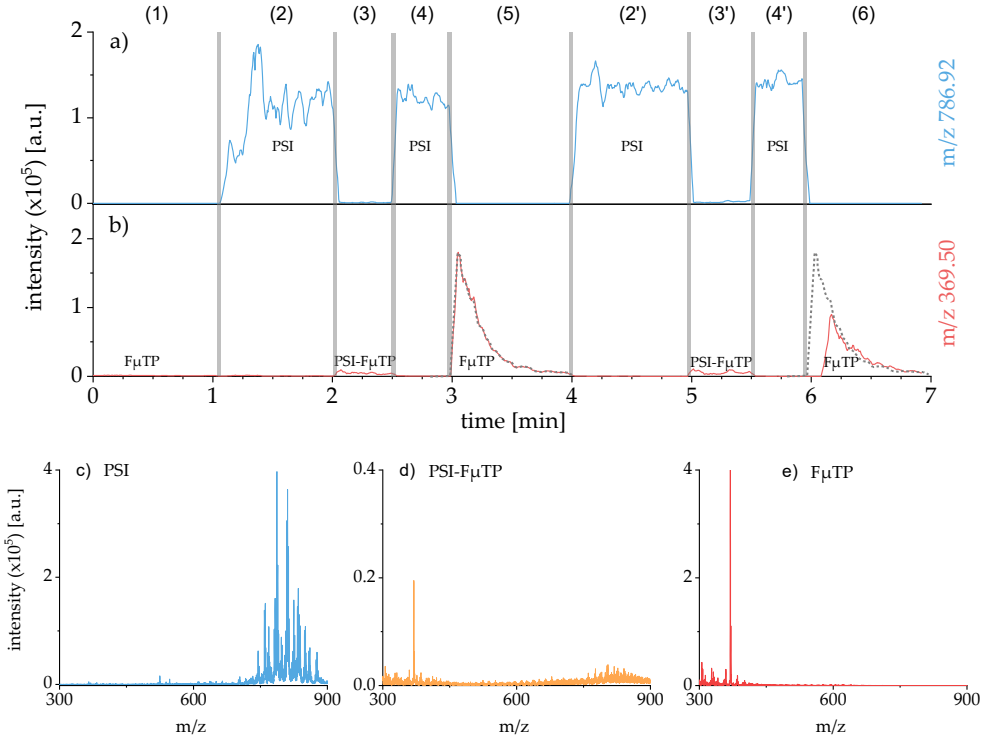

Figure 42: Three different modes of the paper spray ionisation coupled with the flexible micro tube plasma (PSI-FµTP) are performed. The measurement can be separated in 9 periods which are numbered at the top. Relevant ion currents are shown in chromatogram a and b. The diagrams c - e below show spectra of the different modes. High signals of polar lipids can be observed in the periods (2), (4), (2') and (4'), here the PSI mode is activated solely. In the PSI-FµTP-mode low abundant signals are obtained, which can be seen in the periods (3) and (3'). Using only the FµTP results in a spontaneous, very intense cholesterol signal which loses intensity in a tailing shape. This degradation of intensity indicates a desorption process. To exclude an evaporation process of cholesterol afterwards to the PSI, the procedure of the periods (2) to (5) are repeated in the regions (2') to (6), with the exception that the paper triangle has been removed completely. The spectra in c – e represent peak maxima of the chromatograms a and b and are averaged over 15 scans. This Figure is a modified reprint with permission from Anal Chim Acta. 2022, Vol 1201; 339619. Copyright 2022 Elsevier [108].

By activating the paperspray ionisation mode (PSI mode) in period (2), the PC(36:2) signal appears as expected. A mass spectrum as shown in Figure 42c can be observed and represents the typical electrospray spectrum of the liver sample. Activating the FµTP additionally to the paper spray (PSI-FµTP-mode) leads to the signals in period (3). This highlights the mutual hindrance of the two opposing ionisation mechanisms and shows that it is not caused by a saturated ion trap. The corresponding full scan spectrum generated by this mode is depicted in Figure 42d. The PC(36:2) signal disappears and only a very low abundant cholesterol signal can be detected. The reason for this signal suppression is unclear. Both processes, the electrospray ionisation and the plasma ionisation interfer with each other, resulting in very low ionisation yields of cholesterol. The interferences observed with PSI-FµTP are larger than the interferences of the nESI-FµTP source. Hence, the scale of the PSI-FµTP spectrum of Figure 42d is reduced by one order of magnitude due to the low signal intensity. To check the reproducibility of the PSI mode described above, the FµTP is again deactivated in period (4). Afterwards the voltage amplitude of the paper spray is switched off (period (5)) and the plasma is activated so that the FµTP-mode operates here. A fast, strong increase of the cholesterol signal is obtained with a decay during the following 1.5 min. A full scan spectrum generated by this FµTP-mode is depicted in Figure 42e.

This phenomenon leads to the assumption that cholesterol deposits on the MS inlet capillary surface and accumulates during the paper spray process. Because of the high temperature cholesterol desorbs from the 260 °C hot surface and becomes accessible for the plasma ionisation. The entire procedure of the periods (2) to (5) has been repeated in the periods (2') to (6). However, in contrast to period (5), in period (6) the paper triangle has been removed (at minute 6) prior to the plasma activation, in order to exclude an evaporation of solvent with cholesterol after the PSI mode. For safety reasons all high voltage supplies have been switched off for a few seconds during the removal. Turning off any voltage supply cuts off the first seconds of the cholesterol signal, resulting in a reduced peak area of the cholestadiene signal.

To illustrate this, the first structure of the cholestadiene peak of period (5) is added as an overlay to the peak in period (6). The similar shape (tailing) of both cholesterol signals supports the assumption of a cholesterol deposition on, and desorption from the MS inlet surface. The relative signal intensity of the cholesterol is very high for a short moment. This shows the ratio of the most abundant PC(36:2) signal to the measured cholesterol signal. The cholesterol signal reaches the same intensity of $4x10^5$ as the PC(36:2) signal, which corresponds to a relative abundancy of 100 % to the PC(36:2). As a short reminder, the nESI-FµTP approach has only achieved a relative abundance of 39 % for cholesterol.

Based on the results shown here it can be stated that due to the extremely low intensity of the PSI-FµTP-mode a simultaneous operation of both sources does not make sense from an analytical point of view. For this reason, when combining a paper spray and a plasma such as the FµTP, only a sequential order of the applications lead to a sufficient analysis.

An essential aspect for future developments can be derived from the experiment shown here. If the process of deposition and accumulation (followed by desorption and ionisation) occurs in the coupling of the paper spray with the FµTP, this process will probably also play a role in the coupled nESI-FµTP approach. How large the relative amount of deposited and desorbed cholesterol is to the amount of cholesterol that enters directly the gas-phase remains unknown. However, due to a stable cholesterol signal, the influence should be significantly smaller in the nESI-FµTP approach compared to the PSI-FµTP. This could depend on the different distances between ion source and the MS inlet as the paper spray in the PSI-FµTP is placed 2 mm away from the MS inlet, while the nESI of the nESI-FµTP approach has a distance of 3 mm. This means that droplets of the paper spray would have less time to shrink and release ions until they reach the MS inlet before the evaporation process is completed. Furthermore, an electrospray process can occur in different spray modes resulting in a wide range of initial droplet sizes [30-32]. As described in the fundamentals, these spray modes are dependent on operating parameters such as liquid flow rate, electric

conductivity and spray voltage. Consequently, it is very likely that the nESI and the PSI also produce different sized droplets due to their divergent configurations and possible different spray modes. Reports in the current publications suggest that a significant proportion of droplets differ in size, are capable to remain large and have a long lifetime [116–118]. This can lead to aspiration of these droplets into the MS inlet systems. Having investigated this in 2021, the team around T. Benter found that charged droplets are able to induce fragment signatures after penetrating deep into the vacuum stages of commercial mass spectrometers. As a result, these charged microdroplets can even enter the mass analyser area (Markert et al.) [119].

Moreover, the PSI-FμTP only operates sequentially, whereas the sources of the nESI-FμTP approach are able to operate simultaneously, although the plasma ionisation mechanism dominates when the plasma is activated. In the nESI-FμTP the electrospray remains active and maintains the sample supply, in contrast to the PSI-FμTP. This could lead to an equilibrium or "steady state" of deposition and desorption of cholesterol molecules on and from the hot capillary surface. This generates a stable cholesterol signal in the case of nESI-FμTP. Consequently temperature plays a fundamental role in the entire process of the cholesterol ionisation (and perhaps other lipids) and probably also has a larger influence on the nESI-FμTP approach than previously assumed.

4.4 Detection of volatile biomarker candidates

A number of biomarkers can also be present in form of volatile organic compounds. Accordingly, the screening for volatile compounds in complex samples can be of great benefit. An impressive example is the work of Perdita

Barren, who developed a method for diagnosing Parkinson's disease by analysing volatile organic compounds (VOC) in human sebum samples [120,121]. The paper used in PSI is an excellent collection- and carrier substrate for bringing various matrices easily and rapidly in front of a mass spectrometer. However, an ionisation source is still required. The combination of paper spray ionisation and flexible microtube plasma provides both and could therefore be useful for such an application.

To investigate this application with the PSI-FμTP, two volatile organic compounds are analysed with this technique. These compounds are 2-nonanone and 3-octanone, which are potential biomarker candidates for oral cancer [75]. In order to avoid analysing these compounds in the form of common standards, they have been spiked into a complex total lipid heart extract. This feasibility study focuses on PSI-FμTP analysis of the volatile organic compounds, therefore a detailed identification of the lipids inside the heart extract is not performed. For the first test, 97 µL of the heart extract have been spiked with 1.5 µL of each VOC, resulting in concentrations of 12.3 mg/mL 3-octanone and 12.5 mg/mL 2-nonanone. Applying 5 µL of this sample on a paper triangle results in absolute masses of 61.5 µg and 62.5 µg. For the following analysis, a capillary temperature of 280 °C and a tube lens voltage of 120 V have been selected.

Figure 43a shows the mass spectrum obtained in PSI mode. Similar to the analysis of the liver extract, polar lipids in the mass range of m/z 720 - 930 are detectable. The signal with the highest abundance is observed at m/z 758.8. Suggestions for the identification of the five most abundant lipid signals in the mass range of m/z 720 - 930 can be found in Table A1 of the appendix. This identification is primarily based on matching with the work of Christer S. Ejsing [122]. Database-based matching has been applied as well, but is not very reliable due to the low resolution of the LTQ analyser. MS^2 experiments have not been performed in this part of the work, as the exact composition of the heart extract is not of primary interest and is only applied as complex matrix. The composition of the lipid classes of this total lipid heart extract

according to Avanti® Polar Lipids can be taken from Table A2 of the appendix.

When the spray voltage is switched off and the FμTP is activated as shown in the Figure 43b, intense signals appear at m/z 129.1, m/z 143.1 and m/z 369.5 which correspond to 3-octanone, 2-nonanone and the already known cholestadiene ion which is the product ion of cholesterol. Both ketones are represented by the protonated species $[M+H]^+$. Further lipids in the mass range of m/z 500 to m/z 640 can be detected as well. Additional less polar lipids have already been observed in the analysis of the liver sample and described in detail in the previous chapter. The signals of further less polar compounds detected here remain unidentified due to the focus of this experiment.

The difference between the transition processes (from liquid to the gas phase) of the volatile compounds (3-octanone and 2-nonanone) and the non-volatile cholesterol becomes even clearer with a look at the ion currents in Figure 44. For this purpose, the ion currents of the relevant compounds are

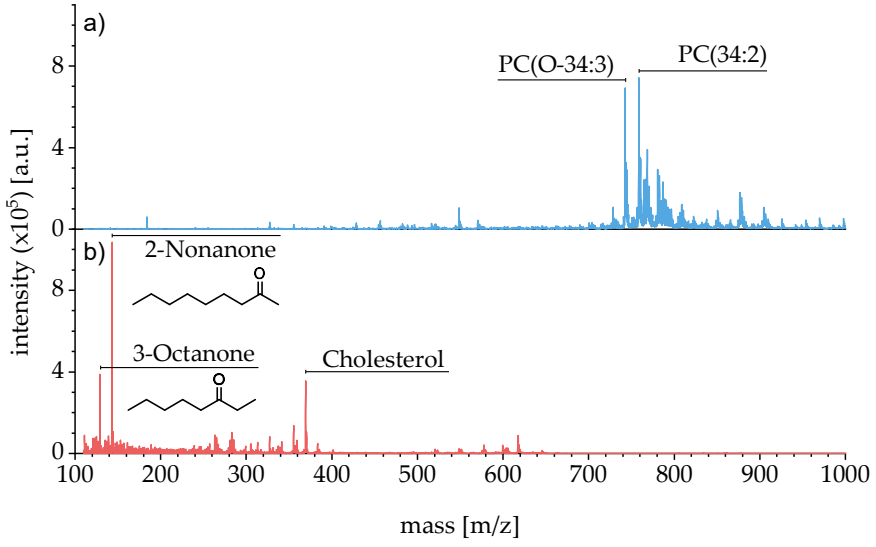

Figure 43: Mass spectra of the bovine heart extract spiked with 3-octanone and 2-nonanone measured with the PSI-FμTP approach. The spectrum in blue (spectrum a) shows the paper spray generated signals of polar lipids. Spectrum b in red shows the active plasma ionisation which leads to the signals of cholesterol and both volatile potential biomarker candidates. Each spectrum consists of 30 scans acquired with a microscan number of three. According to Anal Chim Acta. 2022, Vol 1201; 339619. Copyright 2022 Elsevier [108].

shown as a function of time. At the beginning the paper spray ionisation process is active. The signal of the PC(34:2) at m/z 758.7 (chromatogram a) is stable until the power supply is switched off at minute 0.6. By activating the plasma, the cholesterol signal appears at m/z 369.5 (chromatogram b). After reaching its maximum the signal decreases with a tailing as already observed previously. In contrast to this, the signals of the volatile biomarker candidates 2-nonanone (m/z 143.1; chromatogram c) and 3-octanone (m/z 129.1; chromatogram d) increase slowly and reach their maximum signal intensity first between minute 0.7 – 0.8 min. Afterwards the signals remain constant. The different profiles of the ion currents can be explained by the different transitions of the analytes into the gas phase. While the volatile organic compounds pass directly from the paper substrate into the gas phase, the cholesterol is released after the deposition on and desorption from the hot surface. The question arises whether the volatile compounds rise slowly even though they should evaporate continuously from the paper. This is probably the case, but the ions in front of the MS are in competition due to the temporary large amount of ions. An ion trap is limited to a certain amount

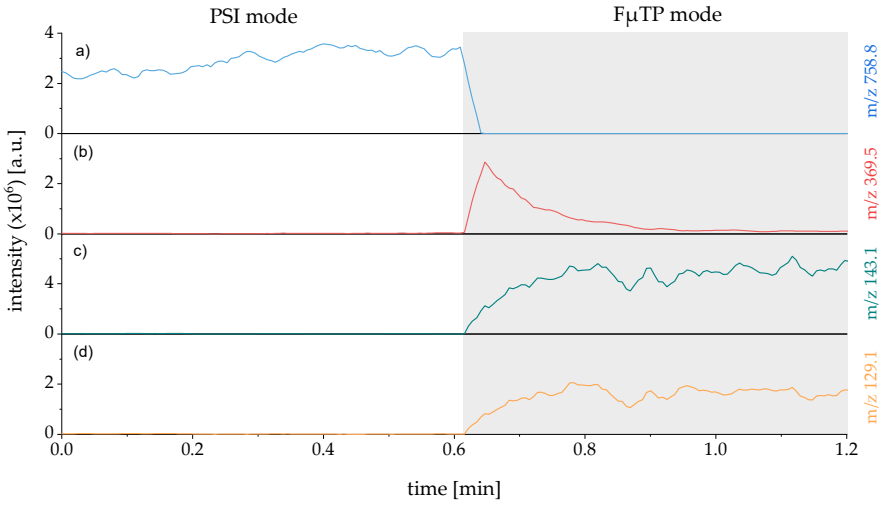

Figure 44: Ion chromatograms of PC(34:2) at m/z 758.7, cholesterol at m/z 369.5 and both potential biomarker candidates 2-nonanone at m/z 143.1 and 3-octanone at m/z 129.1 acquired by PSI-mode and the FμTP-mode. The ion currents show different profiles. The PC signal drops with activating the plasma. In contrast to cholesterol that increases rapidly and fades with a decay, both volatile organic compounds rise slowly and reach a signal plateau. Reprinted with permission of Anal Chim Acta. 2022, Vol 1201; 339619. Copyright 2022 Elsevier [108].

of ions. Due to the direct vicinity and concentration effect of cholesterol on the capillary surface, it has a competitive advantage over the volatile organic compounds. Consequently, it enters the ion trap preferentially for a short period of time. As the amount of cholestadiene ions decreases, the detected amount of the volatile ketones is able to increase.

With these results, the PSI-FµTP approach in addition to the paper spray generated signals of polar lipids allows, the detection of less polar lipids by the plasma and therefore the possibility of the determination of volatile organic compounds. This could be of great interest for the analysis of complex liquid matrices such as sweat, saliva, urine or sebum. In order to assess the performance of this method, a calibration series of the two volatile organic compounds have been performed and the limit of detection has been determined according to the method of Hubaux and Voss, which has already applied previously. The calibration series has been produced with the heart extract as matrix. In addition, a 1:10 (v/v) dilution of the volatile organic compounds in ethanol has been prepared for spiking the samples. To five 1:100 (v/v) dilutions of the heart extract (0.25 mg/mL) different amounts of the volatile organic compounds have been added to the sample generating the concentrations shown in Table 10. 5 µL of a spiked sample have been deposited on the paper triangle resulting in the absolute masses listed in Table 10 as well.

Table 10: Concentrations of the samples and the resulting absolute mass of potential biomarker candidates spotted on the paper.

Sample No.	Concentration [µM]		Concentration [µg/mL]		Abs. mass [ng]	
	2-Nona.	3-Octa.	2-Nona.	3-Octa.	2-Nona.	3-Octa.
1	116.7	127.9	16.6	16.4	83	82
2	233.4	255.8	33.2	32.8	166	164
2	583.5	639.6	83.0	82.0	415	410
4	1167.0	1279.2	166.0	164.0	830	820
5	2334.1	2558.3	332.0	328.0	1660	1640

Figure 45 shows the obtained data with a linear regression and the 95 % confidence intervals. The error of each data point is determined by a quintuple measurement (n = 5). In the case of 2-nonanone, a regression with the coefficient of determination (R^2) of 0.9997 has been achieved, resulting in a limit of detection of 10 ng. For 3-octanone, a regression with a $R^2 = 0.9923$ has been calculated. The slightly higher value also leads to a higher limit of detection of 80 ng. The reason for this deviation is unclear. Pipetting errors during the sample preparation could be a reason. Fictitious molar concentrations calculated on the basis of the used standards and the LOD result in 14 µM for 2-nonanone and 125 µM for 3-octanone.

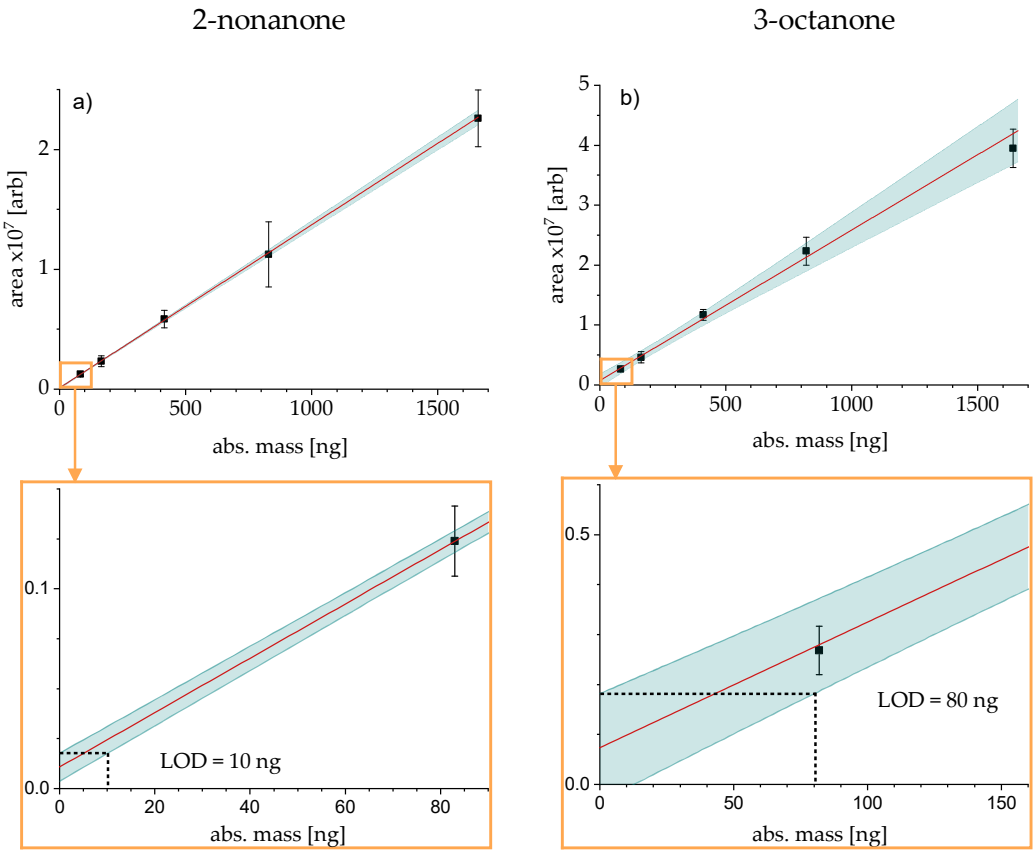

Figure 45: Achieved regressions and LODs of the calibration series of the potential biomarker candidates. Each concentration of 2-nonanone in a (on the left) and 3-octanone in b (on the right) has been analysed five times. The limit of detections are calculated according to the method of Hubaux and Vos and are depicted in the corresponding diagram highlighted in yellow.

Comparative data could not be found in the literature, as the paper spray technique has not been used in a comparable configuration (combined with a plasma for the analysis of VOC) to the current state of knowledge. However, by taking up the already mentioned work of Perdita Barren at the beginning and looking at the examined concentrations, that are in the range of 0.005 µM - 10 µM [120], 2-nonanone is only slightly above the concentration range used for biomarkers detected in Parkinson's disease. The performance of a gas chromatographic separation with a mass spectrometric detector (GC-MS) is clearly not achieved with the results obtained here. However, this study does not claim to outperform this type of method. This investigation serves only as a proof of concept and a successful analysis also depends on the analytical task. The question of whether this method is sufficient for a specific medical diagnosis cannot be answered definitively here, as this would require more studies as well as more specialised knowledge in clinical medicine.

4.5 Summary and conclusion of the PSI-FµTP

In paper spray analyses of a liver extract, unusually long spraying times have been observed. In this context, it has been found that a corona discharge formed after the paper spray ionisation. A strong increase in the source current after paper spray ionisation has also clearly indicated the formation of a corona discharge. The extraction of the source current has been made accessible by an in-house programmed python code. This has not only extended the time of ion production, but has also enabled the ionisation of the less polar cholesterol. There are only a few publications that deal with corona discharges during or subsequent to a paper spray process. However, Kim et al. have been able to achieve a similar effect by combining non-polar

spray solvents such as hexane and very high voltages (6 - 7 kV). Named paper spray chemical ionisation (PSCI), a detection of low polar substances in oil contaminated sediments have been demonstrated.

However, since the current project primarily works with polar solvents, it had to be excluded that the complex liver sample is responsible or partially responsible for the corona discharge observed here. For this reason, a sample standard consisting of reserpine and cholesterol with lower concentrations than the liver sample has been measured with different spray solvents. Here, too, a corona discharge has been observed, which could be detected by the source current as a function of time. The only spray solvent that has not shown a corona discharge was acetontrile. This provides that the formation of a corona discharge is not or only slightly dependent on the sample itself, but rather on the applied solvent.

A corona discharge created with polar solvents subsequent to paper spray ionisation is an interesting phenomenon, but not very efficient in ionisation. For this reason, the flexible microtube plasma has been added to the paper spray. Similar to the nESI-FμTP approach, three ionisation modes are possible. When investigating these different modes, it was found that simultaneous application of the ion sources produces only very weak signals while sequential activation is very efficient. However, the evaluation of the extracted ion signal of the cholesterol showed a decay, which can be explained by cholesterol deposition on the MS inlet surface during the paper spraying process. The high temperature of the surface desorbs the cholesterol and makes it accessible for plasma ionisation. This leads to an intense cholesterol signal. However, since the paper spray is deactivated during plasma ionisation, cholesterol is not replenished and the signal intensity decreases.

In matrices such as urine, sweat or sebum biomarkers or potential biomarker candidates can be present in the form of volatile organic compounds. The combination of paper spray and plasma ionisation is predestined for such an application due to the sample loading on a paper substrate. For this reason, a heart sample has been spiked with volatile potential biomarker candidates (3-octanone, 2-nonanone) and analysed with

the PSI-FμTP approach in the final measurements. It has become clear that it is possible to detect these volatile ketones. When determining the detection limits, 80 ng have been determined for 3-octanone and 10 ng for 2-nonanone. The latter, when converted to a liquid sample (on the basis of the standard solutions used), reaches the upper limit of a concentration series analysed in a study of which describes a successful detection of volatile Parkinson's biomarkers. Whether such a performance is sufficient in clinical medicine cannot be conclusively clarified here.

Two particularly important insights for further developments can be taken from this project. Firstly, it is very likely that the deposition and desorption of cholesterol on and from the hot MS inlet surface plays a role not only in PSI-FμTP experiments, but also in the previously introduced nESI-FμTP approach. Consequently, the electrospray process does not release cholesterol or perhaps other less polar lipids sufficiently. On the other hand, with this PSI-FμTP method (similar to the nESI-FμTP technique) only a sequential combination of both ion sources is possible, which makes the development of a hybrid ionisation source challenging.

Both, the insights obtained from the measurements of the nESI-FμTP approach (e.g. the variation of the MS inlet capillary temperature) and the insights of the current chapter (adsorption and desorption of cholesterol on and from the MS inlet surface) clearly show that thermal energy plays a fundamental role in the coupling of an electrospray-based and a plasma based ion source. In order to make the coupled ionisation system electrospray-plasma independent of the MS inlet temperature, to minimise adsorption and desorption processes and to make other less polar substances accessible, the nano-electrospray is modified in the following.

Furthermore, the fact that both systems cannot be operated simultaneously but rather sequentially illustrates once again that these ion sources are operating under antagonistic conditions. To develop a hybrid ionisation source, a different approach must be applied, which will also be addressed in the final development.

5 Hybrid ionisation via h-nESI-sFμTP

For the development of a hybrid ionisation source that simultaneously ionises polar and less polar compounds, the nESI-FμTP approach introduced at the beginning is applied for futher developments. Two important requirements need to be complied and implemented in order to generate a hybrid ionisation by the nESI-FμTP.

First, the range of analytes accessible by plasma ionisation must be expanded. Currently the detection of different less polar species depends on the MS capillary temperature, which means that either cholesterol or other lipids can be analysed by an activated plasma, but not at the same time (s. chapter 3.5). In addition, very high MS inlet capillary temperatures can lead to undesired effects. This makes an MS temperature-independent ion source necessary. Secondly, the electrospray- and the plasma ionisation must be operated in one single scan cycle to ionise and detect polar and less polar compounds in a spectrum without the use of averaging several spectra.

This chapter focuses on the implementation of these requirements which necessitates some modifications on the nESI-FμTP. The effects and results of these modifications on ionisation will be evaluated and assessed in this chapter. Parts of the data, results and diagrams presented here are currently

in the peer review process and will also be found in a future publication that cannot be referred in this work.

5.1 Coupling a heated nESI with the FμTP

As described in the previous chapter, some of the droplets emitted from the electrospray do not seem to evaporate completely, hitting the hot MS inlet surface and releasing the remaining compounds (low polar) into the gas phase, where they are ionised by the plasma. In order to assist the electrospray process and make the ion source independent from the MS inlet temperature, the nano electrospray used in the previous experiments has been modified with an additional heating element. This supports the release of less polar molecules such as cholesterol (or other lipids) from the μ-droplets into the gas phase, before the droplet reaches the hot capillary surface.

The heating element consists of a heating wire twisted into the shape of a coil. This heating wire is obtained from Thermoexpert GmbH and in detail consists of a resistance heating wire (Inconel®, 1NiCrI05, max. temp. 600 °C, 50 Ω/m at 20 °C) which is embedded in magnesium oxide and sheathed with a stainless steel alloy (type 1.4541) capillary with an outer diameter of 500 μm. This wire is bent to a coil with an inner diameter of 3 mm. In the progress of this approach, three different heating elements have been produced. The first consisted of only one winding, but had little to no effect. The second heating element consisted of 4 windings. The first positive effects were observed here, but a third heating element was produced. This coil has finally been implemented to the setup and consists of 12 turns that are folded in the middle, creating two coils with 6 turns (each ~ 3 mm) in an angle of 90° to each other. One end is mounted on a 3D translation stage with a ceramic

holder. A modified nESI is inserted into the second, angled end of the coil. By utilising a standard laboratory DC power supply (EA-PS-2032-025, Elektro Automatik), it becomes possible to establish a static temperature correlating on the supplied voltage and current. To determine the temperature of the center of the heating element (position of the nESI), a PT-100 temperature sensor (M-3640D, Metex) was positioned inside the heating coil. The sensor does not have any contact with the heating wire surface.

Figure 46 shows the measured temperature as the function of the applied current. Interpreting the data by a parabolic fit shows a very good correlation valid up to a current of 0.61 A. The coefficient of determination could be calculated to R2 = 0.9997. With the following Eq. 21 the temperature T inside the heating element can be calculated with the applied current I, the constant A with 22.62±1.31, the const. B with 66.50±9.72 and the const. C with 611.20±15.25.

Eq. 21

$$T = A + B \cdot I + C \cdot I^2$$

It should be noted that the temperature of the heating element determined here has only been measured once, as it can be assumed that the deviation of the temperature when using the nESI is greater than the error determined in

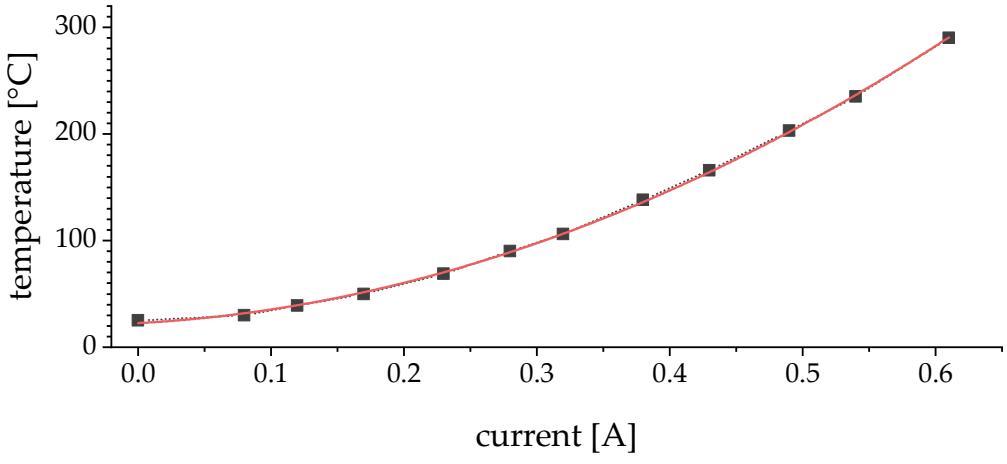

Figure 46: Heating curve of the coil shaped resistance heating wire. The diagram shows the temperature of the heating element as the function of the applied current. The red line represents a parabolic fit to calculate the temperate inside the heating element.

this measurement, due to the fact that the evaporation process removes heat from the heating element. In addition to this, the surface temperature of the heating element is significantly higher compared to the region inside the coil. For these reasons the temperature values determined here can only be considered as an approximation.

An electrospray is very sensitive to high temperatures. Depending on the applied temperature and the solvent used, the electrospray process can stop spraying. To prevent this antagonistic effect, the Taylor cone, which is essential for the spraying process, needs to be protected from the high temperatures of the heating element. The evaporation process should only be accelerated for µ-droplets that have already been ejected from the Tailor cone. The protection of the Taylor cone is ensured here by an additional sheath gas which is guided through a capillary arranged coaxially to the electrospray emitter. This so-called heated nano-electrospray (h-nESI) is constructed of two PEEK tee pieces (UPC-P-728, Upchurch Scientific®) connected with appropriate fittings and sleeves as shown in Figure 47a. The first tee piece accommodates the liquid junction of the sample introduction and a platinum wire electrode for the high voltage supply of the nESI. The high voltage is generated by the MS internal high voltage generator, as already described for the nESI-FµTP and PSI-FµTP approach. A fused silica capillary with an outer diameter of 360 µm and an inner diameter of 50 µm is used as an emitter. The outer polyimide coating is removed by combustion of the tip area. In contrast to the nESI-FµTP approach, the emitter capillary has not been sharpened to a tip, since this setup was first operated on a test basis. The results were excellent, so it was not replaced afterwards. The emitter has been guided through a connector into the second tee piece where it has been inserted to the sheath gas capillary. The second tee piece has been used to connect the nESI emitter, the sheath gas supply and the sheath gas capillary. The latter has an inner diameter of 720 µm and an outer diameter of 1500 µm. The nitrogen flow rate of the sheath gas has been regulated by a mass flow controller (MTC Analytics, model 358529).

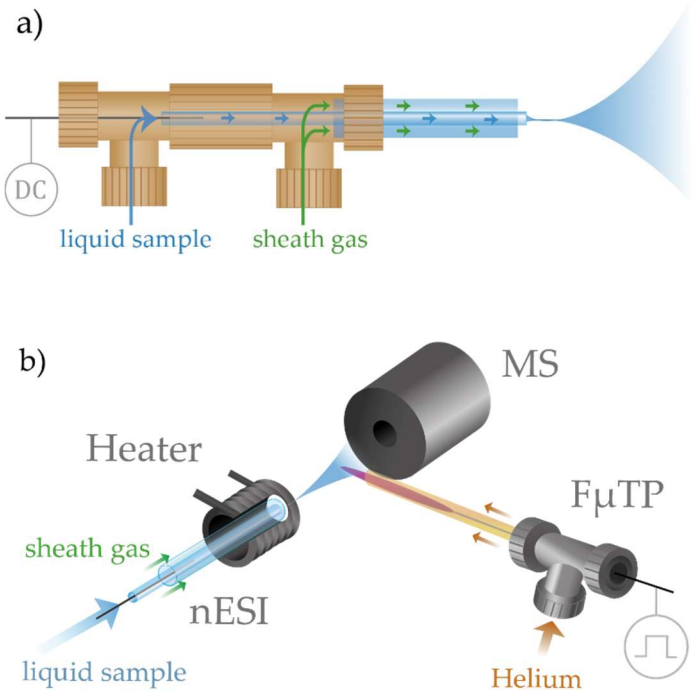

Figure 47: At the top the construction of the nESI with additional sheath gas is shown schematically. The first tee piece is used for sample supply to the emitter. The second tee piece is used to add the sheath gas. The schematic diagram below shows the entire construction with the heated nESI and the FμTP in front of the MS inlet.

The sheath gas capillary ends about 200 µm prior to the nESI emitter, so that the tip protrudes slightly (see Figure 47a). The combination of nESI sheath gas capillary is positioned in the heating element as shown in Figure 47b. The complete h-nESI assemble is placed at a distance of about 2 mm from the MS inlet. The FμTP is located at a right angle to the h-nESI and ends in the ionisation region in front of the MS inlet with a spacing of 0.5 mm. Both nESI (incl. sheath gas and heating element) and the plasma are mounted on separate 3D translation stages and can be positioned independently of each other. The FμTP is identical to that of the previous PSI-FμTP experiments. Figure 48 shows two close-up photographs of the experimental setup and its dimensions in front of the MS inlet. In the following, the combination of the heated nano-electrospray and the flexible microtube plasma developed here will be abbreviated as h-nESI-FμTP.

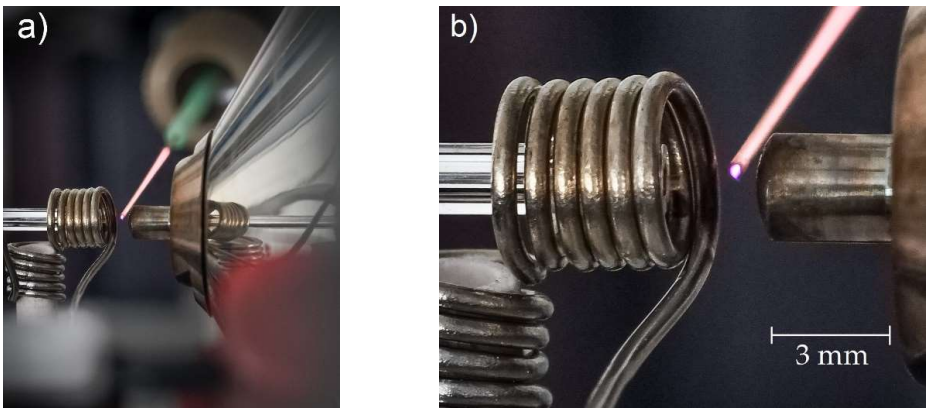

Figure 48: Two close-up photographs of the h-nESI-FμTP setup. The photo on the left shows the dimensions of the ion source compared to the MS inlet. Photo b on the right shows the ionisation region in more detail.

5.2 Identification of less polar lipids

When analysing the complex liver sample with the novel h-nESI-FμTP approach, a strongly changed mass spectrum can be detected with activated plasma compared to the nESI-FμTP spectra. Now a significantly increased number of less polar compounds are accessible. In order to have a reference to the signals generated by the nESI-FμTP and the h-nESI-FμTP with activated plasma, the liver sample has additionally been analysed with the atmospheric pressure chemical ionisation which consists of a thermospray and a corona needle as already described in chapter 2.2.3. The APCI source used here is a commercially distributed Ion Max API source from Thermo Scientific.

Spectra of all three ion sources have been recorded with similar MS instrument parameters. However, different sample flow rates, applied temperatures and voltage amplitudes of the ion sources are unavoidable due to the different constructions. MS and ion source parameters are summarised in detail in the Tables A3a to A3c of the appendix.

The obtained spectra are shown in Figure 49a – c. The spectrum in Figure 49a shows the reference spectrum generated by the APCI. Figure 49b and c show the spectra generated by the nESI-FµTP (centre) and by the novel h-nESI-FµTP (bottom). The APCI spectrum shows a large number of signals, especially in the mass ranges of m/z 300 - 400, m/z 500 - 700 and m/z 800 - 900. These ranges will be descibed as lipid or signal pattern in the following. By using the nESI-FµTP approach, only the cholesterol signal at m/z 369.4 can be observed. In contrast, the modified version with heating element and sheath gas (h-nESI-FµTP) shows a spectrum which is similar to that of the APCI source. A difference can be found mainly in the peak ratios. The signal

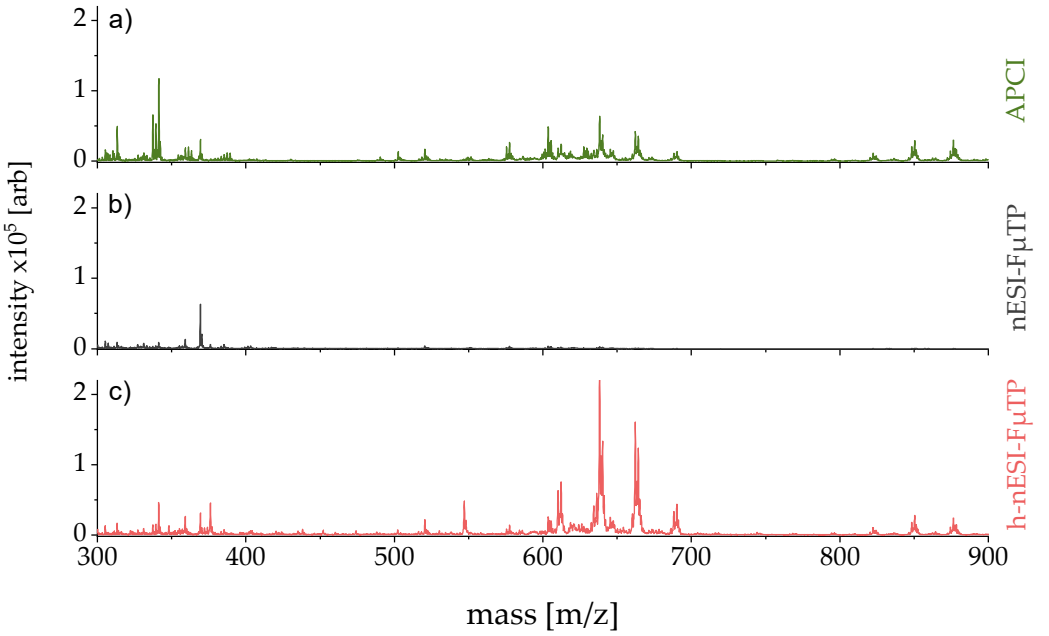

Figure 49: Spectra of total lipid liver extract analysed with APCI (green, spectrum a), with the nESI-FµTP (grey, spectrum b) and with the new h-nESI-FµTP (red, spectrum c). While the nESI-FµTP spectrum can only ionise cholesterol very efficiently, the h-nESI-FµTP shows a spectrum that is very close to the APCI source and even exceeds it in intensity.

pattern in the low mass range (m/z 300 – 400) of the APCI spectrum is more pronounced than in the h-nESI-FµTP spectrum. In contrast to that, the h-nESI-FµTP shows more intense signals in the mass range of m/z 500 - 700. Table 11 shows the 10 most abundant signals of the APCI and the h-nESI-FµTP as well as their relative abundances in comparison. As expected, both the APCI source and the h-nESI-FµTP generate the same spectra, but differ in their signal intensities. The reason for this can be based on the slightly different vaporiser techniques, but it is also very likely that the APCI source generates more fragmentation due to its significantly stronger electrical field at the corona needle tip (DC, 3.9 kV) compared to the somewhat "softer" FµTP (AC, 3.0 kV) which has no bare and point shaped electrode at the capillary's end.

The most intense signals of each lipid pattern of plasma generated spectra have already been mentioned for evaluation purposes in chapter 3.5 of the nESI-FµTP approach. The successful measurement of the missing less polar lipids makes an identification of these most intense signals useful for

Table 11: Comparison of the ten most abundant m/z signals, determined by the heated nESI-FµTP setup and the commercial APCI. This table shows the similarity of both achieved spectra.

m/z	Heated-nESI-FµTP rel. abundance [%]	Ion Max API source rel. abundance [%]
341.4	20.5	100
369.4	15.4	26.7
520.5	9.58	14.2
547.1	22.8	1.9
610.3	26.1	16.1
612.3	24.2	21.1
638.3**	100	55.5
640.3	56.5	32.0
662.3	69.5	36.7
664.3	51.4	30.3
850.4**	11.7	24.6
876.5	9.5	25.3

**signals are used for the evaluation of ongoing experiments.

subsequent investigations. One representative has been chosen from each signal pattern. Similar to the experiment in chapter 3.5, for the signal pattern of m/z 300 - 400 the already introduced cholestadiene ion signal m/z 369.4 is selected. The most intense signal of the mass range m/z 500 – 700 is the m/z 638.3. Finally, as representative of the pattern m/z 800 – 900 the signal at m/z 850.5 has been selected. The identification of these lipid species is based on the comparison with various publications, the LIPID MAPS® database and finally MS^2 experiments [42,95,123,124]. Due to the significantly higher signal intensities, the MS^2 measurements have been performed with the h-nESI-FμTP ion source and an activated plasma. As expected, the identification of these signals indicates clearly the presence of neutral lipid species representing low polar compounds in the liver extract. Acquired with the high resolution orbitrap analyser, the signal at m/z 638.5741 represents an $[M+NH_4]^+$ ion of the diacylglycerol DG(36:2) which has a theoretical monoisotopic m/z of 638.5718 g/mol. Furthermore, the signal at m/z 850.7889 can be assigned to an $[M+NH_4]^+$ ion of the triacylglycerol TG(50:1) with a theoretical monoisotopic m/z of 850.7858. The calculation of the mass deviations results in both cases to 3.6 ppm.

As already explained in the nESI-FμTP chapter 3.2, MS^2 experiments can be used to assign the type of lipid inlcuding the fatty acid chains. By fragmenting the lipids, individual molecular groups can be separated and determined. Figure 50a and b show the corresponding MS^2 fragmentation spectra and the exact peak assignment. Thus, the DG(36:2) signal is represented by a DG(18:0/18:2) and the TG(50:1) by a TG(16:0/16:0/18:1).

Finally, further less polar species have been identified by MS^2 fragmentation and results for the m/z 662.6 to a DG(18:0/20:4) and the m/z 876.7 to a TG(18:1/18:1/16:0). The corresponding MS^2 spectra can be taken from Figures A8 and A9 of the appendix. CID parameters for the MS^2 scans are described in the figure caption of Figure 50.

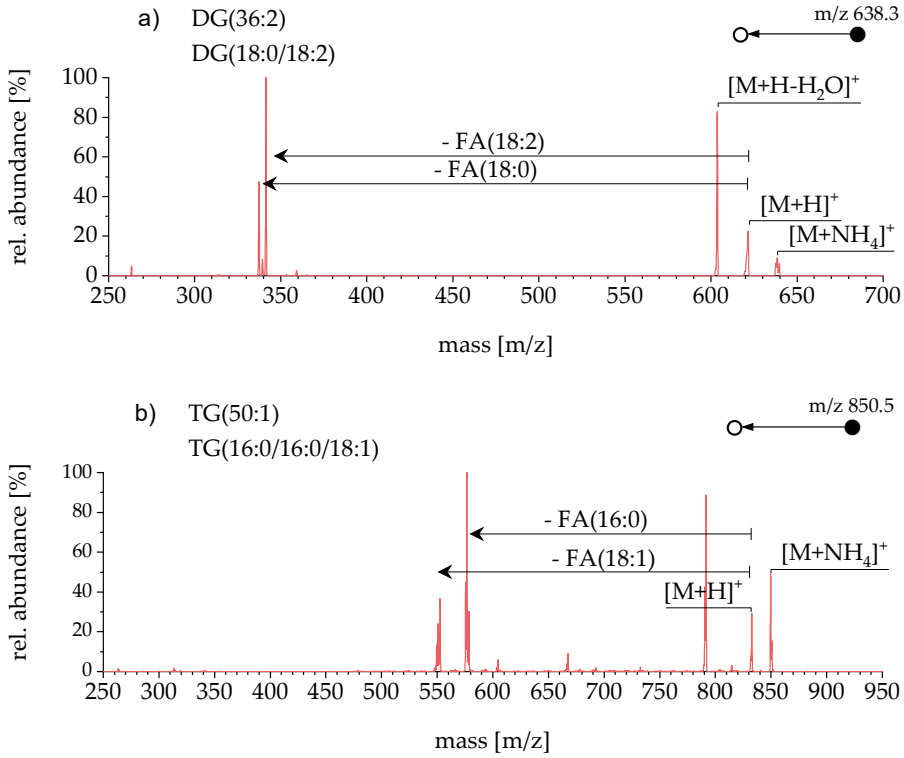

Figure 50: Fragmentation spectra of the signal at m/z 638.3 and m/z 850.5. The top spectrum shows the identification a DG(18:0/20:4). An isolation width of m/z 3 and a normalised collision energy of 4.0 a.u. has been used. The spectrum below has been acquired at a normalised collision energy of 6.0 a.u. (same isolation width) and identifies a TG(16:0/16:0/18:1).

5.3 Improving the ionisation processes

For further measurements, an investigation of the h-nESI-FµTP approach is essential. High signal-to-noise ratios depend on the position and the operating parameter of each individual component. Interactions between the two ion sources make precise signal maximisation difficult. The ability of an

MS device to display m/z signals in real time during a measurement makes this process somewhat easier. The high temperature and metal surface of the heating element can strongly influence the resulting electric field and thus the plasma. If the heating element is moved backwards (away from the inlet) along the nESI emitter axis, the signals of the less polar compounds decrease steadily. In order to get high signal intensities and protect the FμTP from heater influences, the best position of the heating element is identified in a distance of 1 mm to the FμTP (Figure 48, page 108).

The two remaining parameters are the heater temperature and sheath gas flow. First, the heater temperature has successively been increased in order to investigate the influence of the heater temperature on the signals of the mass spectrum. The well-known lipids cholesterol, PC(36:2), DG(36:2) and TG(50:1) serve as representatives for the different lipid classes and the dominating ionisation mechanism. The plasma remains active in this measurement to ensure ion production at higher temperatures when the electrospray process stops. To minimise negative influences on the electrospray process, the voltage amplitude of the plasma is reduced to the minimum of 1.85 kV. At this voltage, the plasma does not dominate, so that disturbance-free operation of the electrospray process is ensured. The result is shown in the diagram of Figure 51, in which the intensities of the extracted ion currents with a mass tolerance of 50 mmu is given as a function of the heater temperature. Each data point consists of 50 measured values and the error is determined by the standard deviation. Furthermore, the MS inlet capillary temperature is kept constant at 280 °C throughout the entire measurement. A minimal sheath gas flow rate is required because otherwise droplets would accumulate at the nESI emitter tip during unstable spraying processes can be pulled into the sheath gas capillary by capillary forces, making a restabilisation of the electrospray impossible. Therefore, the sheath gas is set to a very low flow rate of 5 mL/min.

Within the temperature range of 25 °C to 60 °C shown in Figure 51, the PC(36:2) signal at m/z 786.6 remains constant around $2.9 \cdot 10^5$, indicating that the electrospray remains unaffected by temperature variations. However,

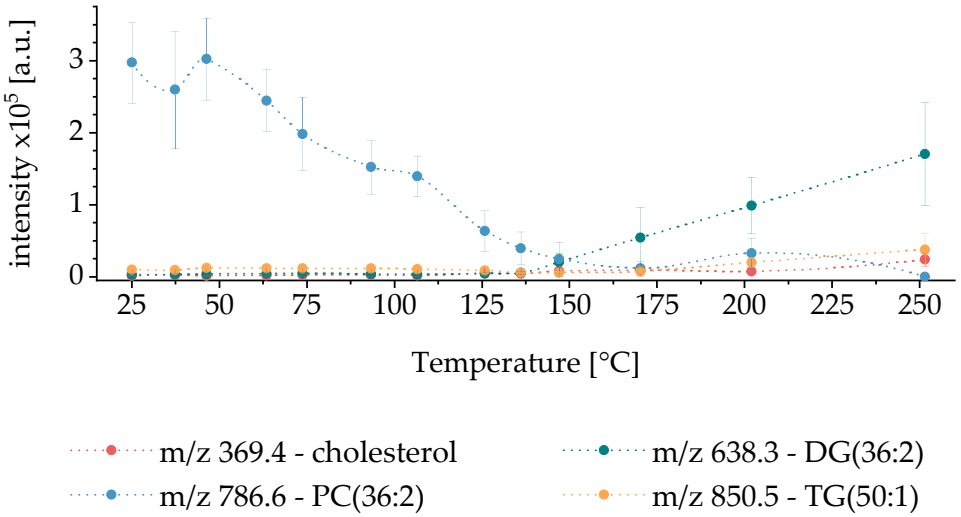

Figure 51: Extracted ion currents of polar and less polar representatives as the function of the heater temperature. The electrospray mechanism decreases with increasing temperature. The plasma-based ionisation mechanism becomes the dominating part at temperatures of 150 °C and higher.

as the temperature is increased from 60 °C to 150 °C, the electrospray signals decrease. The signal reduction may be attributed to evaporation processes interfering with the electrospray mechanism, resulting in lower ion yields. At temperatures exceeding 150 °C, the evaporation process becomes dominant and leads to a strong signal reduction of the nESI spectrum. When the electrospray mechanism interrupts at 150 °C, the less polar lipids (m/z 369.4, m/z 638.3 and m/z 850.5) appear, due to the activated plasma. From here, the plasma-based ionisation mechanism is dominating. To obtain sufficient signals of the DGs and TGs, temperatures above 200 °C are necessary.

Generating an electrospray at high temperatures is not possible. Therefore, the N_2 sheath gas flow should protect the Taylor cone from heat and prevent the electrospray from premature evaporation processes. In order to determine an efficient flow rate, a variation of the sheath gas flow rate is performed at a heater temperature of 200 °C. The signal of the PC(36:2) at m/z 786.6 in Figure 52 represents the performance of the electrospray process. Since only the effect on the electrospray process is examined here, the plasma is not activated.

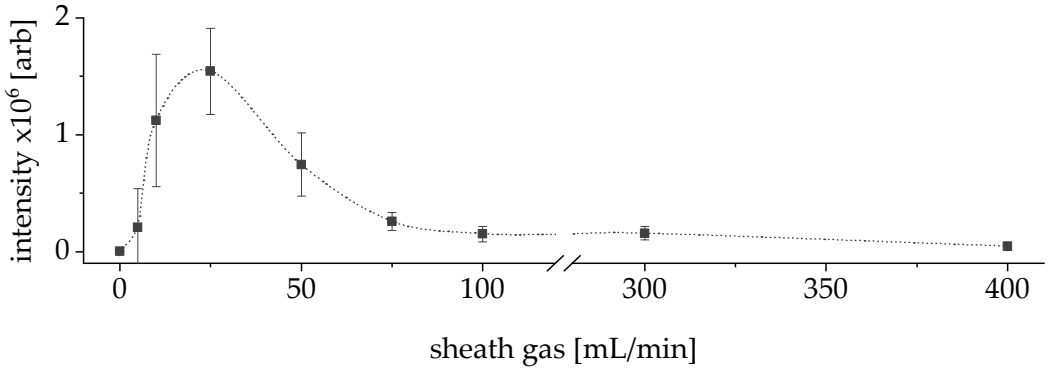

Figure 52: Determination of an efficient sheath gas flow rate. The signal intensity of the PC(36:2) signal generated by the heated nESI at 200 °C is depicted as the function of the sheath gas flow rate. Starting without a sheath gas, no ions can be detected. Evaporation effects disrupt the electrospray process. Applying the sheath gas protects the electrospray from heat and the signal increases, but flow rates of 40 mL/min and above reduces the signal intensity.

At the beginning the N_2 sheath gas flow is off and no electrospray-generated ions can be observed. The process is interrupted by the heater temperature of 200 °C. By slightly increasing the flow rate to 5 mL/min, the electrospray ionisation starts, but shows very instable signal intensities. The PC(36:2) rises with increasing sheath gas flow rate. The highest intensity of the m/z 786.6 signal can be observed at 25 mL/min. Nitrogen flow rates above 25 mL/min lead to a reduction of the PC(36:2) signal. The reason for the rapid decrease in the signal with only slightly higher sheath gas flows is unknown in detail. A possible explanation for this could be a change of the electrospray mode caused by sheath gas initiated turbulences at the emitter tip [125].

This measurement shows that a good balance between temperature and sheath gas flow rate is absolutely important to obtain satisfying signals. Due to the dependence of heater temperature and sheath gas flow rate, readjustment of both parameters may be necessary and can lead to deviations from the values determined here in subsequent experiments.

5.4 Voltage induced hybrid ionisation

As described in chapter 3.5 of the nESI-FµTP approach, increasing the plasma voltage amplitude above a certain threshold leads to the switch of the ionisation mechanisms. In the case of the nESI-FµTP, this transition occurs abruptly due to the strong influence of the plasma to the electrosopray mechanism. By using the h-nESI-FµTP and the detection of the very high abundant DG(36:2), an occurring transition can be identified more sensitively. Under the premise that a transition state between both competing ionisation mechanisms exists, it should be possible to detect it by a small-step voltage variation. Another positive outcome of this experiment is the determination of an efficient plasma voltage amplitude for the FµTP-mode in this dual ionisation source. Therefore, a variation of the plasma voltage is performed as shown in Figure 53. Here the extracted ion currents of the four polar and less polar representatives are shown as the function of the applied plasma voltage amplitude. Every data point contains 50 scans with a micro scan number of three. The error bars are calculated by the standard deviation. A heater temperature of 202°C (4.9 V; 0.49 A) has been used and the sheath gas flow rate has been set to 25 mL/min. A voltage amplitude of 2.6 kV is applied to the h-nESI.

At plasma voltages up to 1.4 kV the intensity of the electrospray-generated PC(36:2) signal remains constant. Further increasing of the plasma voltage leads to a reduction of the PC(36:2) signal. The less polar lipids cholesterol, DG(36:2) and TG(50:1), firstly appear at 1.8 kV, but the electrospray ionisation mechanism still dominates. At 1.85 kV polar and less polar lipids are detectable. At this point a transition state can be successfully generated and is marked as $U_{transition}$ in Figure 53. Here both ionisation mechanisms coexist, which is shown in the spectrum of Figure 54 on page 118. This spectrum shows only one single scan cycle (of 50 scans, 3 micro scans) of the

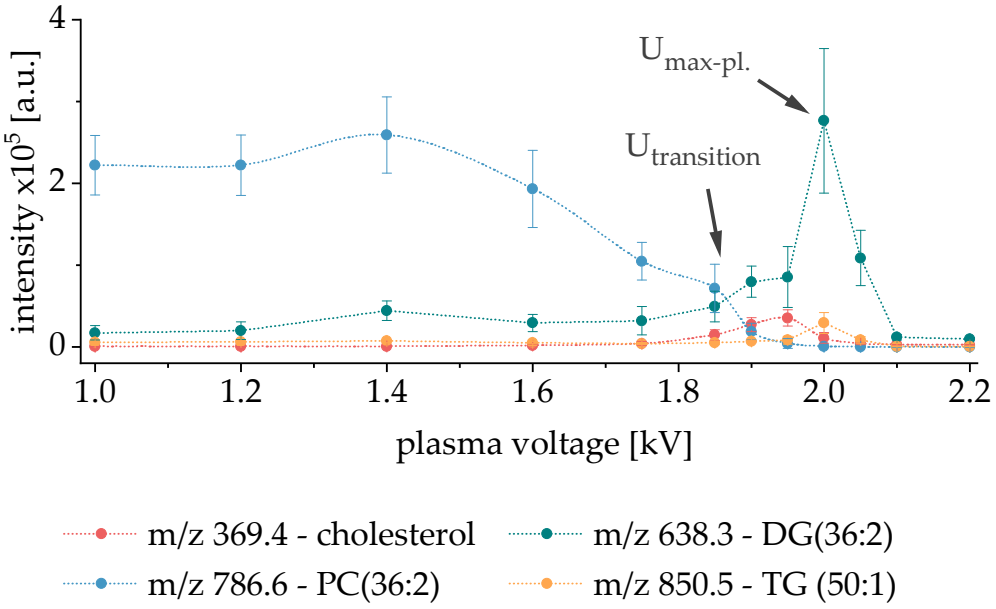

Figure 53: Plasma voltage variation of the h-nESI-FμTP approach to detect a transition state between the electrospray- and the plasma ionisation mechanisms. The extracted ion currents (EICs) of four polar and less polar lipid representatives are shown as the function of the applied plasma voltage amplitude. A transition from one to another ionisation mechanism can be observed at 1.85 kV, which is marked as $U_{transition}$. Here both ionisation pathways occur simultaneously. Furthermore, a signal maximum of the plasma-based ionisation mechanism can be detected at 2.0 kV. The latter is marked by $U_{max\text{-}pl.}$.

data points generated in the transition state at 1.85 kV. Here, different polar lipids like PC and LPC as well as less polar lipids like cholesterol, DGs and TGs are accessible simultaneously in one single MS scan cycle.

Further increasing the voltage to 1.9 kV and more leads to a decrease of the electrospray signals until they finally disappear completely. An increase in the intensities of the low polar lipids can be observed up to the maximum at 2.0 kV which is marked as $U_{Max\text{-}pl.}$ in Figure 53. After reaching this maximum, the plasma-generated signals strongly decrease. It can be assumed that the plasma with its very high voltages disturbs the electrospray. The sample introduction is inhibited and the plasma-generated signals decrease until the electrospray interrupts completely.

The here generated transition state clearly shows that a hybrid ionisation of both, polar and less polar lipids, is in principle possible to be generated.

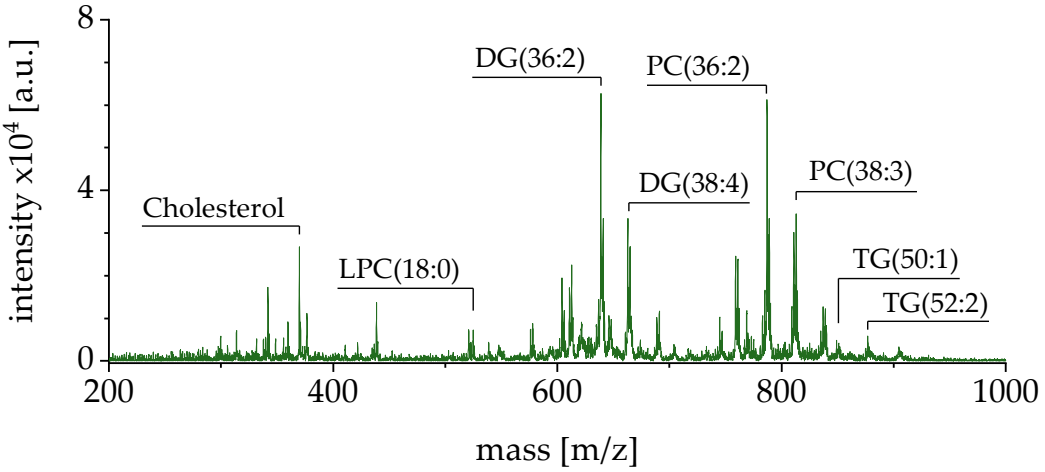

Figure 54: Mass spectrum observed in the transition state from the electrospray- to the plasma ionisation mechanism. This spectrum represents only one scan cycle of the data measured at 1.85 kV plasma voltage amplitude.

However, due to the change in mechanism, the electrospray is not working efficiently any more and the plasma is not operating efficiently yet, so that reduced signal intensities are the consequence.

5.5 Hybrid ionisation by fast switching of the ion source

Last measurements and various investigations in this work have shown that different ideal conditions of the two competing ionisation sources exist. Furthermore, through various modifications and investigation steps these ideal conditions have been achieved, so that the change between the states "ideal electrospray ionisation" and "ideal plasma ionisation" only depends on the activation and deactivation of the plasma. While an electrospray in this

setup ideally operates at a deactivated plasma (0 kV) or low plasma voltages up to 1.4 kV, the best plasma spectrum is achieved at 2 kV voltage amplitude.

In order to avoid the transition state and its reduced signal intensities, another approach to generate hybrid spectra exists. By a fast-switching process of both ion sources, the ideal voltage amplitudes are exploited to generate hybrid spectra. A basic requirement here is that both ionisation processes take place within one scan cycle, as otherwise only an overlay of both spectra is produced by averaging. Accordingly, the duration of a scan cycle is essential for this approach. Based on the fast switching process, this technique is named heated nano-electrospray switched flexible microtube plasma and will be abbreviated as h-nESI-sFμTP in the following.

Ion trap mass spectrometers, as described in chapter 2.2.5, perform a number of different steps within a scan cycle. In the simplest case, after the AGC-controlled prescan, incoming ions are collected for the subsequent determination of the m/z ratios. Since an ion trap can only accept a certain amount of ions, a limitation of incoming ions is necessary. The parameter responsible for this limitation is the injection time. Specified in milliseconds, this can be set manually in the MS software. However, using the automatic gain control is more common. The amount of ions is pre-defined here and the mass spectrometer determines the required injection time by the prescan.

In theorie, the time of the injection process $t_{inj.}$ consists of the two timed equal periods of electrospray- and plasma ionisation with a duration of $t_{sw.}$.

Eq. 22

$$t_{inj.} \geq 2 \cdot t_{sw.}$$

Converted to frequencies ($f = \frac{1}{t}$), this results in:

Eq. 23

$$\frac{1}{f_{inj.}} \geq 2 \cdot \frac{1}{f_{sw.}}$$

A function, generated by an external function generator, is able to control the plasma by the wave crest (plasma voltage on) and a wave trough (plasma voltage off), which means that both processes are present in one period.

Therefore, the plasma activation frequency $f_{act.}$ must be equal or larger than the injection frequency.

Eq. 24

$$f_{act.} \geq f_{inj.}$$

If this condition is fulfilled, every injection cycle contains an electrospray and a plasma ionisation process. This situation is schematically drawn in Figure 55a. Aimed injection times of a Thermo LTQ MS device are typically below one millisecond. Assuming an injection time of 1 ms leads to injection frequencies of 1000 Hz. Consequently, $f_{act.}$ should be $\geq$ 1000 Hz. The basic frequency of the AC plasma high-voltage generator for plasma ignition remains unchanged at 20 kHz, which theoretically corresponds to 40 individual plasma ignitions in the positive half cycle and 80 ignitions in the full period of a 1 ms ion injection cycle.

If the condition of Eq. 24 is not fulfilled, it can lead to unbalanced signal ratios between the electrospray- and plasma-based generated ion signals. For example, if only the half activation frequency is used (500 Hz) so that $f_{act.} = \frac{1}{2} \cdot f_{inj.}$, different artefacts may occur. A phase shift of exactly half a period of the ionisation frequency will produce balanced hybrid spectra (Figure 55b). However, if the phases are exactly synchronised in position (Figure 55c), no hybrid spectra will be produced, since one injection cycle is supplied either by the electrospray or by the plasma. It should be noted that Figure 55 shows a

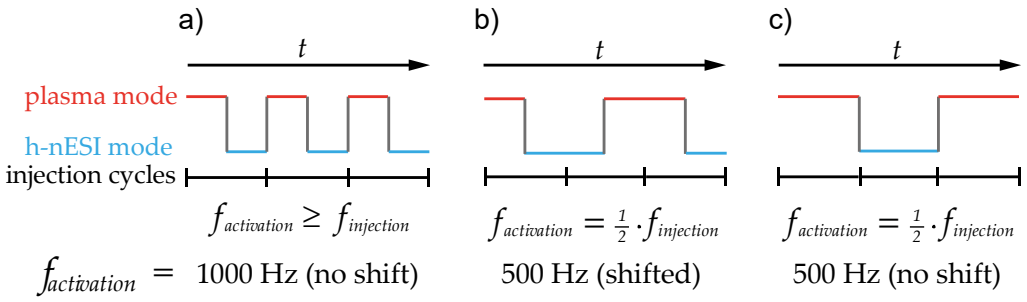

Figure 55: Schematic representation of three possible signal characteristics of injection cycle and ionisation modes. On the left, the activation frequency is larger or equal to the injection period of 1000 Hz. The other two diagrams show a halfed activation frequency (500 Hz) with and without shifting by half a period.

schematic representation of the injection time, other scan cycle processes are not included.

Since the activation frequency of the ion source cannot be triggered by trigger pulses of the MS, an exact superposition of both frequencies as well as an exact shift of the activation frequency by half a period of $f_{inj.}$ is very unlikely. The most probable scenario is a random shift which results in different unbalanced signal ratios in the spectra. Accordingly, hybrid spectra are formed, but they could be associated with large errors and thus standard deviations in a measurment of several scan cycles.

In order to evaluate an optimal plasma activation frequency, a variation of this has been performed in the range from 1 Hz to 2000 Hz. As already described, the plasma voltage is generated by an in-house built square wave high voltage generator. This also provides the connection of an external function generator via TTL signal transmission. With the help of the external function generator (HM8130, HAMEG) the basic plasma frequency of 20 kHz can be overlaid with a square wave function specified by the external function generator, thus activates and deactivates the plasma. This enables a successive activation of both sources and finally leads to the switching between the two ionisation techniques in a suitable frequency range.

A limitation in the switching frequency of the plasma HV generator has been observed before the experiment was performed. When comparing the activation frequency applied by the external function generator with the voltage output of the plasma HV generator using an oscilloscope, errors in the function become increasingly apparent with activation frequencies above 2000 Hz. This allows a practical use of this combination only up to frequencies of 2000 Hz.

For the evaluation of this experiment the ion currents of the representatives PC(36:2), DG(36:2) as well as cholesterol are acquired. Thirteen different activation frequencies have been measured between 1 Hz and 2000 Hz. Each measurement corresponds to 50 scan cycles. To exclude unidentifiable averaging artefacts in these fast ionisation processes, the spectra are recorded

with a micro scan number of one. Since the standard deviation depends on the signal intensity, it is difficult to compare the standard deviations of different signal heights. For this reason, the relative standard deviation is used here. This value is normalised to the intensity and therefore independent from different signal heights. The signal intensity is represented by the average of all acquired scans of a measurement. Both parameters, the relative standard deviation and the averaged intensity, are shown in the diagrams of Figure 56 as a function of the activation frequency. Using selected ion chromatograms in Figure 57, certain unintended processes like averaging artefacts can be identified easier.

The entire experiment has been performed twice with the AGC set to a target number of ions of $5 \cdot 10^4$ and twice without the AGC and an injection time of 1 ms. Only the first series of the measurements is shown here in order to maintain the focus of this manuscript. The diagrams of the second measurements can be found in Figures A10 – A11 of the appendix. In mass spectrometry analysis, measurements are usually performed with AGC. For this reason, the results of the measurement with activated AGC are presented and discussed first.

In the range of very low frequencies between 1 Hz - 100 Hz, the intensities of the lipids in Figure 56a show strongly different ion signal profiles. While the PC(36:2) increases only slightly, the DG(36:2) increases strongly. The cholesterol signal, on the other hand, slightly decreases in intensity. The relative standard deviation in Figure 56b indicates very large errors for all three signals. Here activation frequencies below 100 Hz are too low and several subsequent spectra are obtained solely by electrospray or plasma-loaded injection cycles. This cannot be derived from the signal intensities or the relative standard deviations of Figure 56, but it is recognisable in the ion chromatograms of Figure 57a and 57b on page 124. As expected, the switching processes are clearly visible in the spectra acquired with frequencies between 1 Hz and 20 Hz. At these frequencies several subsequent scan cycles represent only one ionisation process. In addition to this, an anti-cyclic characteristic of the polar and the less polar species can be observed and is highlighted by grey

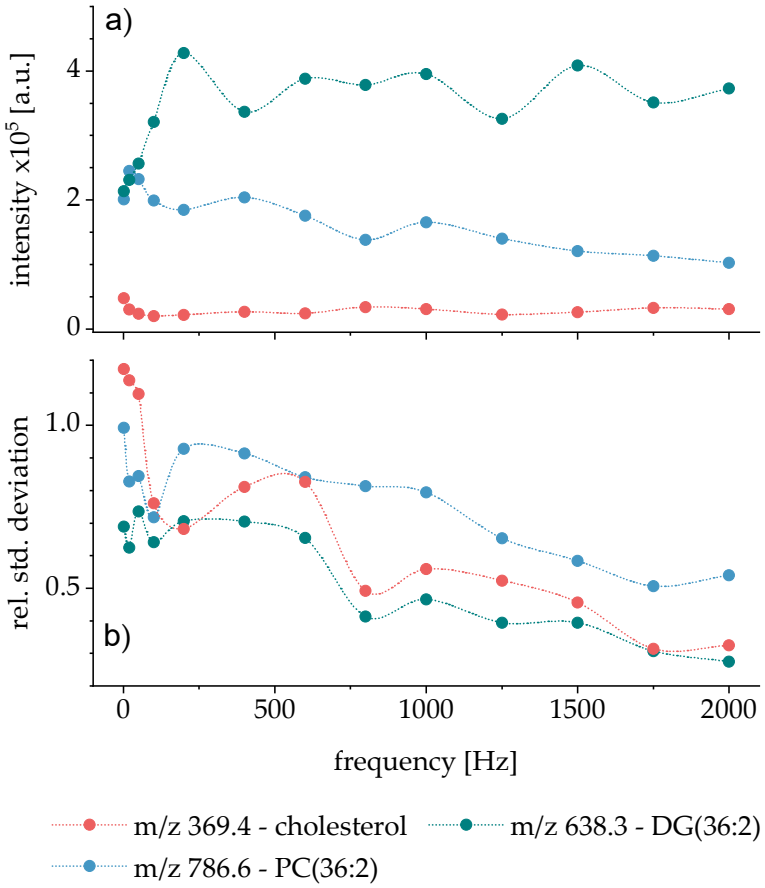

Figure 56: Variation of the activation frequency measured with automatic gain control. By the AGC applied injection times are 0.45 ms on average. The upper diagram shows the signal intensities as a function of the activation frequency. The signal intensities reache their maximum early and remain constant. In b the corresponding value of the relative standard deviation decreases with increasing frequency over the entire measurement range. Each data point consists of 50 scans.

bars. Therefore, no hybrid spectra can be generated at these frequencies. The unexpected small number of only 1 or 2 subsequential spectra formed by a single ionisation process at 20 Hz can be explained by the lenght of the entire scan cycle of 120 ms.

Above 200 Hz the signal intensities reach a plateau and change only slightly even at higher frequencies. Additionally, the relative standard deviation at activation frequencies of ≥ 600 Hz decreases, especially for the less polar compounds, which indicates an increasing signal stability. From here the

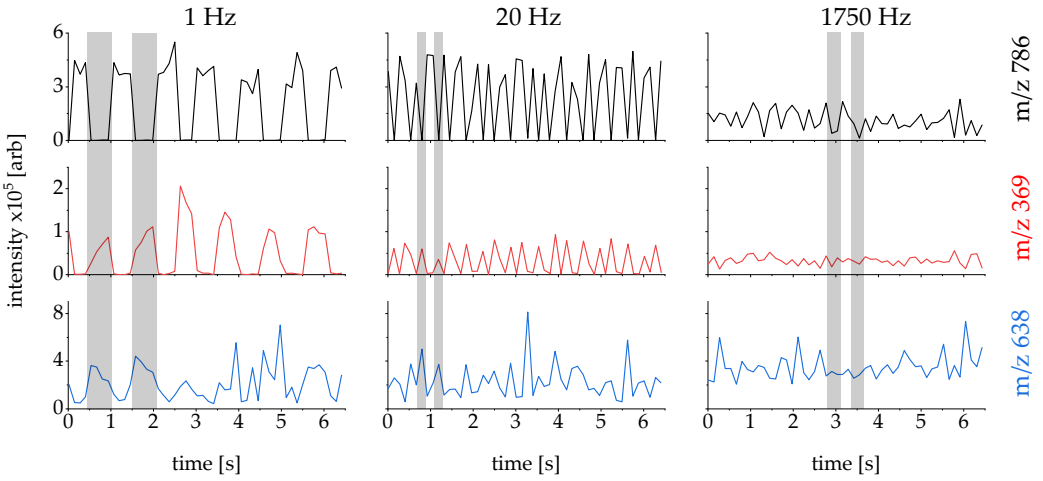

Figure 57: Ion chromatograms of three representatives at selected frequencies. At 1 Hz as well as at 20 Hz, an anticyclic charachteristic of the polar and less polar lipids can be observed. This characteristic is marked in grey bars and disappears with increasing activation frequency.

amount of hybrid spectra in a measurement increases. At 1750 Hz the relative standard deviation seems to reache a minimum. Here further increase in frequency contributes little to no further signal stability and hybrid mass spectra can be detected in every single scan cycle. In theory, an injection time of 0.45 ms corresponds to a frequency of 2222 Hz. This means that an RSD minimum appears here somewhat earlier than expected.

The Figure 58 shows a spectrum of one single scan cycle acquired with a micro scan number of one. Similar to the spectrum of the transition state in Figure 54 on page 118, characteristic ion signals of both ionisation processes can be detected simultaneously. The instrumental effort for hybrid ionisation generated by the fast switching process is higher compared to the hybrid ionization via transition state, but the signal stability and ion yield is significantly increased. For example the absolute intensity of the base peak (signal m/z 638.3) with $3 \cdot 10^5$ is increased compared to that of the transition state with $6 \cdot 10^4$.

When using the AGC, it has to be considered that during the analytical MS run a prescan is performed prior to an injection cycle which calculates the injection time under consideration of the ion target setting. Deactivating the

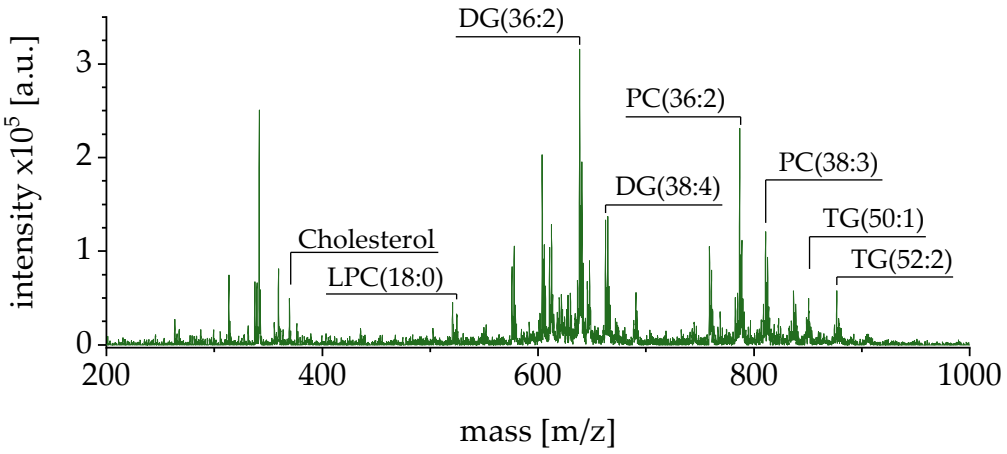

Figure 58: Hybrid mass spectrum of the liver sample generated by the fast switching process of the dual ionisation source at an activation frequency of 1750 Hz. Polar as well as less polar compounds can be identified. This spectrum represents only one single scan cycle with a micro scan number of one and an activated AGC.

AGC and setting the injection time to the fixed value of 1 ms surprisingly reduces the total scan time to 80 ms (compared to 120 ms with AGC). Although the injection time is approximately doubled, the total scan time is reduced by 1/3. Therefore, other scan procedures of the entire scan cycle are skipped when the AGC is switched off.

Due to the nearly doubled injection time, more switching processes can be performed within one ion injection cycle. Accordingly, it can be assumed that the signal stability and thus hybrid spectra occur at lower activation frequencies compared to the measurement with AGC. The results of this measurement with a fixed injection time of 1 ms are depicted in Figure 59. It should be mentioned here that the signals are two orders of magnitude lower than those measured with an activated AGC. This is due to the fact that the automatic gain control also regulates the electronic signal amplification. With deactivated AGC no signal amplification exists and the signals are reduced. However, this does not affect the signal quality as the signal-to-noise remains the same.

Basically, the shape of the averaged intensities and the relative standard deviations of the three different ion signals in Figure 59 are similar to those of the measurement with AGC in Figure 56. The maximum intensities are

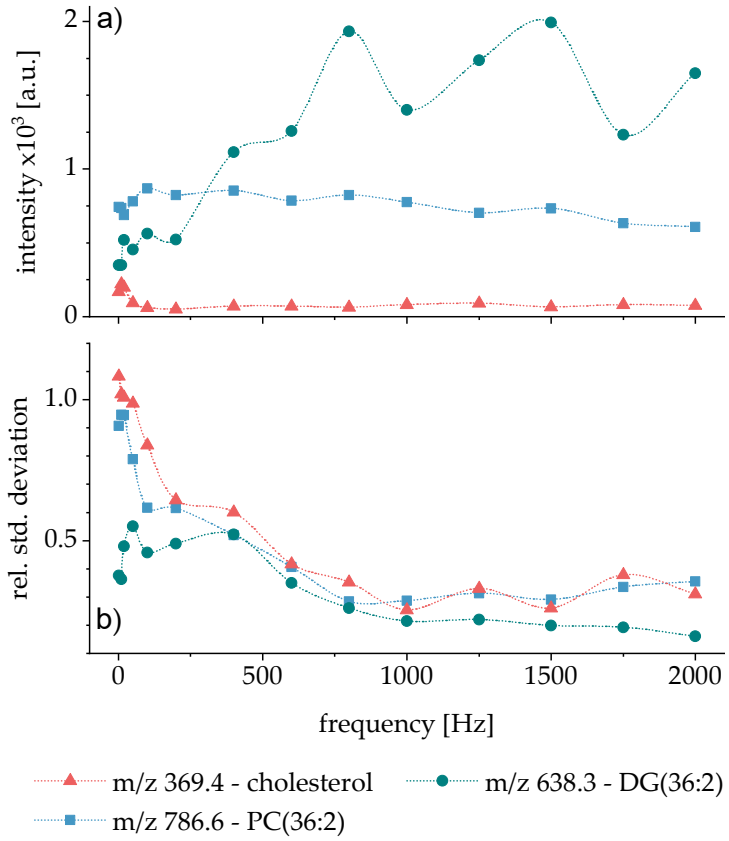

Figure 59: Variation of the activation frequency measured without the AGC. The injection time is set to 1 ms. Signal intensities reach a plateau at higher frequencies compared to the measurement with AGC. In contrast, the relative standard deviation decreases earlier and reaches lower values. Each data point consists of 50 scans.

reached here at higher activation frequencies compared to the measurement with AGC. However, this measurement clearly shows its advantages in the relative standard deviation. While the measurement with AGC only reaches a relative standard deviation of 0.5 at frequencies above 1500 Hz and the potential seems to be exhausted, the measurement with deactivated AGC already reaches this value at 400 Hz. At 1000 Hz, the RSD of the ion currents are below 0.3 and reach a minimum or drop only marginally afterwards. Relative standard deviations of 0.3 or less occur in measurements with AGC only at frequencies above 1750 Hz.

It is noticeable that the relative standard deviations of the polar and less polar compounds diverge significantly less in the measurement without AGC

compared to that with activated AGC (Figure 56b & Figure 59b). Here, at frequencies above of 100 Hz, the relative standard deviations of all signals remain close to each other and have exactly the same profile. This is not given in the first case (activated AGC, Figure 56b on page 123).

Throughout all measurements the intensities of the electrospray signals decrease slightly with increasing activation frequency. This is more pronounced in the measurement with AGC. This trend also can be seen in the spectra of Figure 60. Here both spectra represent an average of the entire MS run with 50 scan cycles.

The spectrum with activated AGC at 1750 Hz on the left clearly shows at m/z 786.6 an SNR reduced by half (SNR = 16) of the electrospray-generated PC(36:2) compared to that of the measurement without AGC at 1000 Hz on the right. If activation frequencies of 3000 Hz are used, the electrospray signals are largely reduced, but can be amplified again by increasing the electrospray voltage to 3.2 kV. This shows that the electrospray seems to respond to an increase in plasma frequency in a similar way to an increase in plasma voltage. From experiments with dielectric barrier nano-electrospray (DB-ESI) sources

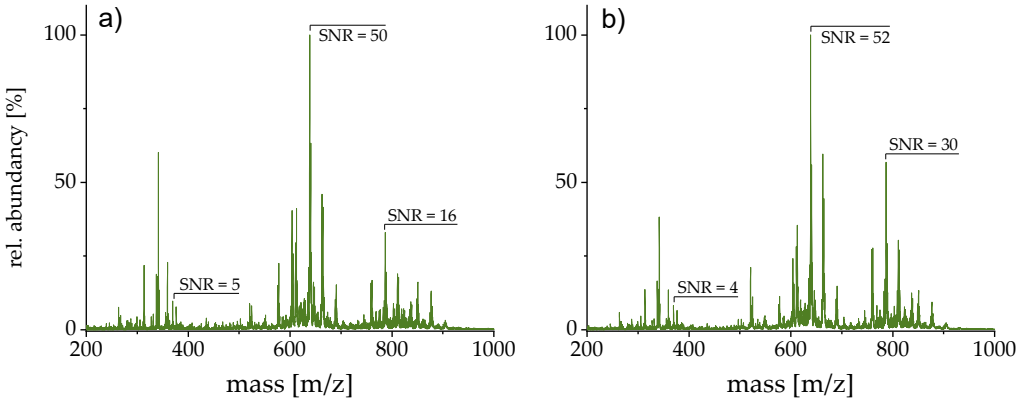

Figure 60: Comparison of the liver spectra generated with the h-nESI-sFμTP in comibination with acitvated AGC on the left and deactivated AGC on the right. In the best measurement with activated AGC at 1750 Hz the signal intensities of polar lipids are reduced compared to those of the best measurement with deactivated AGC at 1000 Hz. In both cases the SNR is divided by 10^4.

it is known that they operate (depending on the distance of the electrode to the emitter tip) efficiently only at frequencies of < 1000 Hz [126,127]. This could indicate that the AC plasma becomes an increasing continuous character for the DC electrospray process as the frequency increases. Charge effects on the glass surface of the plasma capillary, which are also responsible for the difference between plasma ignition voltages and operating voltages, could also be responsible for this quasi-continuous potential at the plasma capillary and thus increasingly influence the electrospray.

Furthermore, a type of anticyclic characteristics of the ion currents, as marked in grey in Figure 57, on closer examination appear not only at low frequencies, but also occur in higher frequencies too, even in another form. In order to examine these artefacts, the comprehensive chart in Figure 61 presents the appearance of hybrid spectra and the ion current courses of the measurement with and without AGC. Here the ion chromatograms of the polar PC(36:2) (blue) and the less polar cholesterol (red) are shown on the right of Figure 61 to highlight the observations. All aspects are sorted by an increasing frequency from top to bottom. Selected sections are marked in grey to clarify the anti-cyclic characteristics in the ion chromatograms of Figure 61.

For this purpose, it is important to keep the theoretically expected frequencies for hybrid ionisation in mind. With activated AGC, an injection frequency or plasma activation frequency of 2222 Hz should be required to generate stable hybrid spectra. Compared to this, the measurement without AGC (fixed injection time of 1 ms) should be generated by an activation frequency of 1000 Hz.

As shown in Figure 61 in the measurement with AGC, the first hybrid spectra can be observed from 100 Hz and in the measurement without AGC from 50 Hz. However, these are only rare and seem to appear completely random. From 800 Hz in the case with AGC and from 400 Hz without AGC, the amount of hybrid spectra increases significantly, but long time periods (~0.8 s) with anti-cyclic characteristics occur, which are exemplary marked in grey. Here, as described in Figure 55, Eq. 24 is not fullfilled and a randomly

Figure 61: Tabular diagram to show and interpret the observations and results of the measurement of the variation of the plasma activation frequency.

shift of the ionisation periods within the injection cycles produce unbalanced signal intensies between electrospray- and plasma-generated signals that show a wave-shaped behavior.

As expected, these wave-shaped artefacts fade out with increasing the activation frequency. At frequency increase up to 1750 Hz (AGC on) and 1000 Hz (AGC off) and decreasing relative standard deviation, these anti-cyclic characteristics are no longer observable and stable hybrid spectra can be achieved. Therefore, the measurement without AGC thus matches the theoretically expected frequency for stable hybrid spectra very accurately at 1000 Hz. The measurement with AGC shows a deviation with 1750 Hz as this is below 2222 Hz, which could be caused by the variation of the injection times. Due to the prescan, the injection time varies between 0.313 and 0.658 ms, resulting in an average injection time of 0.45 ms.

In summary, it can be stated that the occurrence of hybrid spectra as well as the wave-shaped artefacts in the measurement without AGC occur at about half the frequency of the measurement with AGC. A plausible reason for this is the double injection time in the case of the measurement without AGC. Therefore, when using the h-nESI-sFμTP approach, a somewhat higher ion trap injection time is useful to generate hybrid spectra at lower frequencies. On the other hand, increasing the value of the ion target setting (AGC) acts in the same way and leads to an increase in the injection time. This assumption is supposed by a third measurement which is not presented here. In this measurement an activated AGC with an increased ion target setting of $1 \cdot 10^5$ injection is performed and results in injection times of 0.9 ms. Here, the signals show the same behavior as in the measurement without the AGC.

Finally, the signal stability or relative standard deviation approximately below 30 % (AGC off) refers to acquisitions with one micro scan per scan cycle. In order to compare these values with the first nESI-FμTP approach, three acquired spectra (of the heated nESI-sFμTP) have been averaged to calculate the relative standard deviation. This difference in the acquisition and calculation makes a small difference in reults, but is negligible for a first

estimation and comparison. The results of the h-nESI-sFμTP measurement are given in Table 12.

As expected, the relative standard deviations are somewhat higher in the measurement with AGC than in the measurement without AGC. The values of both measurements, but especially the one without AGC, shows clear improvements to the first nESI-FμTP approach. Table 5 on page 49 (chapter 3.3) shows a value of 221 % for the PC(36:2) and a value of 19.2 % for cholesterol in the plasma mode. The nESI reference shows a value of 60.2 % for cholesterol. Still, the stability of the nESI reference in relation to the polar lipid of 6.4 % is not achieved, but both values of the heated nESI-sFμTP without AGC are less than 15 %, which corresponds to a considerable increase in the signal stability compared to the first nESI-FμTP approach. The latter is referred as "good signal quality" in the MS acquisition software Tune Plus.

Table 12: Calculated relative standard deviations of the h-nESI-sFμTP approach for the comparison with RSD of the nESI-FμTP approach and the nESI reference of chapter 3.0.

Signal	Rel. standard deviation
AGC Off, 1000 Hz – PC(36:2)	11.6 %
AGC Off, 1000 Hz – cholesterol	14.1 %
AGC On, 1750 Hz – PC(36:2)	24.0 %
AGC On, 1750 Hz – cholesterol	17.1 %

5.6 Performance of the heated nESI-sFµTP approach

Some of the most important parameters for the performance evaluation of analytical techniques have already been presented and determined in the sections on the nESI-FµTP ion source. Instead of evaluating and discussing the determination of these parameters for the h-nESI-sFµTP approach too, this chapter compares the h-nESI-sFµTP approach with commercially available techniques. For this purpose, the Avanti liver extract has been analysed with seven different modes and techniques. For this comparison, the signal-to-noise ratios (SNR) of the relevant lipids at m/z 369.4, m/z 638.3, m/z 786.6 and m/z 850.5 have been calculated.

Among the commercial techniques there are an nESI (Nanospray Ion Source, Thermo ScientificTM), a HESI (IonMax Interface, HESI Probe, Thermo ScientificTM) and an APCI ion source (IonMax Interface, API Source, Thermo ScientificTM) which have already been used in different chapters of this work. The h-nESI-FµTP technology developed here makes different ionisation modes accessible. These include the heated nano-electrospray and a nano-thermospray with the flexible microtube plasma for ionisation (nTS-FµTP) as well as the hybrid ionisation approaches that are accessible by the transition mode and the fast switching plasma voltage approach. The nTS-FµTP-mode has not been mentioned in this form before, but represents the h-nESI-FµTP where the sheath gas flow has been deactivated as described and shown in Figure 52, so that the nESI spray is interrupted to create a kind of thermospray. Instead of a corona needle, as used in an APCI, the FµTP is used as ionisation technique. For the evaluation of the h-nESI-sFµTP approach, the measurement at 1750 Hz with activated AGC has been used here.

For the four modes of the heated nESI-FµTP setup, namely nESI, h-nESI, h-nESI-FµTP and nTS-FµTP three spectra with a microscan number of one

have been acquired, averaged and interpreted. The acquisitions of the three commercially available ion sources were taken during another experiment and acquired with a microscan number of 3. To keep the data comparable, only one scan has been used here for evaluation. As mentioned above, this difference in acquisition parameters makes a slightly mathematical difference, but the difference in intensities and noise behaviour is not significant. The background noise has been estimated using the median (0.5 quantile) at different m/z ranges. Two reasons make this different m/z ratios important for the noise calculation. On the one hand, each ionisation source shows a specific signal pattern of the large number of different compounds in the complex sample. On the other hand, mass spectra often have zero values, which have a strong influence on the results of the noise values. Thus, areas of the mass spectrum have been chosen that have as little zero values as possible. The number of data points along the mass range for evaluating the noise are 300 in every measurement, which corresponds to a mass range of approximately 25 mass units. The ion source parameters sets are listed in the Tables A4a - g. It should be noted that the commercial HESI and APCI sources are not miniaturised ion sources and have been operated at much higher sample flow rates.

Figure 62 shows the calculated results in the form of a bar chart. The commercial techniques are shown on the left while the dual source and its different modes is shown on the right. The commercial unheated nESI Figure 62a shows polar lipids with a very high SNR. Less polar lipids such as cholesterol as well as di- and triacylglycerides are not accessible or only to very low levels. Both the commercial HESI (not miniaturised) and the h-nESI-mode of the h-nESI-FμTP setup (Figure 62b and d) achieve very similar values. However, compared to the commercial nESI, di- and triacylglycerides with low abundance can be detected here. Cholesterol is not sufficiently measurable with all three electrospray techniques.

As expected, the plasma-based ion sources do not show any polar lipid signals. Here less polar compounds are dominant. While the signal ratios in the APCI are very balanced, the miniaturised variant, the nTS-FμTP-mode

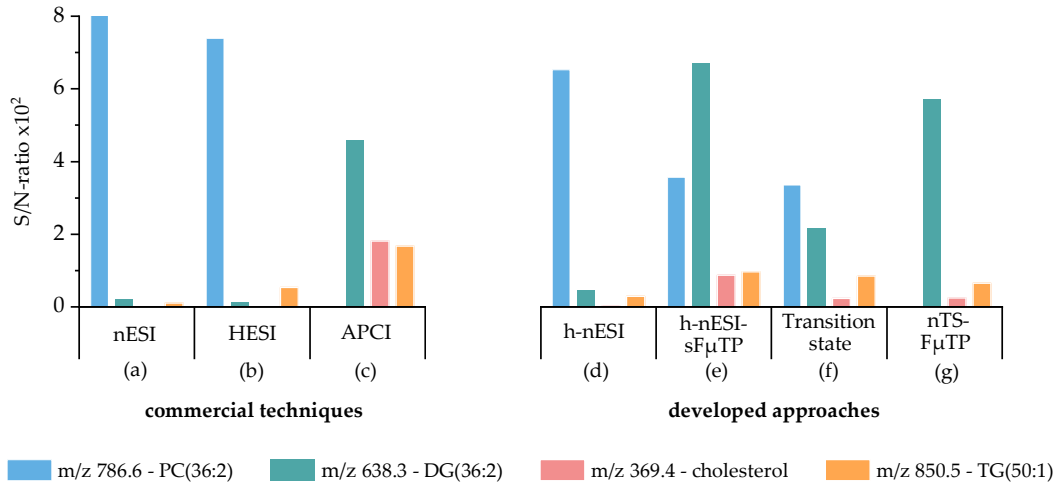

Figure 62: Comparison of three commercial ionisation techniques with the h-nESI-FµTP approach and its different ionisation modes. Here the transition state (f) and the h-nESI-sFµTP approach (e) with a plasma activation frequency of 1750 Hz (with AGC) are the only modes or ion sources that are able to generate hybrid spectra.

of the h-nESI-FµTP, shows very high signals for the diacylglycerides, but cholesterol and triacylglycerides are significantly less intense. The h-nESI-FµTP is the only method that makes hybrid spectra accessible and can do this via two different approaches. As shown in the previous measurements, the transition state, which is generated by setting a specific plasma voltage, produces lower signals related to the less polar lipids.

The signal-to-noise ratios of the polar compounds, on the other hand, are almost the same as in the case of the h-nESI-sFµTP. However, it should be noted that the measurement with activated AGC has been taken into account for the measurement of the switching voltage amplitude (h-nESI-sFµTP). As already shown in the spectrum of Figure 60, increasing the injection time by setting manually or increasing the target ion setting, improves the SNR of the polar compounds by a factor of 2, so that the electrospray signal reaches the intensity of the less polar DG(36:2) and would thus be almost equivalent to the commercial electrospray techniques. Accordingly, the h-nESI-sFµTP approach is the only method that shows both polar and less polar compounds as well as signal to noise ratios that are comparable to commercial technologies. Only the signal stability is reduced compared to the conventional

electrospray ionisation sources. This will have an impact on detection limits, but the benefit of a much larger analyte spectrum has its advantages. It can therefore definitely not be said that the method developed here is better than conventional methods in all aspects. The analytical question of "what is the aim of my analysis and which technique do I need in order to achieve it" still has a major priority.

5.7 Summary and conclusion of the heated nESI-sFμTP

In this chapter, the second stage of development of the coupling between nano-electrospray and flexible micro tube plasma is described, investigated and discussed. From the first and second main chapters of this project, some important aspects for this project have been identified. These include the knowledge that thermal energy is essential for the release of less polar compounds. For this reason, the development of the nESI-FμTP approach introduced at the beginning of this work towards a hybrid ionisation source primarily involves the modification of the nano-electrospray which contains a heating element and a secondary coaxially fitted capillary to the nESI emitter. The latter serves for guiding a sheath gas to protect the electrospray process which is very temperature-sensitive. The heating element consists of a resistance heating wire wound to a coil. In order to estimate the temperatures that occur in this heating element, the temperature at the position of the nESI emitter tip was measured and evaluated as a function of the electrical current flow.

With this modification, it was possible to ionise and detect cholesterol and the other less polar lipids such as DGs and TGs simultaneously and independently of the MS inlet surface temperature. The mass spectrum of the

liver sample generated by h-nESI-FμTP is very similar to the mass spectrum of an APCI source. Despite the higher sample flow rate of the APCI, the approach developed here showed higher signal intensities. Apart from that, the spectra differed only slightly in their signal ratios. Furthermore, this modification now allows the identification of less polar lipids by MS^2 experiment without using an APCI source. The DG(36:2) and the TG(50:1) are identified as DG(18:0/18:2) and a TG(16:0/16:0/18:1) and are selected as representatives for ongoing experiments.

Due to the significantly higher intensities of the DG(36:2) compared to cholesterol, the transition between electrospray ionisation and plasma ionisation can be determined much more sensitively. A specific plasma voltage amplitude for this transition state could be determined at 1.85 kV. Here the electrospray process transitions to a plasma ionisation process and both mechanisms are present simultaneously. Both polar and less polar lipids of the liver sample are detectable in a hybrid spectrum. However, the signals show significantly lower intensities compared to the two initial or single ion sources. Accordingly, this transition state can be used as a hybrid ionisation technique, but it is not very efficient. However, this shows that it is basically possible to generate a hybrid ionisation.

Another possibility to generate hybrid spectra can be achieved by a fast switching process between both ionisation modes. In order to generate a hybrid ionisation in that way, a single scan cycle must include both ionisation processes. Each scan cycle of an ion trap mass spectrometer consists of different steps, whereby the ion injection is of special importance for the fast switching process. The injection time, which represents the duration of the ion accumulation process inside the ion trap, can either be set manually or can be controlled automatically via automatic gain control with the ion target setting of the ion trap. Both possibilities of ion accumulation (with and without AGC) were realised and compared. With active AGC and an ion target setting of $5x10^4$, an injection time of about 0.45 ms resulted. In the case of the measurement without AGC the injection time was set to 1 ms, which was approximately doubled.

In theorie, each injection cycle should be filled with at least one electrospray and one plasma process. A requirement for the stable hybrid spectra is an activation frequency equal or higher than the injection frequency of the ion trap. Depending on the injection time, the first hybrid spectra occur at activation frequencies of 100 Hz (AGC on) and 50 Hz (AGC off). A strong anti-cyclic characteristic can be observed between the electrospray- and plasma ionisation-generated signals. With increasing frequencies this changes into hybrid spectra, but an anticyclic behaviour of the signals can be observed over longer periods. These wave-shaped characteristics or artefacts are created by unbalanced trap fills produced by activation frequencies that are too low.

The characteristics or artefacts start to fade with increasing activation frequency of about 1250 Hz (with AGC) and at 800 Hz (without AGC). Stable hybrid spectra with relative standard deviations of > 30 % and without anti cyclic behaviour can be obtained at plasma activation frequencies of 1750 Hz (with AGC) and 1000 Hz (without AGC).

In principle, it can be stated that the measurement without AGC, that corresponds to a larger injection time, results in overall more stable signals at already lower activation frequencies. The relative standard deviations of the h-nESI-sFμTP approach also show a significant improvement compared to the initial nESI-FμTP approach and are less than 15 % in the measurement without AGC.

Comparing the signal quality by using Signal-to-noise ratios the less polar compounds like DGs and TGs are almost the same for both the measurement with and without AGC. A difference exists in the SNR of the polar lipids like PCs, which is mainly related to the injection time.

Finally, the h-nESI-sFμTP approach and its different modes have been compared with commercial ionisation techniques. As expected, only the h-nESI-FμTP with the two approaches of "transition mode" and "fast plasma voltage swichting" is able to ionise polar and less polar compounds simultaneously within one MS injection cycle and consequently to generate hybrid spectra.

From a performance point of view, the hybrid ion source developed here with the h-nESI-sFμTP approach compares very well with already established, commercial techniques. The slightly less efficient measurement with AGC (or short injection times) shows signal-to-noise ratios equivalent to the commercial techniques which present the h-nESI-sFμTP as sufficiently effective. Therefore, the development of the h-nESI-FμTP represents a powerful tool to extract more information and new insights from complex samples in a single MS run.

6 Conclusion and outlook

In mass spectrometry, electrospray ionisation is an excellent way of ionising polar compounds. In the analysis of complex samples such as blood or tissue, this technique quickly reaches its limits, as less polar compounds are very difficult and very often inaccessible. Unless a second mass spectrometric analysis with another ionisation technique such as APCI or APPI is applied, only parts of the sample can be analysed successfully and the fraction of less polar compounds remains unknown. To prevent the loss of substantial information in ESI-MS analysis or to avoid additional time-consuming analysis, an ion source is necessary that efficiently ionises both polar and less polar compounds.

Developing a new variant of ionisation is extremely complex and probably not very successful, as the variety of different properties, such as the molecular polarity, is extremely large. A more effective approach is the combination of two ion sources to generate hybrid spectra, which leads to the starting point of this work: The coupling of a nano-electrospray and a flexible micro tube plasma, which was investigated and evaluated in detail in the first main chapter of the nESI-FμTP approach.

Detailed summaries as well as advantages and disadvantages of all the techniques and approaches introduced here have already been extensively presented and discussed in the conclusions of the respective state of development. For this reason, the overall process or course of development of

this work is highlighted here but without going into detailed parameters or results.

A complex liver extract containing a large number of polar and less polar compounds has been used to investigate the performance of each state of development. In addition to the nESI-mode, which can be used to ionise polar lipids, the nESI-FμTP approach has shown that very high cholesterol signals can be measured by activating the plasma. In order to investigate this combination as technique for analysing cholesterol in electrospray mass spectrometry, some important parameters such as long-term stability, reproducibility, linear dynamic range, limit of detection and interferences with cholesteryl esters have been determined and assessed. As powerful as this approach of a consecutive ionisation source is, two aspects are of great disadvantage. On the one hand, the significantly larger number of less polar lipids in the liver sample can only be accessed by increasing the MS inlet capillary temperature resulting in a signal reduction of the cholesterol. On the other hand, a simultaneous or hybrid ionisation is not possible with this technique because of the antagonistic effects between the electrospray and plasma processes. The technical realisation of this combination becomes the major challenge. The transition between both processes cannot be stabilised. Nevertheless, this method represents a new possibility for the determination of the less polar cholesterol when analysing liquid samples by electrospray mass spectrometry.

Another coupling was carried out as a side project within the scope of this work. In order to investigate the possibility of a plasma ionisation source with the electrospray-related paperspray ionisation, this resulted in partly surprising and partly helpful insights. When analysing the liver sample by paperspray ionisation mass spectrometry, a corona discharge subsequent to the electrospray mechanism was observed. This fact has been investigated in detail, but has been identified as not efficient. Thus, paper spray ionisation has also been coupled with flexible microtube plasma. The investigation of this coupling confirmed the assumption that temperature (in this case the MS inlet capillary temperature) plays an essential role in the overall process of

evaporation and ionisation of less polar compounds. While the signals from the nESI-FμTP source produced constant and stable signals, even over a longer period of time, the paperspray ionisation stopped completely when the plasma was activated. This consequently led to the interruption of the analyte supply, but instead of an immediate termination of the signal a decay of the intensity could be observed. This indicates that cholesterol and possibly other compounds are deposited on the MS inlet capillary and will be subsequently desorbed by the high temperatures at the MS inlet. Released into the gas phase, these can be ionised here by the plasma. This process probably also plays a role in the first type of coupling (nESI-FμTP). Here the electrospray remains and ensures the analyte supply even when the plasma is activated, presumably a kind of equilibrium is created between deposition and desorption/ionisation of cholesterol that leads to stable signals.

The coupling of the paper spray ionisation and the flexible microtube plasma also demonstrated the detection of less polar volatile compounds, such as the potential oral cancer biomarker candidates 2-nonanone and 3-octanone, which desorb directly from the paper into the gas phase. For this method the detection limits are evaluated finally.

Most importantly, this coupling led to a solution to one of the problems encountered with the nESI-FμTP approach, which concerned the temperature dependence of the desorption processes of cholesterol and the further less polar compounds (DGs and TGs). It led to a modification of the nano electrospray. The nESI has been equipped with a heating element and an additional sheath gas which has led to the coupling of a heated nano-electrospray with the flexible micro tube plasma. Its development and evaluation is described in the third and last major chapter.

After various investigation steps, the h-nESI-FμTP approach showed that it is possible to ionise and detect cholesterol and other less polar compounds simultaneously and independently from the MS inlet capillary surface temperature. The very strong signal of the diacylglycerol DG(36:2) allows the detection of the transition from electrospray mechanism to the plasma based ionisation mechanism much more sensitively when the plasma voltage is

increased stepwise. A transition state can be achieved at a certain plasma voltage. At this voltage, polar and less polar compounds are ionised simultaneously and hybrid spectra can be generated now. However, the ionisation techniques interfere with each other under this condition, so that an efficient ionisation is not possible and the signal intensities are reduced significantly.

By investigating all important ion source parameters, it is possible to change between a very efficient electrospray and an efficient plasma. This switch is now only dependent on one parameter, the plasma voltage, which leads to a new approach. By rapidly activating and deactivating the plasma, hybrid spectra can be generated when the plasma activation frequency exceeds a certain threshold depending on the ion trap injection cycle. The latter leads to very good signal intensities and stabilities. The signal-to-noise ratios of the h-nESI-sFµTP hybrid ion source developed here are thus comparable to those of commercial techniques.

A disadvantage of the h-nESI-FµTP approach is the limitation in plasma activation frequencies up to 2000 Hz. The plasma activation frequency of < 2000 Hz is just sufficient for ion trapped MS devices. Significantly faster devices such as triple quadrupole MS devices can probably not be operated with this technique. However, the latter would have to be evaluated by experiments with non-ion trap devices. Trigger signals from the MS could be helpful, leading to a clocked activation frequency and thus possibly reducing the required plasma activation frequencies.

Another important factor in the ionisation of molecules via ion sources are matrix effects. These are disturbances in the analysis that can be caused by a complicated sample matrix. Since matrix effects occur in ESI as well as in APCI, it is plausible that a combination is also affected by matrix effects. For this reason the standard addition method that considers matrix effects, has been chosen in the present work. Nevertheless, a subsequent study should investigate to assess matrix effects in order to estimate these for other methods.

Furthermore, although the hybrid ion source developed here covers a very large polarity range of molecules, there exist molecules that cannot be ionised with it either. For example, non-polar molecules based exclusively on hydrocarbon atoms such as α-cholestane or β−carotenes or others cannot be ionised and detected with this approach. Here a coupling with an APPI source could be efficient. An APPI source would also have the advantage that no additional voltage source has to be brought into the region of the electrospray, but a challenge can be the often required dopands.

Nevertheless, the independence of the here developed ion source from the mass spectrometer, makes the h-nESI-sFμTP approach also interesting other techniques in which ionisation source are essential. An example for this can be the ion mobility spectrometry. Here the gate time is in the same time regime as the injection time of a mass spectrometer.

Finally, this work focused on the positive ion mode of mass spectrometers. However, for a complete picture of the ion source developed here, the negative mode should also be experimentally investigated and assessed so that the negative ion mode becomes accessible for analysis.

In conclusion, the approach developed here not only provides very satisfactory results, but also demonstrates the possibility of a hybrid ionisation source for mass spectrometry, which can be of great advantage in the rapid untargeted and targeted analysis of complex samples. This technique is not only limited to the analysis of complex samples in clinical or life science fields, but can also be applied to other research fields and may lead to further research insights.

7 Abbreviations, Figures and Tables

7.1 Abbreviations

a.u.	Arbitrary Unit
AAC	Ammonium acetate
AC	Alternating Current
ACN	Acetontrile
AGC	Automatic Gain Control
APCI	Atmospheric Pressure Chemical ionisation
API	Atmospheric Pressure Ionisation
APPI	Atmospheric Pressure Photo Ionisation
CE	Cholesteryl ester
CEM	Chain Ejection Model
CID	Collision Induced Dissociation
CRM	Charge Residue Model
DART	Direct Analysis in Real Time
DBDI	Dielectric Barrier Discharge Ionisation
DC	Direct Current
DG	Diacylglyceride
EIC	Extracted Ion Current
ESI	Electrospray Ionisation
EtOH	Ethanol
FμTP	Flexible Microtube Plasma
FC	Free Cholesterol
FTMS	Fourier-Transformation Mass Spectrometry
HDL	High Density Lipoprotein
HESI	Heated Electrospray Ionisation
h-nESI	Heated nano-Electrospray Ionisation
HV	High Voltage
IEM	Ion Evaporation Model

LC	Lqiuid Chromatography
LDL	Low Density Lipoprotein
LDR	Linear Dynamic Range
LOD	Limit of Detection
LTP	Low Temperature Plasma
MeOH	Methanol
MS	Mass Spectrometer
MSX	Multiplexed MS-MS Scan
nESI	nano-Electrospray Ionisation
PC	Phosphatidylcholine
PE	Phosphatidylethanolamine
PEEK	Polyether Ether Ketone
ppb	part per billion
ppm	part per million
PRM	Parallel Reaction Monitoring
PSI	Paper Spray Ionisation
PSI	Paper Spray
RSD	Relative Standard Deviation
SNR	Signal-to-Noise Ratio
TG	Triacylglyceride
TIC	Total Ion Current
VOC	Volatile Organic Compounds

7.2 Figures

7.3 Tables

8 References

[1] F. Lottspeich (Ed.), Bioanalytik, 3rd ed., Springer, Spektrum, Akad. Verl., Berlin, Heidelberg, 2012.

[2] E.C. Considine, The Search for Clinically Useful Biomarkers of Complex Disease: A Data Analysis Perspective, Metabolites 9 (2019). https://doi.org/10.3390/metabo9070126.

[3] J.H. Gross, Massenspektrometrie: Ein Lehrbuch, Springer Spektrum, Berlin, 2013.

[4] S. Kromidas (Ed.), Das HPLC-MS-Buch für Anwender, Wiley-VCH, Weinheim, Germany, 2017.

[5] M. Yamashita, J.B. Fenn, Electrospray ion source. Another variation on the free-jet theme, J. Phys. Chem. 88 (1984) 4451–4459. https://doi.org/10.1021/j150664a002.

[6] C.S. Ho, C.W.K. Lam, M.H.M. Chan, R.C.K. Cheung, L.K. Law, L.C.W. Lit, K.F. Ng, M.W.M. Suen, H.L. Tai, Electrospray Ionisation Mass Spectrometry: Principles and Clinical Applications, The Clinical Biochemist Reviews 24 (2003) 3–12.

[7] L. Konermann, E. Ahadi, A.D. Rodriguez, S. Vahidi, Unraveling the mechanism of electrospray ionization, Analytical chemistry 85 (2013) 2–9. https://doi.org/10.1021/ac302789c.

[8] M. Mann, The ever expanding scope of electrospray mass spectrometry-a 30 year journey, Nature communications 10 (2019) 3744. https://doi.org/10.1038/s41467-019-11747-z.

[9] J.B. Fenn, M. Mann, C.K. Meng, S.F. Wong, C.M. Whitehouse, Electrospray ionization for mass spectrometry of large biomolecules, Science (New York, N.Y.) 246 (1989) 64–71. https://doi.org/10.1126/science.2675315.

[10] J.B. Fenn, Electrospray wings for molecular elephants (Nobel lecture), Angewandte Chemie (International ed. in English) 42 (2003) 3871–3894. https://doi.org/10.1002/anie.200300605.

[11] A. Albert, C. Engelhard, Characteristics of low-temperature plasma ionization for ambient mass spectrometry compared to electrospray ionization and atmospheric pressure chemical ionization, Anal. Chem. 84 (2012) 10657–10664. https://doi.org/10.1021/ac302287x.

[12] D.I. Carroll, I. Dzidic, R.N. Stillwell, M.G. Horning, E.C. Horning, Subpicogram detection system for gas phase analysis based upon atmospheric pressure ionization (API) mass spectrometry, Anal. Chem. 46 (1974) 706–710. https://doi.org/10.1021/ac60342a009.

[13] M.M. Siegel, K. Tabei, F. Lambert, L. Candela, B. Zoltan, Evaluation of a dual electrospray ionization/atmospheric pressure chemical ionization source at low flow rates (~50 μ L/min) for the analysis of both highly and weakly polar compounds, J. Am. Soc. Mass Spectrom. 9 (1998) 1196–1203. https://doi.org/10.1016/S1044-0305(98)00085-3.

[14] S.-C. Cheng, S.-S. Jhang, M.-Z. Huang, J. Shiea, Simultaneous detection of polar and nonpolar compounds by ambient mass spectrometry with a dual electrospray and atmospheric pressure chemical ionization source, Anal. Chem. 87 (2015) 1743–1748. https://doi.org/10.1021/ac503625m.

[15] D.S. Kulyk, D.J. Swiner, T. Sahraeian, A.K. Badu-Tawiah, Direct Mass Spectrometry Analysis of Complex Mixtures by Nanoelectrospray with Simultaneous Atmospheric Pressure Chemical Ionization and Electrophoretic Separation Capabilities, Anal. Chem. 91 (2019) 11562–11568. https://doi.org/10.1021/acs.analchem.9b01456.

[16] Q. Liu, J. Lan, R. Wu, A. Begley, W. Ge, R. Zenobi, Hybrid Ionization Source Combining Nanoelectrospray and Dielectric Barrier Discharge Ionization for the Simultaneous Detection of Polar and Nonpolar Compounds in Single Cells, Anal. Chem. 94 (2022) 2873–2881. https://doi.org/10.1021/acs.analchem.1c04759.

[17] S. Brandt, F.D. Klute, A. Schütz, U. Marggraf, C. Drees, P. Vogel, W. Vautz, J. Franzke, Flexible Microtube Plasma (FμTP) as an Embedded Ionization Source for a Microchip Mass Spectrometer Interface, Anal. Chem. 90 (2018) 10111–10116. https://doi.org/10.1021/acs.analchem.8b01493.

[18] C. Drees, A. Schütz, G. Niu, J. Franzke, W. Vautz, S. Brandt, Stepwise optimization of a Flexible Microtube Plasma (FμTP) as an ionization source for Ion Mobility Spectrometry, Analytica chimica acta 1127 (2020) 89–97. https://doi.org/10.1016/j.aca.2020.06.018.

[19] A. Knodel, U. Marggraf, N. Ahlmann, S. Brandt, D. Foest, B. Gilbert-López, J. Franzke, Standardization of Sandwich-Structured Cu-Glass Substrates Embedded in a Flexible Diode Laser-Plasma Interface for the Detection of Cholesterol, Anal. Chem. 92 (2020) 4663–4671. https://doi.org/10.1021/acs.analchem.0c00311.

[20] D. Moreno-González, D. Castilla-Fernández, P. Vogel, G. Niu, S. Brandt, C. Drees, J.F. García-Reyes, A. Molina-Díaz, J. Franzke, Evaluation of a novel

controlled-atmosphere flexible microtube plasma soft ionization source for the determination of BTEX in olive oil by headspace-gas chromatography/mass spectrometry, Analytica chimica acta 1179 (2021) 338835. https://doi.org/10.1016/j.aca.2021.338835.

[21] Sebastian Brandt, Entwicklungen und Kombinationen miniaturisierter Probenzufuhr- und Ionisierungssysteme. Dissertation, Fakultät Physik.

[22] P.W. Atkins, J. de Paula, Physikalische Chemie, 4th ed., Wiley-VCH, Weinheim, 2012.

[23] E. Riedel, C. Janiak, Anorganische Chemie, 10th ed., De Gruyter, Berlin, 2022.

[24] A.L. Hickey, C.N. Rowley, Benchmarking quantum chemical methods for the calculation of molecular dipole moments and polarizabilities, J. Phys. Chem. A 118 (2014) 3678–3687. https://doi.org/10.1021/jp502475e.

[25] H.-D. Belitz, W. Grosch, P. Schieberle, Food Chemistry, 4th ed., Springer Berlin Heidelberg; Imprint: Springer, Berlin, Heidelberg, 2009.

[26] J.L. Boyer, Bile formation and secretion, Comprehensive Physiology 3 (2013) 1035–1078. https://doi.org/10.1002/cphy.c120027.

[27] Z. Jastrzebski, J. Kortas, K. Kaczor, J. Antosiewicz, Vitamin D Supplementation Causes a Decrease in Blood Cholesterol in Professional Rowers, Journal of nutritional science and vitaminology 62 (2016) 88–92. https://doi.org/10.3177/jnsv.62.88.

[28] J. Semmens, I. Rouse, L.J. Beilin, J.R. Masarei, Relationship of plasma HDL-cholesterol to testosterone, estradiol, and sex-hormone-binding globulin levels in men and women, Metabolism: clinical and experimental 32 (1983) 428–432. https://doi.org/10.1016/0026-0495(83)90002-1.

[29] E. Ikonen, Cellular cholesterol trafficking and compartmentalization, Nature reviews. Molecular cell biology 9 (2008) 125–138. https://doi.org/10.1038/nrm2336.

[30] M. Maekawa, G.D. Fairn, Complementary probes reveal that phosphatidylserine is required for the proper transbilayer distribution of cholesterol, Journal of cell science 128 (2015) 1422–1433. https://doi.org/10.1242/jcs.164715.

[31] M. Cassader, G. Ruiu, R. Gambino, N. Alemanno, F. Veglia, G. Pagano, Hypercholesterolemia in non-insulin-dependent diabetes mellitus: different effect of simvastatin on VLDL and LDL cholesterol levels, Atherosclerosis 99 (1993) 47–53. https://doi.org/10.1016/0021-9150(93)90049-Z.

[32] L.S. Eberlin, A.L. Dill, A.B. Costa, D.R. Ifa, L. Cheng, T. Masterson, M. Koch, T.L. Ratliff, R.G. Cooks, Cholesterol sulfate imaging in human prostate

cancer tissue by desorption electrospray ionization mass spectrometry, Anal. Chem. 82 (2010) 3430–3434. https://doi.org/10.1021/ac9029482.

[33] J.W. GOFMAN, M. HANIG, H.B. JONES, M.A.A.X. LAUFFER, E.Y. LAWRY, L.A. LEWIS, G.V. MANN, F.E. MOORE, F. OLMSTED, J.F. YEAGER, E.C. ANDRUS, J.H. BARACH, J.W. BEAMS, J.W. FERTIG, I.H. PAGE, J.A. SHANNON, F.J. STARE, P.D. WHITE, Evaluation of Serum Lipoprotein and Cholesterol Measurements as Predictors of Clinical Complications of Atherosclerosis, Circulation 14 (1956) 689–741. https://doi.org/10.1161/01.CIR.14.4.689.

[34] J.L. Goldstein, M.S. Brown, A century of cholesterol and coronaries: from plaques to genes to statins, Cell 161 (2015) 161–172. https://doi.org/10.1016/j.cell.2015.01.036.

[35] M.G. Martín, F. Pfrieger, C.G. Dotti, Cholesterol in brain disease: sometimes determinant and frequently implicated, EMBO reports 15 (2014) 1036–1052. https://doi.org/10.15252/embr.201439225.

[36] F.D. Porter, G.E. Herman, Malformation syndromes caused by disorders of cholesterol synthesis, Journal of lipid research 52 (2011) 6–34. https://doi.org/10.1194/jlr.R009548.

[37] H.J. Pownall, C. Rosales, B.K. Gillard, A.M. Gotto, High-density lipoproteins, reverse cholesterol transport and atherogenesis, Nature reviews. Cardiology 18 (2021) 712–723. https://doi.org/10.1038/s41569-021-00538-z.

[38] C.C. Schwartz, J.M. VandenBroek, P.S. Cooper, Lipoprotein cholesteryl ester production, transfer, and output in vivo in humans, Journal of lipid research 45 (2004) 1594–1607. https://doi.org/10.1194/jlr.M300511-JLR200.

[39] D. Lütjohann, I. Björkhem, S. Friedrichs, A. Kerksiek, A. Lövgren-Sandblom, W.-J. Geilenkeuser, R. Ahrends, I. Andrade, D. Ansorena, I. Astiasarán, L. Baila-Rueda, B. Barriuso, S. Becker, L. Bretillon, R.W. Browne, C. Caccia, U. Ceglarek, A. Cenarro, P.J. Crick, G. Fauler, G. Garcia-Llatas, R. Gray, W.J. Griffiths, H. Gylling, S. Harding, C. Helmschrodt, L. Iuliano, H.-G. Janssen, P. Jones, L. Kaipiainen, F. Kannenberg, M.J. Lagarda, V. Leoni, A.M. Lottenberg, D.S. MacKay, S. Matysik, J. McDonald, M. Menendez-Carreño, S.B. Myrie, V. Sutti Nunes, R.E. Ostlund, E. Polisecki, F. Ramos, T.C. Rideout, E.J. Schaefer, G. Schmitz, Y. Wang, C. Zerbinati, U. Diczfalusy, H.-F. Schött, First international descriptive and interventional survey for cholesterol and non-cholesterol sterol determination by gas- and liquid-chromatography-Urgent need for harmonisation of analytical methods, The Journal of steroid biochemistry and molecular biology 190 (2019) 115–125. https://doi.org/10.1016/j.jsbmb.2019.03.025.

[40] S. Böcker, M.C. Letzel, Z. Lipták, A. Pervukhin, SIRIUS: decomposing isotope patterns for metabolite identification, Bioinformatics (Oxford, England) 25 (2009) 218–224. https://doi.org/10.1093/bioinformatics/btn603.

[41] J. Krank, R.C. Murphy, R.M. Barkley, E. Duchoslav, A. McAnoy, Qualitative analysis and quantitative assessment of changes in neutral glycerol lipid molecular species within cells, Methods in enzymology 432 (2007) 1–20. https://doi.org/10.1016/S0076-6879(07)32001-6.

[42] Sud M., Fahy E., Cotter D., Brown A., Dennis E., Glass C., Murphy R., Raetz C., Russell D. and Subramaniam S., LIPID MAPS Structure Database (LMSD), 2006, https://www.lipidmaps.org/databases/lmsd/browse, accessed 18 April 2023.

[43] C. Stenby Ejsing, Molecular characterization of the lipidome by mass spectrometry. Dresden, Techn. Univ., Diss., 2007.

[44] J.K. Pauling, M. Hermansson, J. Hartler, K. Christiansen, S.F. Gallego, B. Peng, R. Ahrends, C.S. Ejsing, Proposal for a common nomenclature for fragment ions in mass spectra of lipids, PloS one 12 (2017) e0188394. https://doi.org/10.1371/journal.pone.0188394.

[45] J.K. Pauling, M. Hermansson, J. Hartler, K. Christiansen, S.F. Gallego, B. Peng, R. Ahrends, C.S. Ejsing, ALEX123 Lipid Calculator, 2017, http://www.alex123.info/, accessed 23 December 2022.

[46] L.-H. Li, E.P. Dutkiewicz, Y.-C. Huang, H.-B. Zhou, C.-C. Hsu, Analytical methods for cholesterol quantification, Journal of food and drug analysis 27 (2019) 375–386. https://doi.org/10.1016/j.jfda.2018.09.001.

[47] H.C. Köfeler, A. Fauland, G.N. Rechberger, M. Trötzmüller, Mass spectrometry based lipidomics: an overview of technological platforms, Metabolites 2 (2012) 19–38. https://doi.org/10.3390/metabo2010019.

[48] K. Yang, X. Han, Accurate quantification of lipid species by electrospray ionization mass spectrometry - Meet a key challenge in lipidomics, Metabolites 1 (2011) 21–40. https://doi.org/10.3390/metabo1010021.

[49] H.C. Köfeler, R. Ahrends, E.S. Baker, K. Ekroos, X. Han, N. Hoffmann, M. Holčapek, M.R. Wenk, G. Liebisch, Recommendations for good practice in MS-based lipidomics, Journal of lipid research 62 (2021) 100138. https://doi.org/10.1016/j.jlr.2021.100138.

[50] T. Züllig, H.C. Köfeler, HIGH RESOLUTION MASS SPECTROMETRY IN LIPIDOMICS, Mass spectrometry reviews 40 (2021) 162–176. https://doi.org/10.1002/mas.21627.

[51] A. Cappiello (Ed.), Advances in LC-MS instrumentation, 1st ed., Elsevier, Amsterdam, 2007.

[52] R.B. Cody, J.A. Laramée, H.D. Durst, Versatile new ion source for the analysis of materials in open air under ambient conditions, Anal. Chem. 77 (2005) 2297–2302. https://doi.org/10.1021/ac050162j.

[53] J.D. Harper, N.A. Charipar, C.C. Mulligan, X. Zhang, R.G. Cooks, Z. Ouyang, Low-temperature plasma probe for ambient desorption ionization, Anal. Chem. 80 (2008) 9097–9104. https://doi.org/10.1021/ac801641a.

[54] N. Na, M. Zhao, S. Zhang, C. Yang, X. Zhang, Development of a dielectric barrier discharge ion source for ambient mass spectrometry, J. Am. Soc. Mass Spectrom. 18 (2007) 1859–1862. https://doi.org/10.1016/j.jasms.2007.07.027.

[55] H. Hayen, A. Michels, J. Franzke, Dielectric barrier discharge ionization for liquid chromatography/mass spectrometry, Anal. Chem. 81 (2009) 10239–10245. https://doi.org/10.1021/ac902176k.

[56] P. Vogel, U. Marggraf, S. Brandt, J.F. García-Reyes, J. Franzke, Analyte-Tailored Controlled Atmosphere Improves Dielectric Barrier Discharge Ionization Mass Spectrometry Performance, Anal. Chem. 91 (2019) 3733–3739. https://doi.org/10.1021/acs.analchem.9b00112.

[57] A. Schütz, S. Brandt, S. Liedtke, D. Foest, U. Marggraf, J. Franzke, Dielectric Barrier Discharge Ionization of Perfluorinated Compounds, Anal. Chem. 87 (2015) 11415–11419. https://doi.org/10.1021/acs.analchem.5b03538.

[58] D.B. Robb, T.R. Covey, A.P. Bruins, Atmospheric pressure photoionization: an ionization method for liquid chromatography-mass spectrometry, Anal. Chem. 72 (2000) 3653–3659. https://doi.org/10.1021/ac0001636.

[59] T.J. Kauppila, J.A. Syage, T. Benter, Recent developments in atmospheric pressure photoionization-mass spectrometry, Mass spectrometry reviews 36 (2017) 423–449. https://doi.org/10.1002/mas.21477.

[60] F.W. McLafferty, F. Turecek, Interpretation of mass spectra: Zahlr. Tab, 4th ed., University Science Books, Mill Welley, 1993.

[61] R.B. Cole (Ed.), Electrospray ionization mass spectrometry: Fundamentals, instrumentation, and applications, 1st ed., Wiley, New York, NY u.a., 1997.

[62] P. Kebarle, M. Peschke, On the mechanisms by which the charged droplets produced by electrospray lead to gas phase ions, Analytica chimica acta 406 (2000) 11–35. https://doi.org/10.1016/S0003-2670(99)00598-X.

[63] G. Taylor, Disintegration of water drops in an electric field, Proc. R. Soc. Lond. A 280 (1964) 383–397. https://doi.org/10.1098/rspa.1964.0151.

[64] L.T. CHERNEY, Structure of Taylor cone-jets: limit of low flow rates, J. Fluid Mech. 378 (1999) 167–196. https://doi.org/10.1017/S002211209800319X.

[65] A. Gomez, K. Tang, Charge and fission of droplets in electrostatic sprays, Physics of Fluids 6 (1994) 404–414. https://doi.org/10.1063/1.868037.

[66] R.C. Murphy, Challenges in Mass Spectrometry-based Lipidomics of Neutral Lipids, Trends in analytical chemistry TRAC 107 (2018) 91–98. https://doi.org/10.1016/j.trac.2018.07.023.

[67] S.F. Gallego, K. Højlund, C.S. Ejsing, Easy, Fast, and Reproducible Quantification of Cholesterol and Other Lipids in Human Plasma by Combined High Resolution MSX and FTMS Analysis, J. Am. Soc. Mass Spectrom. 29 (2018) 34–41. https://doi.org/10.1007/s13361-017-1829-2.

[68] M. Höring, C.S. Ejsing, M. Hermansson, G. Liebisch, Quantification of Cholesterol and Cholesteryl Ester by Direct Flow Injection High-Resolution Fourier Transform Mass Spectrometry Utilizing Species-Specific Response Factors, Anal. Chem. 91 (2019) 3459–3466. https://doi.org/10.1021/acs.analchem.8b05013.

[69] G. Rovelli, M.I. Jacobs, M.D. Willis, R.J. Rapf, A.M. Prophet, K.R. Wilson, A critical analysis of electrospray techniques for the determination of accelerated rates and mechanisms of chemical reactions in droplets, Chemical science 11 (2020) 13026–13043. https://doi.org/10.1039/d0sc04611f.

[70] N.B. Cech, C.G. Enke, Relating electrospray ionization response to nonpolar character of small peptides, Anal. Chem. 72 (2000) 2717–2723. https://doi.org/10.1021/ac9914869.

[71] S. Müller, Optimierung, Charakterisierung und Anwendung der Dielectric Barrier Discharge Ionisation Source, Technische Universität Dortmund, 2014.

[72] S.S. Hodgman, R.G. Dall, L.J. Byron, K.G.H. Baldwin, S.J. Buckman, A.G. Truscott, Metastable helium: a new determination of the longest atomic excited-state lifetime, Physical review letters 103 (2009) 53002. https://doi.org/10.1103/PhysRevLett.103.053002.

[73] M.v. Ardenne, G. Musiol, U. Klemradt (Eds.), Effekte der Physik und ihre Anwendungen, 3rd ed., Deutsch, Frankfurt am Main, 2005.

[74] E.C. Horning, M.G. Horning, D.I. Carroll, I. Dzidic, R.N. Stillwell, New picogram detection system based on a mass spectrometer with an external ionization source at atmospheric pressure, Anal. Chem. 45 (1973) 936–943. https://doi.org/10.1021/ac60328a035.

[75] P. Vogel, C. Lazarou, O. Gazeli, S. Brandt, J. Franzke, D. Moreno-González, Study of Controlled Atmosphere Flexible Microtube Plasma Soft Ionization Mass Spectrometry for Detection of Volatile Organic Compounds as Potential Biomarkers in Saliva for Cancer, Anal. Chem. 92 (2020) 9722–9729. https://doi.org/10.1021/acs.analchem.0c01063.

[76] M. Allers, A.T. Kirk, M. Eckermann, C. Schaefer, D. Erdogdu, W. Wissdorf, T. Benter, S. Zimmermann, Positive Reactant Ion Formation in High Kinetic Energy Ion Mobility Spectrometry (HiKE-IMS), J. Am. Soc. Mass Spectrom. 31 (2020) 1291–1301. https://doi.org/10.1021/jasms.0c00114.

[77] S.B. Olenici-Craciunescu, A. Michels, C. Meyer, R. Heming, S. Tombrink, W. Vautz, J. Franzke, Characterization of a capillary dielectric barrier plasma jet for use as a soft ionization source by optical emission and ion mobility spectrometry, Spectrochimica Acta Part B: Atomic Spectroscopy 64 (2009) 1253–1258. https://doi.org/10.1016/j.sab.2009.10.001.

[78] A. von Keudell, V. Schulz-von der gathen, Einführung in die Plasmaphysik II: Niedertemperaturplasmen - Vorlesungsskript. Wintersemester 2022/23, Bochum, 2023.

[79] S. Brandt, Entwicklungen und Kombinationen miniaturisierter Probenzufuhr- und Ionisierungssysteme, TU Dortmund, 2020.

[80] G. Kaklamanos, E. Aprea, G. Theodoridis, Mass Spectrometry: Principles and Instrumentation, in: Encyclopedia of Food and Health, Elsevier, 2016, pp. 661–668.

[81] Thermo Fisher Scientific Inc., LTQ Series Hardware Manual, 2015, https://assets.thermofisher.com/TFS-Assets/CMD/manuals/Man-97055-97072-LTQ-Series-Hardware-Man9705597072-EN.pdf, accessed 4 September 2023.

[82] R.A. Zubarev, A. Makarov, Orbitrap mass spectrometry, Anal. Chem. 85 (2013) 5288–5296. https://doi.org/10.1021/ac4001223.

[83] Thermo Fisher Scientific Inc., Scan Speed vs Cycle Time on a Ion Trap Mass Spectrometer - Product Support Bulletin PSB 119, https://assets.thermofisher.com/TFS-Assets/CMD/Warranties/PSB119-Scan-Speed-vs-Cycle-Time-EN.pdf, accessed 5 September 2023.

[84] D.A. Skoog, J.J. Leary, Instrumentelle Analytik: Grundlagen - Geräte - Anwendungen ; mit 86 Tabellen, Springer, Berlin, Heidelberg, New York, Barcelona, Budapest, Hongkong, London, Mailand, Paris, Santa Clara, Singapur, Tokio, 1996.

[85] K. Cammann, Instrumentelle analytische Chemie: Verfahren, Anwendungen und Qualitätssicherung, 1st ed., Spektrum Akademischer Verlag, Heidelberg, 2011.

[86] J. Inczédy, T. Lengyel, A.M. Ure, Compendium of analytical nomenclature: Definitive rules 1997, 3rd ed., Blackwell Science, Osney Mead, Oxford, Malden, MA, 2000, 1998.

[87] P.A. Tipler, Physik, 1st ed., Spektrum, Akad. Verl., Heidelberg, 1995.

[88] M. Belter, A. Sajnóg, D. Barałkiewicz, Over a century of detection and quantification capabilities in analytical chemistry--historical overview and trends, Talanta 129 (2014) 606–616. https://doi.org/10.1016/j.talanta.2014.05.018.

[89] A. Hubaux, G. Vos, Decision and detection limits for calibration curves, Anal. Chem. 42 (1970) 849–855. https://doi.org/10.1021/ac60290a013.

[90] R. Baker, High-performance liquid chromatography-ultraviolet method for the simultaneous determination of potential synthetic and hydrolytic impurities in urapidil fumarate, Journal of chromatography 393 (1987) 447–453. https://doi.org/10.1016/S0021-9673(01)94243-8.

[91] Y. Hayashi, R. Matsuda, R.B. Poe, Probabilistic approach to confidence intervals of linear calibration, The Analyst 121 (1996) 591. https://doi.org/10.1039/AN9962100591.

[92] J. Tellinghuisen, Calibration: Detection, Quantification, and Confidence Limits Are (Almost) Exact When the Data Variance Function Is Known, Anal. Chem. 91 (2019) 8715–8722. https://doi.org/10.1021/acs.analchem.9b00119.

[93] Avanti Polar Lipids Inc., Phospholipid Profile, Liver Total Lipids Extract (Bovine) 181104, https://avantilipids.com/product/181104, accessed 28 April 2023.

[94] A. Tran, L. Wan, Z. Xu, J.M. Haro, B. Li, J.W. Jones, Lithium Hydroxide Hydrolysis Combined with MALDI TOF Mass Spectrometry for Rapid Sphingolipid Detection, J. Am. Soc. Mass Spectrom. 32 (2021) 289–300. https://doi.org/10.1021/jasms.0c00322.

[95] G. Vale, S.A. Martin, M.A. Mitsche, B.M. Thompson, K.M. Eckert, J.G. McDonald, Three-phase liquid extraction: a simple and fast method for lipidomic workflows, Journal of lipid research 60 (2019) 694–706. https://doi.org/10.1194/jlr.D090795.

[96] C.S. Ejsing, E. Duchoslav, J. Sampaio, K. Simons, R. Bonner, C. Thiele, K. Ekroos, A. Shevchenko, Automated identification and quantification of glycerophospholipid molecular species by multiple precursor ion scanning, Anal. Chem. 78 (2006) 6202–6214. https://doi.org/10.1021/ac060545x.

[97] C. Wu, D.R. Ifa, N.E. Manicke, R.G. Cooks, Rapid, direct analysis of cholesterol by charge labeling in reactive desorption electrospray ionization, Anal. Chem. 81 (2009) 7618–7624. https://doi.org/10.1021/ac901003u.

[98] D. Foest, A. Knodel, R. Ahrends, C. Coman, J. Franzke, S. Brandt, Flexible Microtube Plasma for the Consecutive-Ionization of Cholesterol in Nano-

Electrospray Mass Spectrometry, Anal. Chem. 95 (2023) 8423–8432. https://doi.org/10.1021/acs.analchem.2c04052.

[99] H.M.N.H. Irving, Compendium of analytical nomenclature Definitive rules 1977, Pergamon Press, Oxford, England, Elmsford, New York, 1978.

[100] I.W. Duncan, P.H. Culbreth, C.A. Burtis, Determination of free, total, and esterified cholesterol by high-performance liquid chromatography, Journal of chromatography 162 (1979) 281–292. https://doi.org/10.1016/S0378-4347(00)81515-7.

[101] A. Álvarez-Sala, G. Garcia-Llatas, R. Barberá, M.J. Lagarda, DETERMINATION OF CHOLESTEROL IN HUMAN MILK: AN ALTERNATIVE TO CHROMATOGRAPHIC METHODS, Nutricion hospitalaria 32 (2015) 1535–1540. https://doi.org/10.3305/nh.2015.32.4.9139.

[102] C.S.J.W. Briche, D. Carter, K.S. Webb, Comparison of gas chromatography and liquid chromatography mass spectrometric measurements for high accuracy analysis of cholesterol in human serum by isotope dilution mass spectrometry, Rapid communications in mass spectrometry RCM 16 (2002) 848–853. https://doi.org/10.1002/rcm.646.

[103] K. Lian, P. Zhang, W. Wang, T. Dai, L. Li, Determination of Total Cholesterol in Serum by Gas Chromatography-Mass Spectrometry, Asian J. Chem. 26 (2014) 2646–2648. https://doi.org/10.14233/ajchem.2014.15780.

[104] H.-Y. Hsieh, L.-H. Li, R.-Y. Hsu, W.-F. Kao, Y.-C. Huang, C.-C. Hsu, Quantification of Endogenous Cholesterol in Human Serum on Paper Using Direct Analysis in Real Time Mass Spectrometry, Anal. Chem. 89 (2017) 6146–6152. https://doi.org/10.1021/acs.analchem.7b00943.

[105] M.S. Gardner, L.G. McWilliams, J.I. Jones, Z. Kuklenyik, J.L. Pirkle, J.R. Barr, Simultaneous Quantification of Free Cholesterol, Cholesteryl Esters, and Triglycerides without Ester Hydrolysis by UHPLC Separation and In-Source Collision Induced Dissociation Coupled MS/MS, J. Am. Soc. Mass Spectrom. 28 (2017) 2319–2329. https://doi.org/10.1007/s13361-017-1756-2.

[106] G. Liebisch, M. Binder, R. Schifferer, T. Langmann, B. Schulz, G. Schmitz, High throughput quantification of cholesterol and cholesteryl ester by electrospray ionization tandem mass spectrometry (ESI-MS/MS), Biochimica et biophysica acta 1761 (2006) 121–128. https://doi.org/10.1016/j.bbalip.2005.12.007.

[107] D. Foest, A. Knodel, S. Brandt, J. Franzke, Coupling paper spray ionization with the flexible microtube plasma for the determination of low polar biomarkers in mass spectrometry, Analytica chimica acta 1201 (2022) 339619. https://doi.org/10.1016/j.aca.2022.339619.

[108] P.A. James, S. Oparil, B.L. Carter, W.C. Cushman, C. Dennison-Himmelfarb, J. Handler, D.T. Lackland, M.L. LeFevre, T.D. MacKenzie, O. Ogedegbe, S.C. Smith, L.P. Svetkey, S.J. Taler, R.R. Townsend, J.T. Wright, A.S. Narva, E. Ortiz, 2014 evidence-based guideline for the management of high blood pressure in adults: report from the panel members appointed to the Eighth Joint National Committee (JNC 8), JAMA 311 (2014) 507–520. https://doi.org/10.1001/jama.2013.284427.

[109] C. Tsioufis, C. Thomopoulos, Combination drug treatment in hypertension, Pharmacological research 125 (2017) 266–271. https://doi.org/10.1016/j.phrs.2017.09.011.

[110] F. Allain, PyMSFile Reader, 2023, https://github.com/frallain/pymsfilereader.

[111] A. Li, H. Wang, Z. Ouyang, R.G. Cooks, Paper spray ionization of polar analytes using non-polar solvents, Chemical communications (Cambridge, England) 47 (2011) 2811–2813. https://doi.org/10.1039/c0cc05513a.

[112] D. Kim, U.H. Yim, B. Kim, S. Cha, S. Kim, Paper Spray Chemical Ionization: Highly Sensitive Ambient Ionization Method for Low- and Nonpolar Aromatic Compounds, Anal. Chem. 89 (2017) 9056–9061. https://doi.org/10.1021/acs.analchem.7b01733.

[113] H. Kim, H. Lee, D. Kum, H. Tae, S. Cha, D. Kim, S. Kim, Mechanism behind the paper spray chemical ionization phenomenon and the choice of solvent, Journal of mass spectrometry JMS 56 (2021) e4602. https://doi.org/10.1002/jms.4602.

[114] R.D. Espy, A.R. Muliadi, Z. Ouyang, R.G. Cooks, Spray mechanism in paper spray ionization, International Journal of Mass Spectrometry 325-327 (2012) 167–171. https://doi.org/10.1016/j.ijms.2012.06.017.

[115] J. McKenna, E.S. Dhummakupt, T. Connell, P.S. Demond, D.B. Miller, J. Michael Nilles, N.E. Manicke, T. Glaros, Detection of chemical warfare agent simulants and hydrolysis products in biological samples by paper spray mass spectrometry, The Analyst 142 (2017) 1442–1451. https://doi.org/10.1039/C7AN00144D.

[116] P. Nemes, I. Marginean, A. Vertes, Spraying mode effect on droplet formation and ion chemistry in electrosprays, Anal. Chem. 79 (2007) 3105–3116. https://doi.org/10.1021/ac062382i.

[117] J.N. Smith, R.C. Flagan, J.L. Beauchamp, Droplet Evaporation and Discharge Dynamics in Electrospray Ionization, J. Phys. Chem. A 106 (2002) 9957–9967. https://doi.org/10.1021/jp025723e.

[118] A.M. Gañán-Calvo, J. Dávila, A. Barrero, Current and droplet size in the electrospraying of liquids. Scaling laws, Journal of Aerosol Science 28 (1997) 249–275. https://doi.org/10.1016/S0021-8502(96)00433-8.

[119] C. Markert, M. Thinius, L. Lehmann, C. Heintz, F. Stappert, W. Wissdorf, H. Kersten, T. Benter, B.B. Schneider, T.R. Covey, Observation of charged droplets from electrospray ionization (ESI) plumes in API mass spectrometers, Analytical and bioanalytical chemistry 413 (2021) 5587–5600. https://doi.org/10.1007/s00216-021-03452-y.

[120] D.K. Trivedi, E. Sinclair, Y. Xu, D. Sarkar, C. Walton-Doyle, C. Liscio, P. Banks, J. Milne, M. Silverdale, T. Kunath, R. Goodacre, P. Barran, Discovery of Volatile Biomarkers of Parkinson's Disease from Sebum, ACS central science 5 (2019) 599–606. https://doi.org/10.1021/acscentsci.8b00879.

[121] E. Sinclair, C. Walton-Doyle, D. Sarkar, K.A. Hollywood, J. Milne, S.H. Lim, T. Kunath, A.M. Rijs, R.M.A. de Bie, M. Silverdale, D.K. Trivedi, P. Barran, Validating Differential Volatilome Profiles in Parkinson's Disease, ACS central science 7 (2021) 300–306. https://doi.org/10.1021/acscentsci.0c01028.

[122] Christer S. Ejsing, Molecular characterization of the lipidome by mass spectrometry. Dissertation, Dresden, 2006.

[123] W.-C. Lee, T.-J. Wu, C.-H. Cheng, Y.-C. Wang, H.-C. Hung, J.-C. Lee, T.-H. Wu, H.-S. Chou, C.-F. Lee, K.-M. Chan, Elevation of Lipid Metabolites in Deceased Liver Donors Reflects Graft Suffering, Metabolites 13 (2023). https://doi.org/10.3390/metabo13010117.

[124] P. Seubnooch, M. Montani, S. Tsouka, E. Claude, U. Rafiqi, A. Perren, J.-F. Dufour, M. Masoodi, Characterisation of hepatic lipid signature distributed across the liver zonation using mass spectrometry imaging, JHEP reports innovation in hepatology 5 (2023) 100725. https://doi.org/10.1016/j.jhepr.2023.100725.

[125] J. Wang, Y. Zhang, W. Zhang, Z. Fan, Research Progress of Electrostatic Spray Technology over the Last Two Decades, J. Energy Eng. 147 (2021) 35. https://doi.org/10.1061/(ASCE)EY.1943-7897.0000763.

[126] I. Reginskaya, A.-K. Stark, M. Schilling, D. Janasek, J. Franzke, Dielectric barrier electrospray-polarity cycle and trigger, Anal. Chem. 85 (2013) 10738–10744. https://doi.org/10.1021/ac401582s.

[127] A.K. Stark, M. Schilling, D. Janasek, J. Franzke, Characterization of dielectric barrier electrospray ionization for mass spectrometric detection, Analytical and bioanalytical chemistry 397 (2010) 1767–1772. https://doi.org/10.1007/s00216-010-3749-x.

9 Appendix

Supporting information to chapter 3.2 "Application to liver extract".

MS^2 spectra of the polar Lipid identification by nESI-MS:

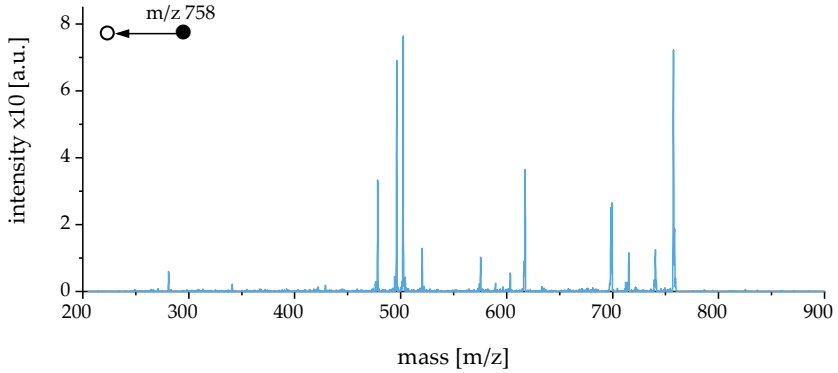

Figure A1: MS^2 spectrum of m/z 758 that leads to the identification of PC(34:2).

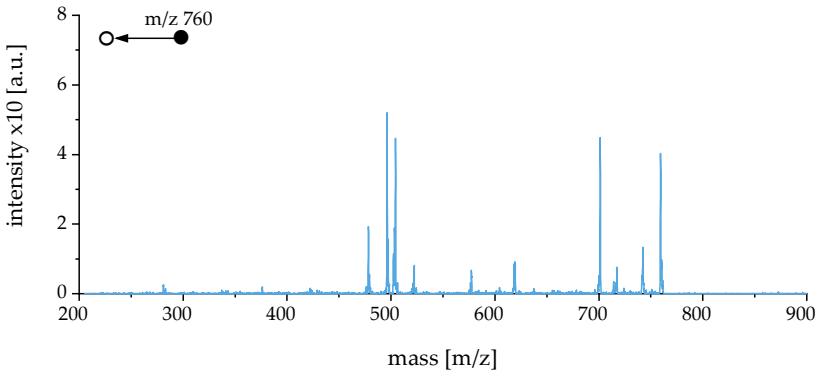

Figure A2: MS^2 spectrum of m/z 760 that leads to the identification of PC(34:1).

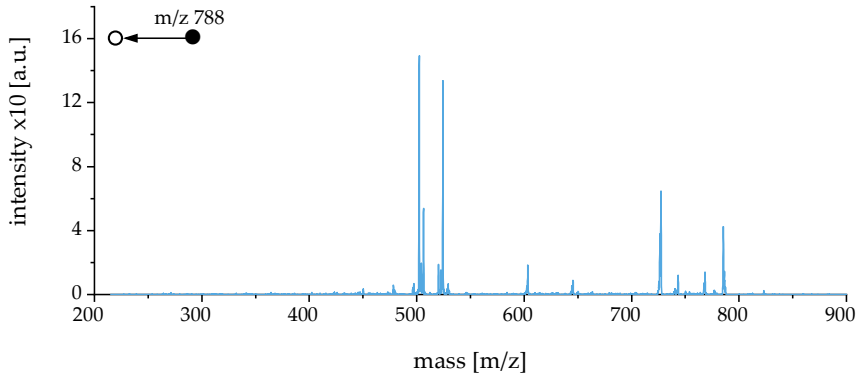

Figure A3: MS² spectrum of m/z 788 that leads to the identification of PC(36:1).

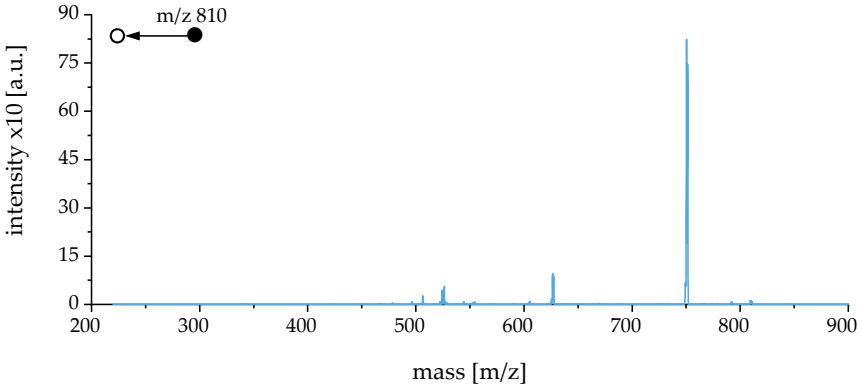

Figure A4: MS² spectrum of m/z 810 that leads to the identification of PC(38:4).

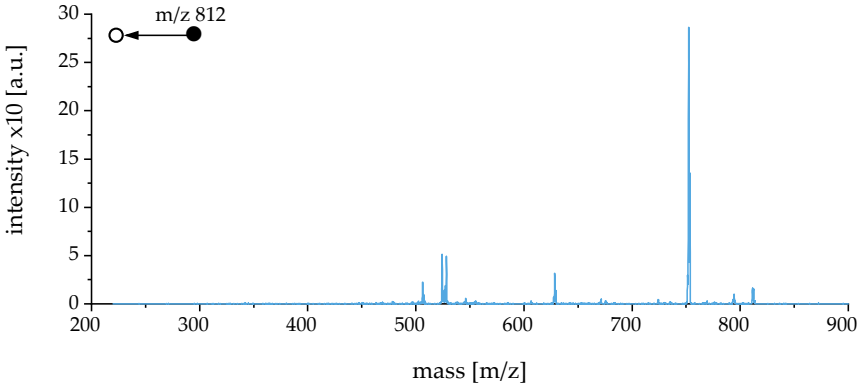

Figure A5: MS² spectrum of m/z 812 that leads to the identification of PC(38:3).

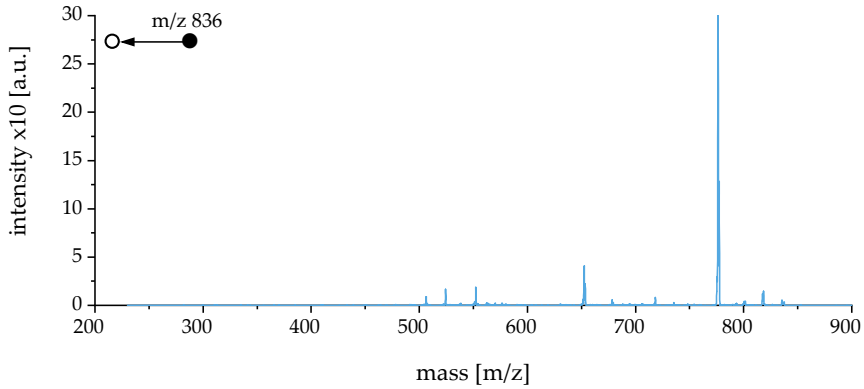

Figure A6: MS^2 spectrum of m/z 812 that leads to the identification of PC(40:5).

Supporting information to chapter 3.3 "Signal quality and stability".

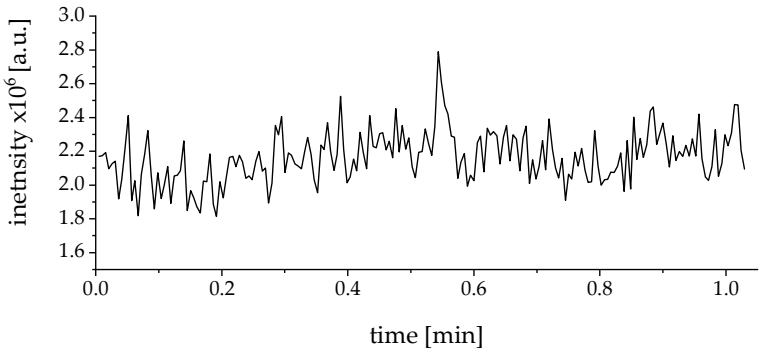

Figure A7: EIC of m/z m/z 786 of the nESI reference measurement.

Supporting information to chapter 4.4 "Detection of volatile biomarker candidates".

Table A1. Identification of five high abundant polar lipids of the total heart extract. According to reference [122].

m/z	Rel. abundance	Corresponding lipid species	Ion type
742.71	90.7	PC(O-34:3)	$[M+H]^+$
744.69	41.8	PC(O-34:2)	$[M+H]^+$
758.70	100.0	PC(34:2)	$[M+H]^+$
760.71	46.4	PC(34:1)	$[M+H]^+$
768.62	56.7	PC(O-36:4)	$[M+H]^+$

Table A2. Composition of the total liver lipid extract of a bovine according to Avanti lipids.

Component	Fraction (wt/wt) [%]
Phosphatidylcholine	5.4
Phosphatidylethanolamine	6.8
Phosphatidylinositol	2.5
Phosphatidic acids	1.1
Cardiolipin	2.3
Unknown	32.1

Supporting information to chapter 5.1. "Coupling a heated nESI with the FμTP".

Applied ionisation source parameters of the measurement in Figure 49.

Table A3a: Commercial Thermo IonMax API (APCI).

Parameter	Value
Corona voltage	3.9 kV
Vaporizer temperature	300 °C
Tube lens voltage	110 V
Capillary voltage	10 V
Inlet capillary temperature	280 °C
Number of scans (averaged)	50
Number of micro scans	3

Table A3b: Parameters of the nESI-FμTP approach.

Parameter	value
nESI voltage	2.1 kV
FμTP voltage amplitude	2.5 kV
Tube lens voltage	65 V
Capillary voltage	10 V
Inlet capillary temperature	320 °C
Number of scans (averaged)	50
Number of micro scans	3

Table A3c: Parameter of the heated-nESI-FµTP approach.

	Parameter	value
H-nESI	voltage	3.0 kV
	liquid flow	2 µL/min
	temperature	160 °C
	sheath gas flow	off
Plasma/ FµTP	voltage amplitude	2.2 kV
	frequency / form	20 kHz / square-wave
	helium gas flow	30 mL/min
MS	tube lens voltage	100 V
	capillary voltage	10 V
	inlet capillary temperature	280 °C
	number of scans (averaged)	50
	number of micro scans	3

Supporting information to chapter 5.2. "Identification of less polar lipids".

MS^2 spectra of the less polar lipid identification by heated nESI-FµTP-MS:

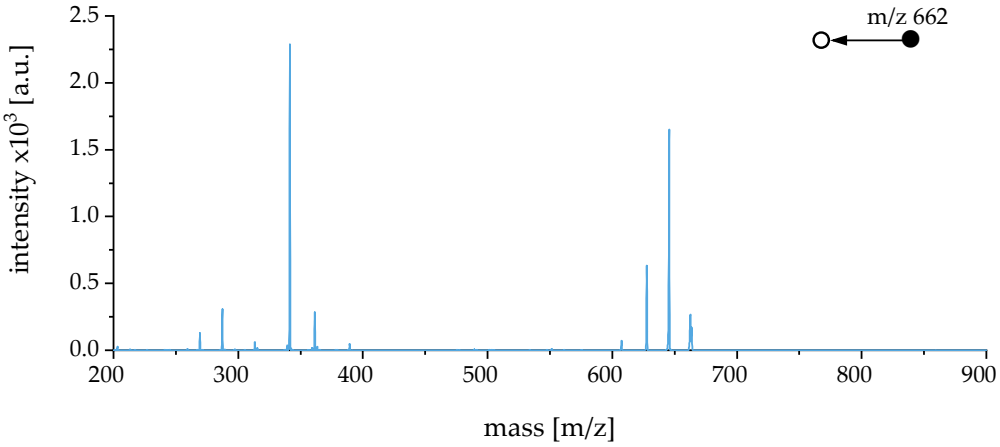

Figure A8: MS^2 spectrum of m/z 662 that leads to the identification of DG(18:0/20:4).

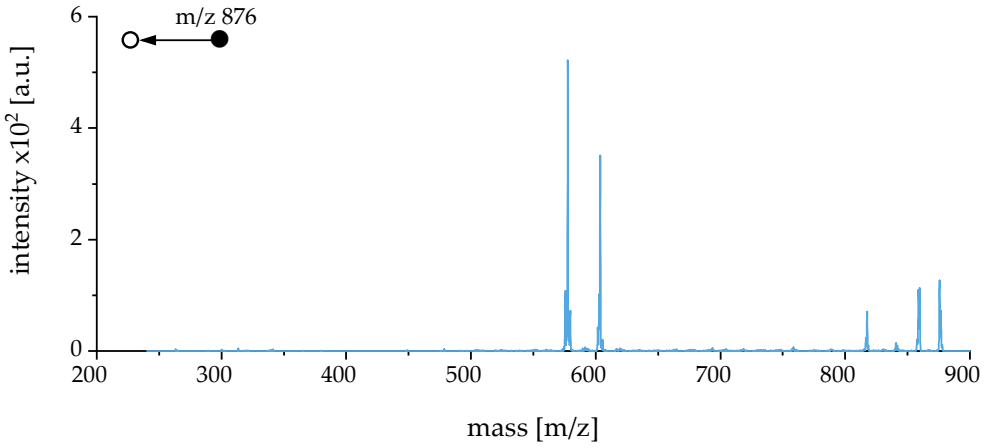

Figure A9: MS² spectrum of m/z 876 that leads to the identification of TG(18:1/18:1/16:0).

Supporting information to chapter 5.5. "hybrid ionisation by fast switching of the ion source".

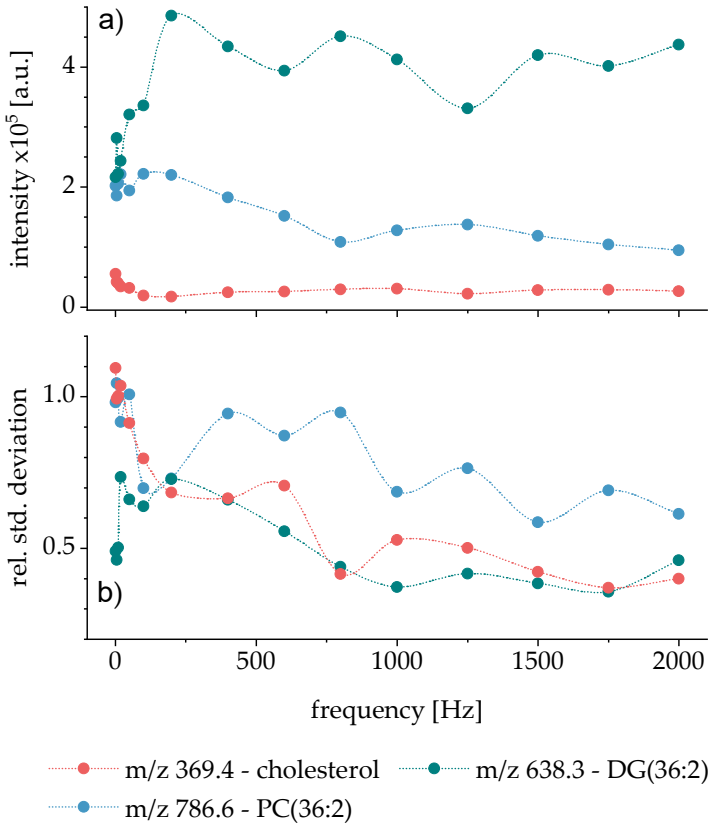

Figure A10: Second measurement with the heated nESI-sFμTP – AGC activated.

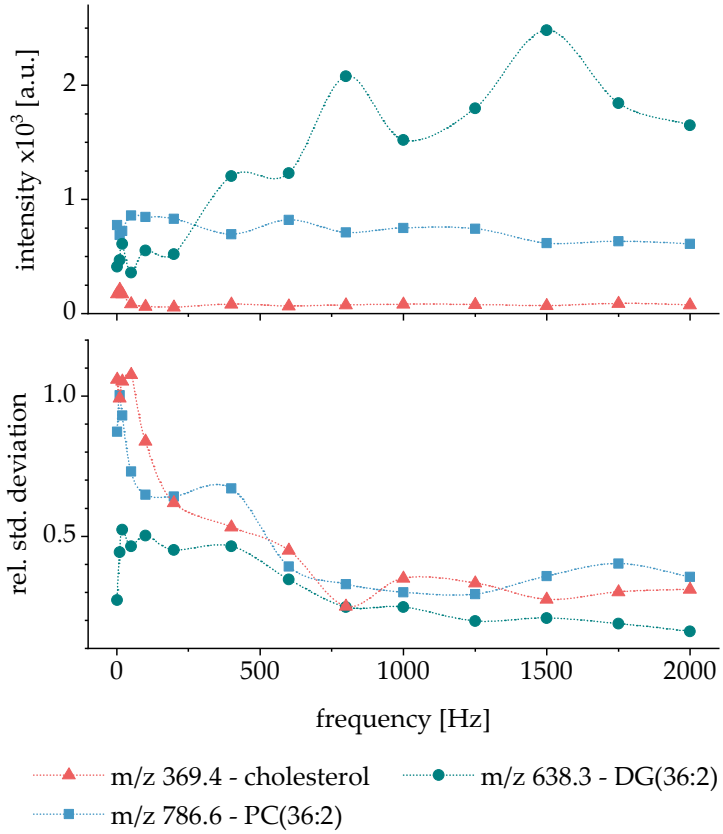

Figure A11: Second measurement with the heated nESI-sFμTP – AGC off 1 ms injection time.

Supporting information to chapter 5.6. "Performance of the heated of the heated nESI-sFμTP".

Applied ionisation source parameters of the measurement in Figure 62.

Table 4a: Parameter of the **nESI reference**.

	Parameter	Value
nESI	Voltage	2.1 kV
	Liquid flow	1 µl/min
MS	Tube lens voltage	90 V
	Capillary voltage	95 V
	Inlet capillary temperature	280 °C

b) Parameter of the Thermo IonMax API - **HESI II** probe.

	Parameter	Value
H-ESI	Voltage	2.8 kV
	Liquid flow	10 µL/min
	Temperature	43 °C
	Sheath gas / Aux gas flow	5 / 5 arb
MS	Tube lens voltage	110 V
	Capillary voltage	15 V
	Inlet capillary temperature	280 °C

c) Parameter of the commercial Thermo IonMax API - **APCI** probe.

	Parameter	Value
APCI	Voltage	3.9 kV
	liquid flow	15 µL/min
	temperature	300 °C
	sheath gas / Aux gas flow	5 / 5 arb
MS	tube lens voltage	110 V
	capillary voltage	10 V
	Inlet capillary temperature	280 °C

d) Parameter for the **heated nESI**.

	Parameter	Value
nESI	voltage	2.2 kV
	liquid flow	3 µl/min
	temperature	200 °C
	sheath gas	25 mL/min
MS	tube lens voltage	100 V
	capillary voltage	10 V
	inlet capillary temperature	280 °C

e) Parameter of the heated **nESI-sFµTP approach**.

	Parameter	Value
nESI	voltage	2.2 kV
	liquid flow	3 µl/min
	temperature	200 °C
	sheath gas	25 mL/min
sFµTP	voltage	2.2 kV
	helium gas flow	30 mL/min
	activation frequency	1750 Hz
MS	tube lens voltage	100 V
	Capillary voltage	10 V
	inlet capillary temperature	280 °C

f) Parameter for the heated nESI in **transition mode**.

	Parameter	Value
nESI	voltage	2.6 kV
	liquid flow	5 µl/min
	temperature	200 °C
MS	tube lens voltage	100 V
	capillary voltage	10 V
	inlet capillary temperature	280 °C

g) Parameters of the **nTS-FµTP**.

	Parameter	Value
nESI	voltage	2.6 kV
	liquid flow	3 µl/min
	temperature	160 °C
	sheath gas	0 mL/min
sFµTP	voltage	3 kV
	helium gas flow	30 mL/min
MS	tube lens voltage	120 V
	Capillary voltage	10 V
	inlet capillary temperature	280 °C